Methane Measurements in Selected Ocean Areas: Eastern Tropical North Atlantic Ocean and Southwestern Labrador Sea

Als Diplomarbeit vorgelegt von

Annette Kock

IFM-GEOMAR, Leibniz-Institut für Meereswissenschaften an der Christian-Albrechts-Universität Kiel

August 2007

Index

1. Introduction: The Ocean as Source for Atmospheric Methane

1.1 Atmospheric Methane

Methane (CH_4) is the most abundant hydrocarbon in the atmosphere. On a 100 years time horizon, the global warming potential of one molecule methane is 21 times higher than that of one molecule carbon dioxide. Atmospheric methane accounts for more than 20 % of the greenhouse effect, therefore being the second most important greenhouse gas apart from carbon dioxide (IPCC 2007). Atmospheric methane levels have been increasing since the beginning of the industrial revolution from pre-industrial values of 0.7 ppm to a present value of about 1.8 ppm (ETHERIDGE, STEELE ET AL. 1998) [FIG. 1]. Decreasing annual growth rates in the last years were discussed as evidence for the approach of a new steady-state (DLUGOKENCKY, HOUWELING ET AL. 2003), although recent studies found indications for a further increase of atmospheric methane (LELIEVELD 2006).

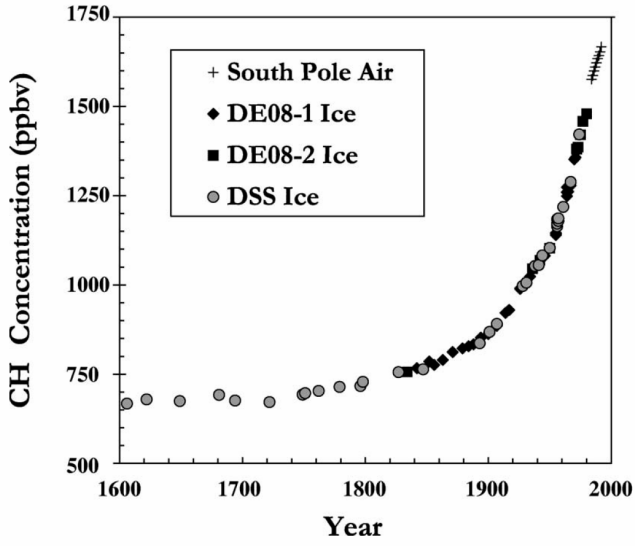

Figure 1: Atmospheric methane mixing ratio during the last 400 years. Source: (ETHERIDGE, STEELE ET AL. 1998). Information was obtained from Antarctic ice cores for times up to 1950 and completed by in-situ measurements for the last decades.

Global annual methane emissions were estimated by the fourth IPCC report (IPCC) to be 582 Tg. A variety of anthropogenic and natural sources contribute to the total emissions (KVENVOLDEN AND ROGERS 2005) [FIG. 2]. Anthropogenic sources are methane release during exploitation of fossil energy resources and waste disposal, but also intensive rice cultivation and livestock farming. In total, about 70 % of the total annual emissions are estimated to be of anthropogenic origin.

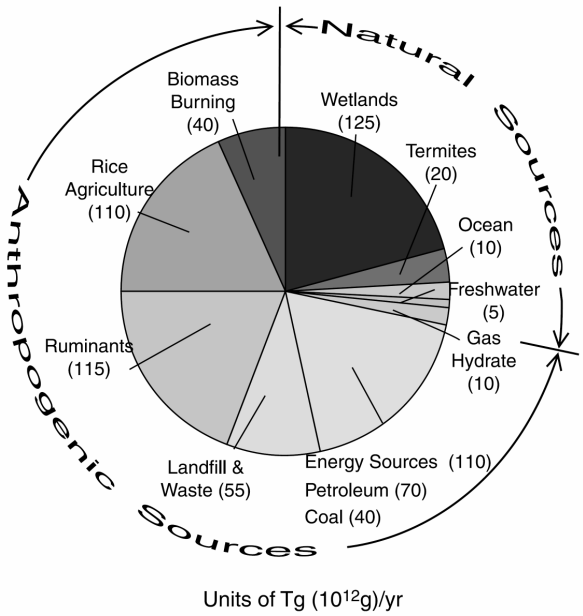

Figure 2: Natural and anthropogenic emissions of methane to the atmosphere. Source: (KVENVOLDEN AND ROGERS 2005).

Natural sources of methane are wetlands, the digestive tracts of termites, gas hydrates and, being a minor source of about 10 Tg yr^{-1}, the oceans [FIG. 2]. Estimates of source strengths show high uncertainties, however (HOUWELING, KAMINSKI ET AL. 1999). KVENVOLDEN AND ROGERS (2005) reported that terrestrial methane seepage from geological sources should also be taken into account, and most recently KEPPLER ET AL. (2006) suggested a so far unknown process of methane production by terrestrial plants that may also contribute significantly to methane emissions.

Oxidation of methane by OH-radicals in the troposphere is by far the main sink for atmospheric methane. About 90 % of the methane is removed in this way. A significant amount of CH_4 is exported to the stratosphere where it is

involved in complex ozone decomposition reactions. Another minor sink is the oxidation in dry soils (WUEBBLES AND HAYHOE 2002).

1.2 Methane in the Oceans

Methane concentrations in the ocean are influenced by a variety of geological, oceanographic and biological factors that are closely interconnected. FIG. 3 illustrates the involved processes.

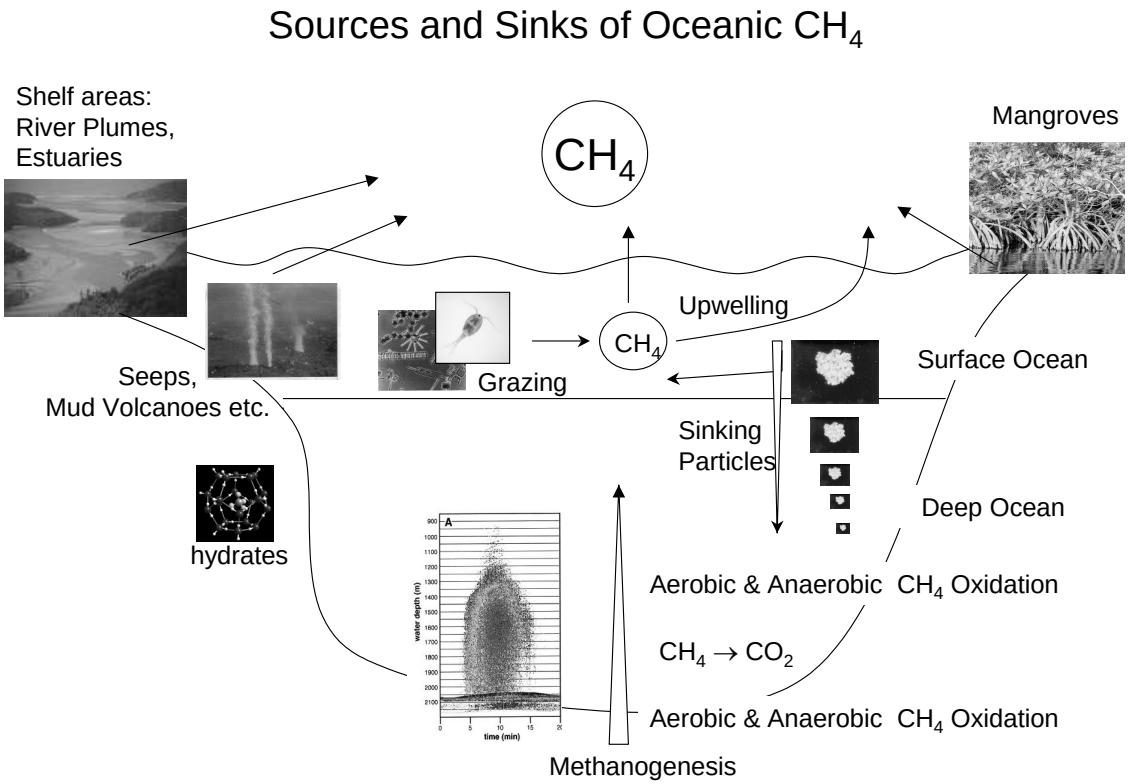

Figure 3: Overview of processes that influence the oceanic methane emissions to the atmosphere. Modified from BANGE (2006, unpublished).

Methane in the ocean water column is either of geological or biogenic origin. Geological sources are hydrothermal systems, natural gas and groundwater seeps and gas hydrates, all releasing methane from the sediments into the water column (ETIOPE 2004).

Methane from biogenic sources emerges as the end product of a sequence of organic matter decomposition steps. The methane production step is performed by archaea, converting mainly acetate or carbon dioxide to methane:

$$CH_3COOH \rightarrow CH_4 + CO_2 \quad [1]$$

$$CO_2 + 4H_2 \rightarrow CH_4 + 2H_2O \quad [2]$$

Methanogens require a strictly anaerobic environment and are outcompeted for substrates (acetate and hydrogen) by sulfate reducers (CICERONE AND OREMLAND 1988). Thus, methanogenesis is restricted to environments where oxygen and sulfate are depleted. Other methanogenic pathways using non-competitive organic substrates as methanol, dimethyl sulfide, methylated amines and methane thiol can occur in zones where sulfate is abundant, but may play only a minor role for the total methane production (CICERONE AND OREMLAND 1988). However, only a few oceanic basins show anoxic conditions and none are sulfate-free. Therefore, methanogenesis should not occur in the ocean water column, but in anoxic sediments below the sulfate reduction zone [FIG. 4] (REEBURGH 2007).

Consumption of methane occurs in the water column as well as in the sediments. Two oxidation pathways are known: In oxygenated environments, methane is oxidized to CO_2 by methanotrophic bacteria (CICERONE AND OREMLAND 1988):

$$CH_4 + 2O_2 \rightarrow CO_2 + 2H_2O \quad [3]$$

BOETIUS ET AL. (2000) identified a consortium of sulfate reducers and methanogens performing anaerobic oxidation of methane (AOM). The underlying process is the coupled reduction of sulfate with “reverse methanogenesis”, i.e. the oxidation of methane to carbon dioxide [FIG. 4] (VALENTINE AND REEBURGH 2000):

1) Reverse methanogenesis:

$$CH_4 + 2H_2O \rightarrow CO_2 + 4H_2 \qquad [4]$$

2) Sulfate reduction:

$$SO_4^{2-} + 4H_2 + H^+ \rightarrow HS^- + 4H_2O \qquad [5]$$

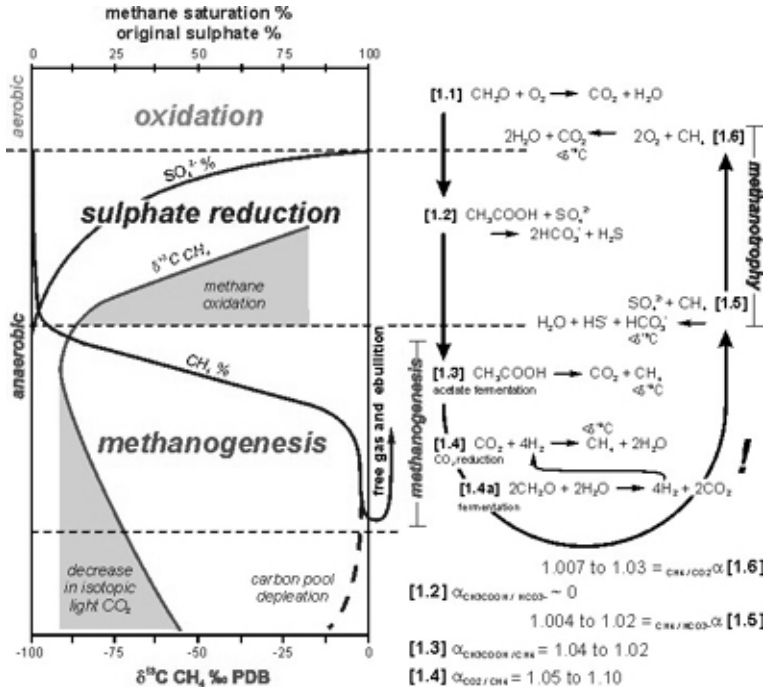

Figure 4: The marine methane cycle. Methane production and consumption in different environments. Source: GREINERT (1998).

Methane released from deep sediments is usually oxidized rapidly in the water column before reaching the surface ocean. Except from bottom waters with CH_4 plumes from mud volcanoes etc., the open ocean deep water column is usually undersaturated with respect to atmospheric equilibrium. Typical saturation values in the deep ocean range from 30 % to 50 % (REHDER, KEIR ET AL. 1999), while the surface ocean is known to be in atmospheric equilibrium or slightly supersaturated (BANGE, BARTELL ET AL. 1994; BATES, KELLY ET AL. 1996). Open ocean emissions have been estimated to range from 0.4 to 0.8 ± 0.6 Tg yr^{-1} (BATES, KELLY ET AL. 1996; KELLEY AND

JEFFREY 2002), confirming that the open ocean represents a small source for atmospheric methane.

On the shelf, however, where bottom depths do not exceed 200 m, significant amounts of methane can reach the ocean surface. Thus, shelf areas might contribute 75 % to the total oceanic methane emissions to the atmosphere (BANGE, BARTELL ET AL. 1994), showing high spatial variations, though. Supersaturations range from 110 % in open shelf waters to several thousand percent in estuaries and river plumes (BANGE 2006).

Although methanogenesis is restricted to anaerobic environments, measurements of dissolved methane in the water column revealed a methane maximum in the well-oxygenated subsurface layer throughout the ocean. This phenomenon cannot be explained by advection of coastal waters alone (SCRANTON AND BREWER 1977), but suggests the occurrence of in-situ methane production in anoxic microniches or of methane production by a so far unidentified pathway. Several methane sources associated with anaerobic microenvironments have been discussed: KARL AND TILBROOK (1994) suggested a connection of the subsurface methane maximum to the accumulation of particulate organic mater (POM) in the pycnocline. They measured methane fluxes from sinking organic particles sufficient to explain the subsurface methane maximum. DE ANGELIS AND LEE (1994) argued that the subsurface methane maximum could result from methane production in zooplankton guts. Other pathways such as CH_4 production by phytoplankton have been suggested, but have not been quantified yet.

1.2.1 Methane in Coastal Upwelling Areas

In coastal upwelling areas water masses from the depth of the subsurface methane maximum in 100-200m are brought to the surface. These waters usually show significantly enhanced surface methane concentrations in consequence of enhanced methane production in the subsurface layer of the upwelling-induced high productivity zone (SANSONE, POPP ET AL. 2001).

Methane air-sea fluxes from upwelling regions were estimated from several measurements in the Arabian Sea (NAQVI, BANGE ET AL. 2005) and the California Current region (REHDER, COLLIER ET AL. 2002; SANSONE, GRAHAM ET AL. 2004). MONTEIRO ET AL. (2006) obtained a time series of methane concentrations from a mooring station deployed in the Benguela Current upwelling system, but no sea-air fluxes were calculated.

Estimates of methane emissions were calculated for the coastal upwelling in the Arabian Sea and range from 0.5 to 0.9 Gg during an upwelling period of 4 months, indicating that coastal upwelling regions are “hot spots” of methane emissions to the atmosphere (BANGE, RAMESH ET AL. 1998).

For the Northwest African upwelling system, methane data are sparse. GEBHARDT AND BANGE (2006) report slight supersaturations from underway measurements during the Poseidon 320 cruise in March/April 2005. FORSTER ET AL. (2007) calculated sea-air fluxes from the area off Mauritania using data from 3 depth profiles taken in fall 2003 during a cruise of the Atlantic Meridional Transect (AMT) programme. Flux densities were calculated to 2.31 – 4.04 µmol m^{-2} d^{-1} (26.7 – 46.7 pmol m^{-2} s^{-1}).

1.2.2 Methane in the Labrador Sea

Deep convection is known to take place in distinct areas in the Southern Ocean and the North Atlantic Ocean, transporting considerable amounts of surface waters into the deep ocean. Deep water formation in the Labrador Sea is a well investigated phenomenon, yet only few measurements of methane concentrations have been performed so far.

In the subpolar regions the ocean represents a net sink for methane, indeed. REHDER ET AL. (1999) found surface methane concentrations in the North Atlantic Ocean to be in equilibrium with the atmosphere. In contrast to most parts of the oceans they found no subsurface methane maximum as indicator for biological methane production. The methane distribution in the Labrador Sea water column is mainly influenced by oceanographic properties. Similar to the Apparent Oxygen Utilization (AOU), Methane saturation levels reflect the age of water masses as consumption is the only biological process affecting methane concentrations.

1.3 Objectives of the Thesis

In this study methane concentration measurements from two contrasting oceanic regions (the coastal upwelling region off Mauritania and the deep water formation site in the Labrador Sea) are presented: Continuous surface measurements and methane depth profiles were taken during the SOPRAN (**S**urface **O**cean **Pr**ocesses in the **An**thropocene) cruise Poseidon 348 in the Eastern Tropical North Atlantic Ocean(ETNA) in February 2007. Additionally, CH_4 depth profiles were measured during the Maria S. Merian cruise MSM 05/2 in the southwestern Labrador Sea in May/June 2007.

The results in this study are a contribution to the investigation of the largely unknown CH_4 cycle in the ocean.
The specific objectives were:

1) To determine the surface and depth distribution of methane in the Eastern Tropical North Atlantic Ocean,
2) To quantify the methane emissons to the atmosphere from the upwelling area off Mauritania and
3) To determine the methane depth distribution in the deep water formation site in the Labrador Sea and compare it with data from 1997.

2 Materials & Methods

2.1 Overview of the Analytical System

Concentrations of dissolved methane were measured gas chromatographically using (A) a static and (B) a continuous equilibration method. FIG. 5 shows the analytical set-up for both methods. Detailed descriptions of both methods are given in sections 2.4 and 2.5.

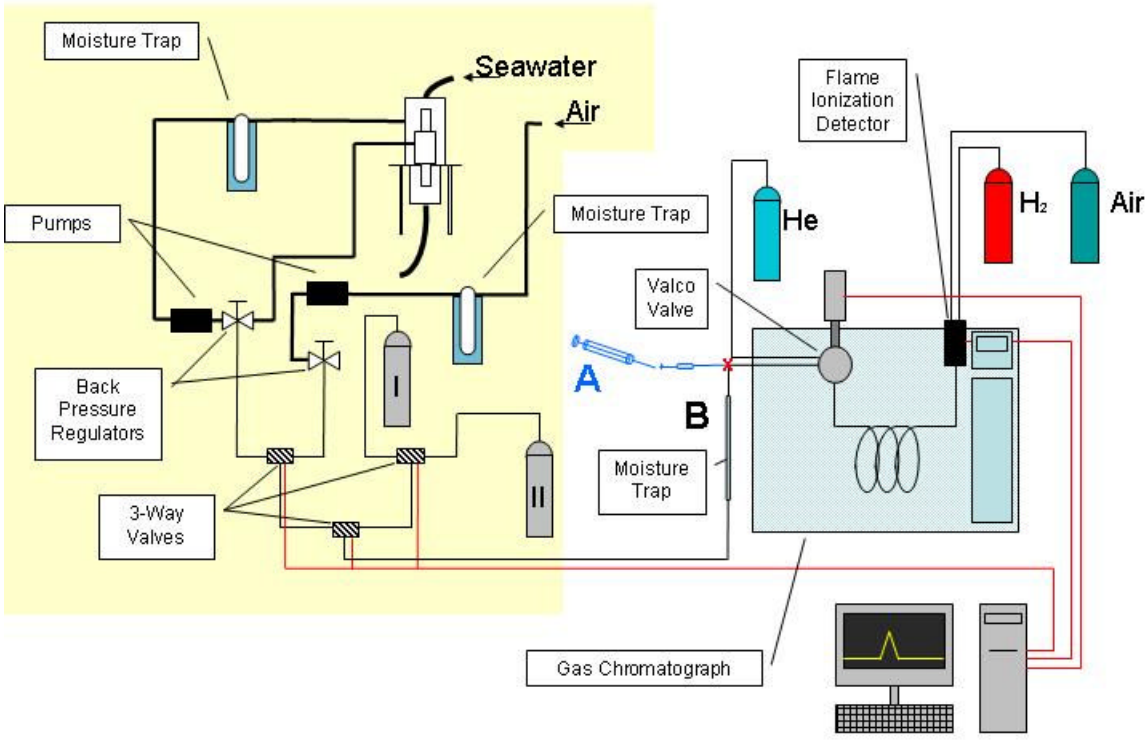

Figure 5: Experimental set-up for A) discrete measurements and B) continuous measurements. The shaded box illustrates the system of valves and pumps installed to switch between the source gases. I and II are standard gas mixtures. The red cross (x) indicates the location where the valve system was disconnected when changing from continuous to discrete measurements.

2.2 Gas Chromatographic Analysis

For all measurements, a Hewlett Packard 5890 Series II gas chromatograph, equipped with a flame ionization detector (FID), was used [FIG. 6].

Figure 6: The HP 5890 II gas chromatograph used for discrete sample analysis. View inside the oven with Valco valve, sample loop and column. For continuous analysis, an identical GC, but equipped with a second column and an electron capture detector for N_2O analysis, was used.

Samples were injected into the gas chromatograph using a 10 mL gas tight syringe, passing a moisture trap (filled with Sicapent®) before entering a 6-port (for discrete samples) or 12-port (for continuous measurements) Valco valve.

The Valco valve could be switched into two positions: In the LOAD position, the column was flushed with carrier gas only, while an injected sample was lead into a sample loop of 2 mL volume. In the INJECT position, the sample loop was connected to the column and flushed by the carrier gas stream. This ensured a constant sample volume injected into the column. The Valco valve was installed inside the oven and moved by an electric actuator which could be switched manually.

To separate methane from the other gas components a stainless steel column (1.83 m length, 3.2 mm OD, 2.2 mm ID) packed with washed molsieve 5A (mesh 80/100, Alltech GmbH, Germany) was used. Helium (Helium 5.0, Air Liquide GmbH, Düsseldorf) was used as carrier gas at a flow rate of 25 mL min^{-1}. The oven temperature was held at a constant temperature of 60°C.

The FID is a widespread detector to determine hydrocarbons in gas samples. In a flame of hydrogen and air the sample molecules are ionized at temperatures of about 2000 °C and detected as an electric current between two electrodes that are installed beneath the flame. The FID is sensitive to organic compounds that can easily be oxidized, but insensitive to the main air components like nitrogen and oxygen.

The linear correlation between signal intensity and sample gas concentration over a wide concentration range makes the FID applicable particularly for quantitative trace analysis of hydrocarbons. The detector temperature during the measurements was 250°C and the flow rates of the flame gases were 120 mL min^{-1} (Air) and 20 mL min^{-1} (Hydrogen).

2.3 Standard Gas Mixtures

We used two sets of standard gas mixtures with CH_4 in synthetic air. These mixtures were gravimetrically prepared by DEUSTE-Steininger GmbH (Mühlheim, Germany). The standard mixtures have been calibrated against the NOAA scale in the laboratories of the Max Planck Institute for Biogeochemistry in Jena. The CH_4 dry mole fractions of the standards were: 1.779 ± 0.002 ppm and 2.543 ± 0.002 ppm.

2.4 Discrete Water Samples

Discrete samples from the water column were taken on a section along 18°N during R/V Poseidon cruise P348 and on two sections during R/V Maria S. Merian cruise MSM 05/2 (for detailed descriptions of the cruise tracks see sections 3 and 4). For each water depth, triplicate samples were taken from the Niskin bottles at all stations during MSM 05/2 and at the first 4 stations during P348. Duplicate samples were taken for the rest of the stations during P348.

The P348 samples were poisoned with 0.2 mL of mercury chloride ($HgCl_2$, aq, 1 mmol L^{-1}) for storage and transport to IFM-GEOMAR, while the samples taken during MSM 05/2 were not treated with mercury chloride but measured on board within 48 h after sampling (see also section 2.8.1).

Samples were analyzed with a static equilibration method: A headspace of 10 mL Helium (5.0, Air Liquide GmbH, Düsseldorf) was added to a opaque glass vial (24 mL) and left to equilibrate with the liquid phase for at least 2 h. Afterwards subsamples were taken from the headspace with a gas-tight syringe extracting approximately 9.5 mL of the headspace volume [FIG. 7]. The subsample was injected manually into the gas chromatographic system.

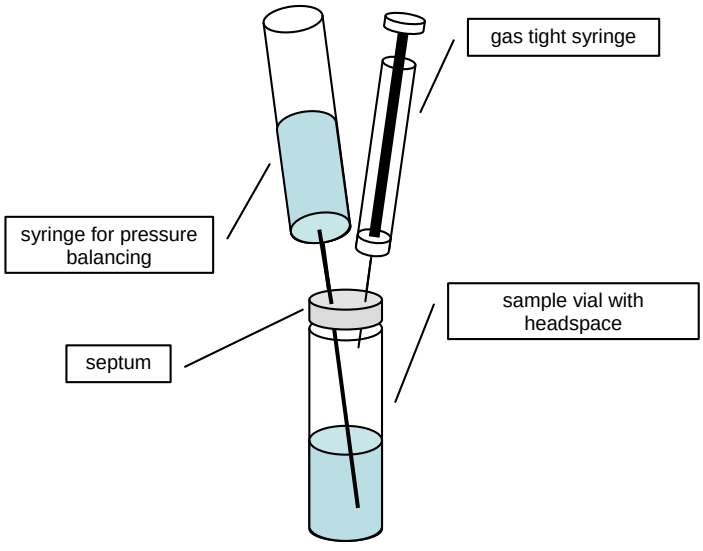

Figure 7: Headspace equilibration method.

The methane dry mole fraction in the headspace x_{Hs} was determined from the FID signal peak area using two standard gas mixtures for calibration. Six of each standard were injected every day before and after the sample measurements. These twelve standard measurements were taken for daily calibration.

The methane content n_{Hs} [nmol] was calculated according to the Ideal Gas Law:

$$n_{Hs} = x_{Hs} \frac{pV_{Hs}}{RT_{eq}} \quad [6]$$

where: $p =$ atmospheric pressure during equilibration, assumed to be 10^5 Pa

$V_{Hs} =$ 10 mL = headspace volume

$R = 8.31451 \frac{m^3 Pa}{Kmol}$ = gas constant

$T_{eq} =$ equilibration temperature [K]

The solubility of gases in liquids can be described according to Henry's law:

$$C_W = H \times p \times x_{Hs} \quad [7]$$

where: H = Henry's law constant. The Henry's law constant is specific for the respective gas and is a function of temperature.

In seawater, the salinity effect on the solubility of gases has to be taken into account, too. WEISS (1970) developed a general gas solubility equation which includes the effects of temperature and salinity in the calculation of the dissolved gas concentration C_W from its dry mole fraction in the gas phase x_{Hs} :

$$C_W = \exp\left\{ A_1 + A_2\left(\frac{100}{T_{eq}}\right) + A_3 \ln\left(\frac{T_{eq}}{100}\right) + A_4\left(\frac{T_{eq}}{100}\right) + S\left[B_1 + B_2\left(\frac{T_{eq}}{100}\right) + B_3\left(\frac{T_{eq}}{100}\right)^2 \right] \right\} \times x_{Hs}\, p \qquad [8]$$

where: S = salinity of the water sample

A_1 to B_3 are gas specific coefficients. Their values for methane were determined by WIESENBURG AND GUINASSO (1979). They are listed in TAB. 1, giving the final dissolved CH_4 concentration in nmol L^{-1}.

The exponential term in Equation [8] is called the Bunsen coefficient β and is used equivalent to Henry's law constant.

Table 1: Coefficients to calculate the Bunsen solubility of methane, giving the final dissolved CH4 concentration in nmol L^{-1}.

Co-efficient	A_1	A_2	A_3	A_4	B_1	B_2	B_3
Value	-415.2807	596.8104	379.2599	-62.0757	-0.059160	0.032174	-0.0048198

The total concentration of the sample C_{tot} was obtained by:

$$C_{tot} = C_W + \frac{n_{Hs}}{V_W} \qquad [9]$$

The water phase volume V_W is the difference between the total sample vial volume and the headspace volume. The vial volume was determined by weighing to be 23.95 ± 0.41 mL. Thus, V_W is 13.96 ± 0.41 mL.

Methane saturations ($Sat.$ in %) were calculated with the equilibrium concentration (C_{atm}) based on the actual atmospheric mixing ratio. Equilibrium concentrations were computed according to Eqn. [8], where T_{eq} was replaced by the potential temperature θ (this is the temperature after adiabatic expansion to atmospheric pressure).

$$Sat. = 100 \frac{C_{tot}}{C_{atm}} . \qquad [10]$$

2.5 Continuous Measurements

In the continuous measurements, samples were taken from a shower type equilibrator developed by R. F. Weiss (Scripps Institution of Oceanography, La Jolla, California), shown in FIG. 8.

Figure 8: The equilibrator used for the P348 underway measurements. It is flushed with seawater from the top. The seawater is lead over a sprinkler head and several chambers inside the equilibrator to accelerate the air-sea exchange. The total equilibrator volume was about 8 L.

The total equilibrator volume was approximately 8 L. Seawater was pumped continuously from a depth of 3 m via a submersible pump installed in the ship's moonpool into the equilibrator. The air inside the equilibrator should approach equilibrium with the water phase. Equilibration temperature was recorded automatically once a minute from a temperature sensor installed inside the equilibrator.

The experimental set-up is illustrated in FIG. 5 (see section 2.1). "Equilibrator air" was pumped through the equilibrator in a closed circuit in order to allow dynamic equilibration. To reduce the amount of water entering the valve system two moisture traps (dewars with water/ice mixtures) were installed in both the equilibrator headspace circuit and the ambient air sampling line. The gas sampling lines were connected to a system of 3-way-valves which was

controlled remotely to switch between 4 different sample sources: In addition to the “equilibrator air”, ambient atmospheric air and the two standard gas mixtures were connected to the system.

From each gas stream samples were taken every 22.2 min using a computer program that controlled the switching of the 3-way valves and the Valco valve. The sample loop was flushed for 1.5 min before switching the Valco valve to INJECT. To minimize the waste of standard and equilibrator air the system was purged with ambient air in between two measurements [FIG 9]. The flow of the respective sample gases ranged between 70 and 140 mL min^{-1}.

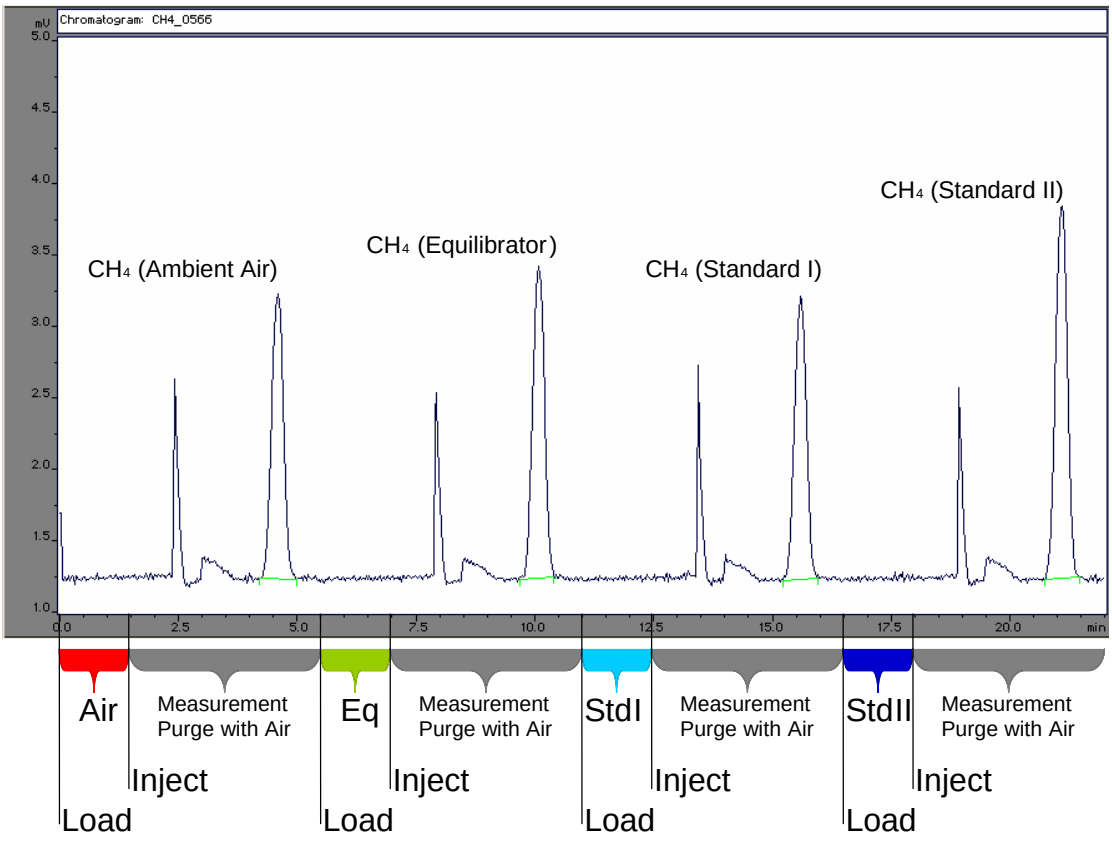

Figure 9: Time schedule of one sampling cycle in the continuous measurements. The colored braces indicate the time the sample loop is flushed with the respective sample gas. One cycle took 22 min and was repeated every 22.2 min.

The standard peak areas of the respective and the following chromatogram were used for calibration to determine the methane dry mole fractions x_{eq} and x_A. The equilibrator methane concentrations C_{eq} were calculated according to Equation [8], using the equilibrator temperature as T_{eq} and x_{eq} instead of x_{Hs}. Salinity values were taken from the ship's thermosalinograph and calibrated against CTD values.

To obtain the surface methane concentrations, the equilibrator methane concentrations have to be corrected for temperature differences between the sea surface temperatures (SST) at the pump's seawater intake and the seawater temperature measured inside the equilibrator. SST was taken from the ship's thermosalinograph, too. The correction was calculated by:

$$C_{SST} = \frac{\beta_{eq}}{\beta_{SST}} \times C_{eq} \qquad [11]$$

x_A was used to calculate the equilibrium methane concentrations in the surface layer according to Equation [8]. Temperature and salinity were taken from the thermosalinograph again.

2.6 Gas Exchange Calculations

To quantify the emissions from the upwelling area, the air-sea gas exchange has to be calculated. The most common approach to describe gas-exchange is the “stagnant film” model, assuming microscale viscous boundary layers both in the water and gas phase where transport processes across the ocean/atmosphere interface are controlled by molecular diffusion only. The air-sea exchange flux F can then be described according to Fick’s first law of diffusion:

$$F = \frac{D}{z}\Delta C \qquad [12]$$

where: D = molecular diffusion coefficient of the gas in the water phase

$\Delta C = C_W - C_A$

z = thickness of the boundary layer.

The quotient $\frac{D}{z}$ is called the gas exchange velocity k.

Several equations exist to express the relationship between gas exchange velocity and wind speed. The expressions used in this study were developed by LISS AND MERLIVAT (1986) and WANNINKHOF (1992). FIG. 10 compares both functions to in-situ measured values for k. The scattering of the values reflects the difficulties to determine k. The equations by WANNINKHOF (1992) and LISS AND MERLIVAT (1986) can be seen as the upper and lower limit for k and thus set the max and min limits for the resulting gas exchange estimates as well.

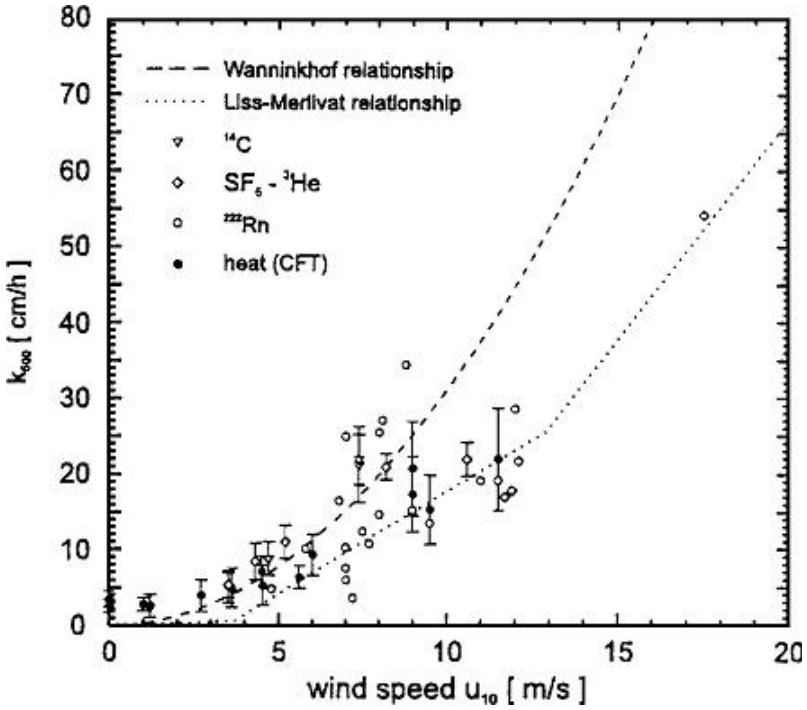

Figure 10: Relationship between the gas transfer coefficient k and the wind speed u_{10} for the models of LISS AND MERLIVAT (1986) and WANNINKHOF (1992), compared to gas transfer coefficient measurements for several gases. Source: JÄHNE AND HAUSSECKER (1998).

The derived equations are:

a) LISS AND MERLIVAT (1986) relationship:

1) for $0 \leq u_{10} \leq 3.6$ m s^{-1}

$$k = 0.17 u_{10} \left(\frac{600}{Sc_{CH_4}} \right)^{2/3} \quad [13]$$

2) for $3.6 < u_{10} \leq 13$ m s^{-1}

$$k = \left(\frac{600}{Sc_{CH_4}} \right)^{1/2} (2.85 u_{10} - 10.26) \quad [14]$$

3) for $u_{10} > 13$ m s^{-1}

$$k = \left(\frac{600}{Sc_{CH_4}} \right)^{1/2} (5.9 u_{10} - 49.91) \quad [15]$$

where: u_{10} = wind speed, normalized to a height of 10 m

b) WANNINKHOF (1992) relationship:

1) for $0 \leq u_{10} \leq 3.6$ m s^{-1}

$$k = 0.31 u_{10}^2 \left(\frac{660}{Sc_{CH_4}} \right)^{3/2} \quad [16]$$

2) for $u_{10} > 3.6$ m s^{-1}

$$k = 0.31 u_{10}^2 \left(\frac{660}{Sc_{CH_4}} \right)^{1/2} \quad [17]$$

During P348 wind speeds were measured at about 22m above sea level. Thus, the measured wind speeds were corrected to 10 m with the equation given in GARRATT (1977).

The Schmidt number (*Sc*) is defined as:

$$Sc = \frac{\nu_{sw}}{D} \quad [18]$$

where: ν_{sw} = kinematic viscosity of seawater, ν_{sw} = f(T, S).

The diffusion of CH_4 in seawater was calculated with the equations given in JÄHNE ET AL. (1987)

2.7 Error Estimation

Mean values were determined for each depth from the triplicate (duplicate) samples. Various error sources can be identified to contribute to the statistic error e.g. the sample vial volume, the accuracy of the added headspace volume and the scattering due to the gas chromatographic analysis. Some of these errors can easily be quantified, others are poorly known.

The standard deviation of the mean CH_4 concentration (C_W) was approximated with ($C_{W\max} - C_{W\min}$) / 1.91, where $C_{W\min}$ and $C_{W\max}$ stand for the minimal and maximal CH_4 concentrations of the triplicate samples, respectively. The factor 1.91 is derived from the statistical method by DAVID (1951).

Mean standard deviation was ±10 % for the discrete P348 samples and ±10 % for MSM 05/2.

Error estimation for the equilibrator measurements is more complicated. The automation of the measurements makes the system less sensitive to sample handling errors, but bears the risk of various systematic errors. These are discussed in chapter 3.6 in detail.

Based on error propagation, BANGE (1994) calculated the relative error of C_W (measured with a comparable analytical system) to be in the range from ± 3 to ± 5 %. Thus, I assume that the mean relative error of C_W for the continuous CH_4 measurements presented in this study are comparable.

2.8 Additional Measurements

2.8.1 Comparison of Poisoned and Unpoisoned Samples

The samples measured onboard during the MSM05/2-cruise were not treated with mercury chloride. To show that biological processes affecting the methane concentration can be neglected for the time between sampling and measurement, a comparison experiment was performed during the cruise. 19 samples were taken from a depth of 300 m at the beginning of the cruise, of which 10 were treated with 0.2 mL mercury chloride ($HgCl_2$, aq) and 9 were left untreated. 9 samples were measured within 48 h after taking them from the Niskin Bottle, 10 after 10 days at the end of the cruise. The results listed in TABLE 2 show that there is no significant difference between poisoned and unpoisoned samples.

An increase of about 15 % could be observed for unpoisoned as well as for poisoned samples, though. This could be a result of small air intrusions into the sample vials, but contaminated samples usually show an enhanced scattering.

Microbial methane production should be inhibited by mercury chloride. However, methane production could arise from enzymatic production even after poisoning the microbes or from abiotic production on a so far unknown pathway. If production happened even in poisoned samples this would directly affect the discrete samples taken during P348.

Table 2: Comparison of unpoisoned and poisoned Samples.

Date of Measurement	Number of Measured Samples		Methane Concentration [nmol L^{-1}]	
	+ $HgCl_2$	Unpoisoned	+ $HgCl_2$	Unpoisoned
01 June.	5	4	2,82 ± 0,37	3,04 ± 0,29
10 June.	5	5	3,30 ± 0,42	3,49 ± 0,14

2.8.2 Comparison of Discrete and Continuous Sampling Measurements

To compare the discrete headspace measurements to the equilibrator measurements, 6 triplicate discrete samples were taken from the water supply that was connected to the equilibrator. Time and the associated equilibrator chromatograms were recorded. The discrete samples were treated with 0.2 mL mercury chloride and were measured two months later at IFM-GEOMAR.

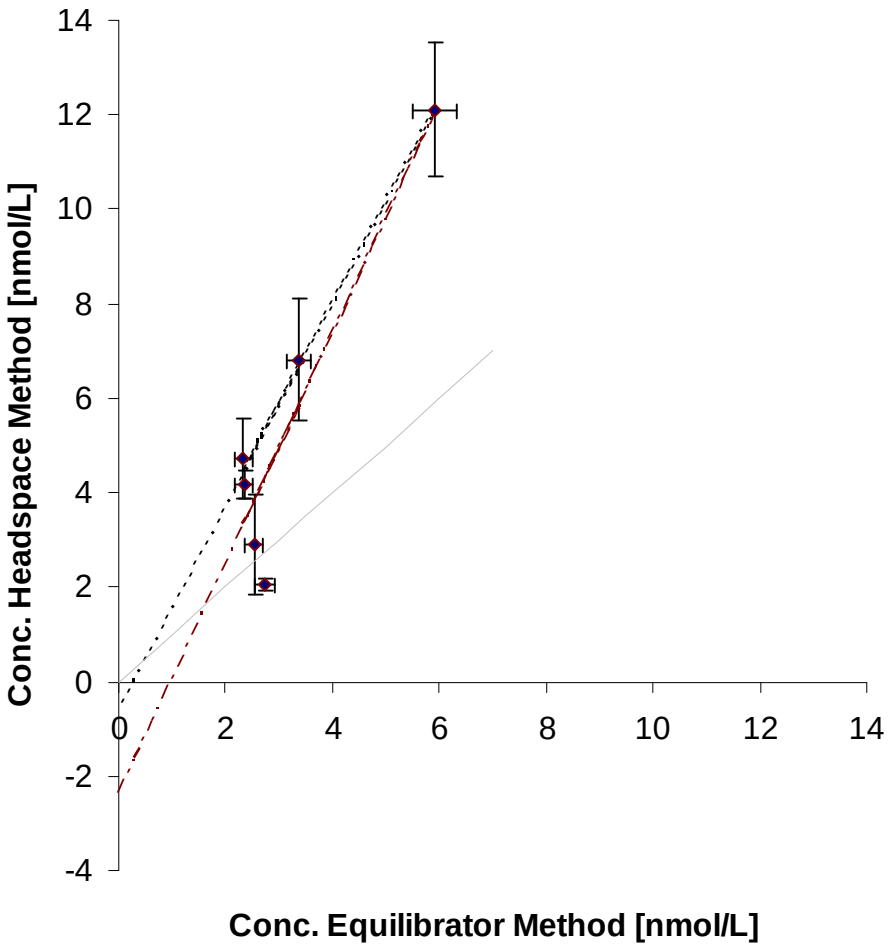

Figure 11: Calibration plot of measured discrete headspace values vs. equilibrator values. The grey line is the 1:1 line. The dashed-pointed line is the linear correlation taking into account all data points. The dashed line is the linear correlation taking into account only the data points with headspace concentrations > 4 nmol L^{-1}.

The results reveal significant differences between the two methods. FIG. 11 shows the plot of discrete headspace vs. equilibrator concentrations. The majority of the discrete headspace concentrations were approximately 2 times higher than the equilibrator concentrations. Linear correlation for all data points gives $y = 2.44x - 2.36$; $r^2 = 0.86$. If only the data points with $C_{Hs} > 4$ nmol L^{-1} are taken into account, the linear correlation is $y=2.141x-0.512$, $r^2=0.995$.

Several aspects must be considered to explain these results:

a) Discrete sampling

– Injection of ambient air into the sample would lead to higher concentrations for the headspace method. The methane mixing ratio in the ambient air is more than 15 times higher than in the equilibrated headspace, so that small contaminations would lead to great errors. The good linear correlation in FIG. 11 suggests that contamination of discrete samples is unlikely to be the reason for the methodical differences, though, since a randomly introduced error would lead to enhanced scattering of the data. Nevertheless, a tendency to higher values due to small intrusions of ambient air cannot be ruled out.

– Microbial methane production during storage should be inhibited as samples were poisoned with mercury chloride. However, the comparison experiment performed during MSM 05/2 reveals a slight increase in methane concentrations for both, unpoisoned and poisoned samples. The occurrence of abiotic methane production or microbial production despite the treatment with mercury chloride has not been reported yet (BANGE AND UHER 2005) but cannot be ruled out completely. This is analysed in a current comparison experiment running for 6 months.

– Methane mixing ratios in the headspace of the discrete samples were much smaller than the mixing ratios of the used standard gas mixtures. Although the FID is expected to show linear behavior in a wide range of mixing ratios the peak areas of the discrete samples are in a range where uncertainties are very high. The mean offset in the calibration curves during the P348 cruise was 521 ± 78 area units, indicating a deviation from linear behavior for low mixing ratios. The peak areas of the discrete samples range from 600 to 4000 area units, which is in a range where a linear fit might be not applicable.

b) Continuous equilibration

– In contrast to the discrete headspace samples, mixing ratios of ambient air and equilibrator air were in the range of the mixing ratios of the standard gas mixtures. Therefore, the error arising from calibration variability is much smaller.

–"True" equilibrium is never reached due to the continuous seawater flow. Equilibration time is dependent on the gas exchange velocity and the concentration gradient between liquid and gaseous phase. For gases with long equilibration times this could lead to a considerable deviation from equilibrium.

– The equilibrator air is affected by occasional venting with ambient air to balance the removal of equilibrator air due to sample gas removal, equilibration of major gas components and export of gas bubbles through the drain (JOHNSON 1999). JOHNSON identified gas bubble formation as the major venting mechanism and measured venting rates of 20 to 40 mL min^{-1}. He derived an equation for disequilibrium due to venting of the equilibrator from CO_2 equilibration measurements:

$$D = \frac{Q_V}{Q_W}\left(\frac{1}{\varepsilon\alpha}\right)\left(1-\frac{C_a\alpha}{C_W}\right) \quad [19]$$

where:

$\frac{Q_V}{Q_W}$ = the ratio of vent flow to water flow through the equilibrator

C_a = the gas concentration in the equilibrator air

C_W = the dissolved gas concentration

α = the solubility coefficient

ε = the equilibrator coefficient, a constant specific to the equilibrator type and volume.

According to this, disequilibrium is dependent on the ratio of vent and water flow, the concentration gradient between water and gas phase and the solubility of the respective gas. From this equation JOHNSON (1999) predicted disequilibrium values for methane at venting rates of 35-80 mL min^{-1} to be in the range of 2-4 %. This would by far not be sufficient to explain the results of P348. However, the equilibrator used during P348 was of the same type but considerably smaller. The equilibrator investigated by JOHNSON featured a headspace volume of 19 L, whereas the one used during P348 possessed a total volume of about 8 L and was filled at least to one third with water. Assuming the venting rates to be similar, about 20 % of the equilibrator air would be replaced in the time of one sampling circle.

– Pressure control of the equilibrator directly influences equilibrium, too. According to Henry's law the concentration of a dissolved gas is proportional to its partial pressure in the gas phase. To explain the difference between the equilibrator and the discrete samples, the equilibrator would have to feature a permanent pressure of 500 mbar, which seems very unlikely under the given conditions.

From analyzing these points, I assume the error resulting from the calibration uncertainties in the discrete measurements to be the main error source, yet in this work equilibrator or headspace concentrations were not corrected due to

the sparse data coverage. More data points are required to confirm a general discrepancy between the methods. Nevertheless, some experiments concerning the error sources should be performed:

– An experiment on the influence of storage on methane concentrations is already performed.

– Venting rates of the used equilibrator should be measured to allow conclusions of the comparability of the equilibrator used during P348 and the one investigated by JOHNSON (1999).

– A dilution series of methane mixing ratios could reveal the behavior of the analytical system in the range of the mixing ratios of the discrete headspace samples. Another possibility is to take a larger sample vial volume in order to increase the headspace mixing ratio. To reach mixing ratios in the range of the standard gases the vials should have a volume of at least 200 mL for samples with low methane concentrations.

3. Methane in the Eastern Tropical North Atlantic Ocean

3.1 Hydrography

The Eastern Tropical North Atlantic (ETNA) covers an area with strongly differing hydrographic properties. On the one hand, the Canary and North Equatorial Currents form the eastern part of the North Atlantic Subtropical Gyre which is typically a zone of very low nutrient-supply and thus low primary production. On the other hand nutrient-rich upwelled water masses initiate zones of high biological productivity off the West African Coast (MITTELSTAEDT 1983).

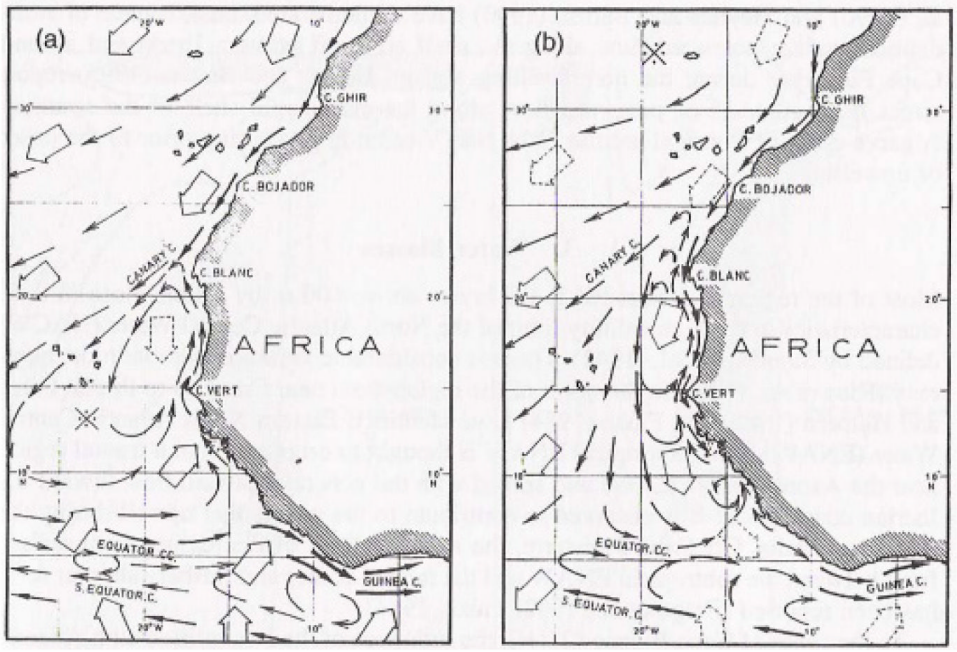

Figure 12: Circulation pattern of surface waters in the eastern tropical north Atlantic, a) in summer, b) in winter (MITTELSTAEDT 1983).

The southwestward directed Canary Current transports comparatively cold waters from the Portugal and Azores Currents. It extends to the North African shelf from the Strait of Gibraltar to Cape Blanc. South of Cape Blanc it gets detached from the coast and turns into the North Equatorial Current, leaving a shadow zone with a local circulation pattern in the Southeast [FIG. 12]. Off the Mauritanian coast waters circulate in a cyclonic gyre with wind driven offshore currents that effect coastal upwelling events at the shelf edge. Coastal upwelling occurs in consequence of offshore Ekman transport due to trade winds along the coastline. It is a typical phenomenon of the eastern boundary currents, where the alongshore trade winds afford the ideal conditions for coastal upwelling: Strong and steady winds are required to induce upwelling events which initiate high primary production (MITTELSTAEDT 1986).

The upwelling front extends over a narrow band of approx. 10 km near the shelf edge from 10 to 25°N (TOMCZAK AND GODFREY 2002). It shows a seasonality following the shifting of the Inter Tropical Convergence Zone (ITCZ) throughout the year. In the region between Cape Vert (10°N) and Cape Blanc (22°N) upwelling takes place in winter, with maximum intensity in February/March (MINAS, CODISPOTI ET AL. 1982). The correlation between the length of the upwelling season and the latitude is shown in FIG. 13.

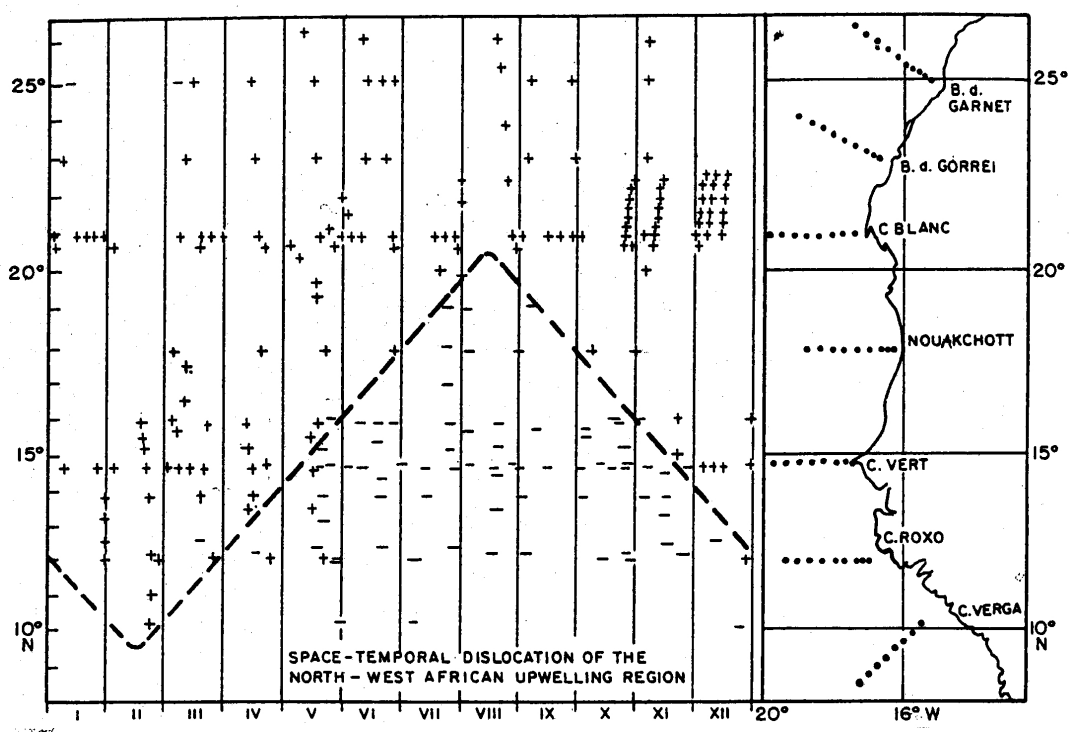

Figure 13: **Latitudinal dependence of the length of the upwelling period. The plus signs (+) indicate stations where upwelling was recognized, the minus signs (–) indicate stations where no upwelling was recognized. Source: MINAS ET AL. (1982).**

The removed water masses are replaced by subsurface waters from a depth of 100 to 200 m. Two different subsurface water masses with different hydrographic properties have been identified to feed the upwelling zone: In the North upwelled waters are strongly influenced by North Atlantic Central Water (NACW) while in the South they show properties of South Atlantic Central Water (SACW). Both NACW and SACW are found between 150 and 600m water depth. SACW is advected by a poleward undercurrent into the northern hemisphere, being nutrient-enriched compared to the NACW (HAGEN 2001). The frontal zone is located at 21°N near the continental shelf (MITTELSTAEDT 1991).

NACW and SACW show distinct differences in temperature, salinity and nutrient-content, but cover the same range of density. The frontal zone is therefore characterized by strong interleaving of the water masses which directly affects nutrient-supply in the upwelled waters, leading to an incoherent distribution of biological productivity (TOMCZAK AND GODFREY 2002).

The situation between 19°N and 21°N is further complicated by the presence of a water mass originating from the Banc d'Arguin. The Banc d'Arguin is a very shallow shelf area south of Cape Blanc [FIG. 14]. Waters advected to the Banc d'Arguin are exposed to strong evaporation, resulting in high salinity waters which leave the Banc d'Arguin through underwater canyons along the shelf break and contribute to the poleward undercurrent (PETERS 1976). Upwelled waters thus might deviate from the SACW as a result of admixture of the Banc d'Arguin waters.

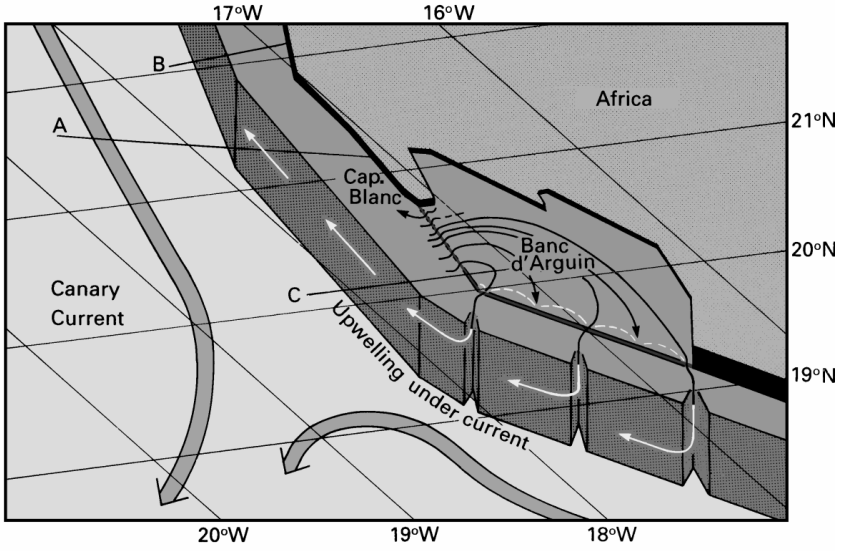

Figure 14: Scheme of the circulation pattern off in the Banc d'Arguin region (TOMCZAK AND GODFREY 2002). Banc d'Arguin waters contribute to the poleward undercurrent (yellow arrows). Blue arrows indicate the surface currents: The alongshore Canary Current in the north and the cyclonic circulation south of Cape Blanc.

3.2 Poseidon cruise P348

The cruise P348 took place onboard the research vessel (R/V) Poseidon from 8 to 26 February 2007. During P348, continuous surface water measurements were performed in the upwelling region between 18°N and 24°N, with main focus on the region between 18°N and 21°N. An E-shaped section was chosen to cover both, open ocean and coastal upwelling regions.

7 depth profiles were taken on a section along 18°N between the Cape Verde Islands and the North African coast including the transition from oligotrophic offshore conditions to the high productivity upwelling region. The P348 cruise track and the positions of the depth profiles are shown in FIG. 15.

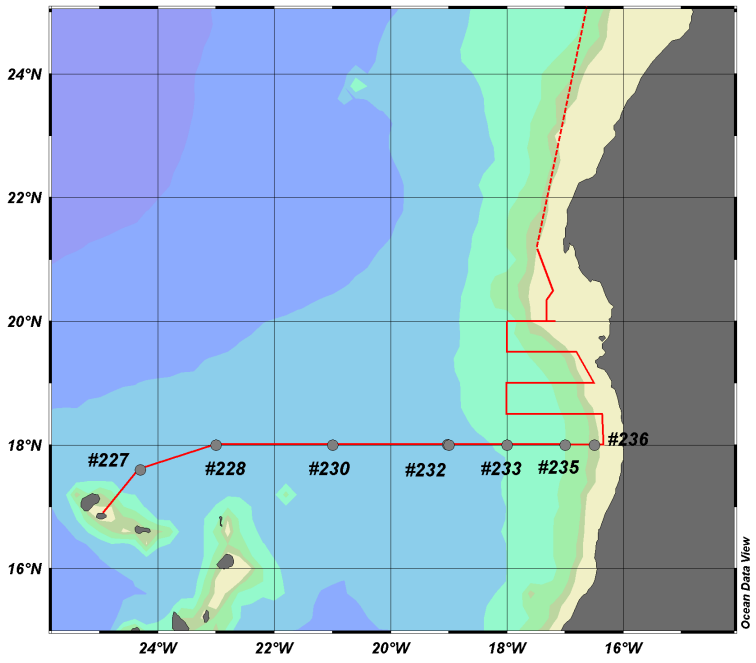

Figure 15: Cruise track of Poseidon 348. Depth profiles were taken on 7 stations, indicated as grey dots. The cruise started with a transit from as Palmas, Gran Canaria to Mindelo, Cape Verde Islands, where the sampling program started. Methane depth profiles were taken on the first part of the cruise along 18°N (marked stations) and underway measurements were performed along the E-shaped section off the Mauritanian coast from #236 to about 24° N.

3.3 Methane in the Surface Waters of the Northwest African Upwelling Region

3.3.1 Atmospheric Methane

The measurements of atmospheric methane showed mixing ratios ranging from 1.8 ppm to 2.5 ppm [FIG. 16]. The observed mixing ratios are in reasonable agreement with the monthly mean CH_4 mixing ratio of 1.836 ± 0.017 ppm measured in February 2007 at the nearest NOAA-Earth System Research Laboratory atmospheric baseline

observatory in Izaña, Tenerife (23.3°N, 16.5°W, elevation 2300 m) [http://www.esrl.noaa.gov/gmd/dv/site/IZO.html; February 2007 data were provided by E. Dlugokencky].

CH_4 mixing ratios from flasks measurements at the newly established atmospheric observatory at Mindelo, Cape Verde Islands, were not available at the time of the writing of this thesis (M. Heimann, MPI for Biogeochemistry, Jena, personal communication, 2007).

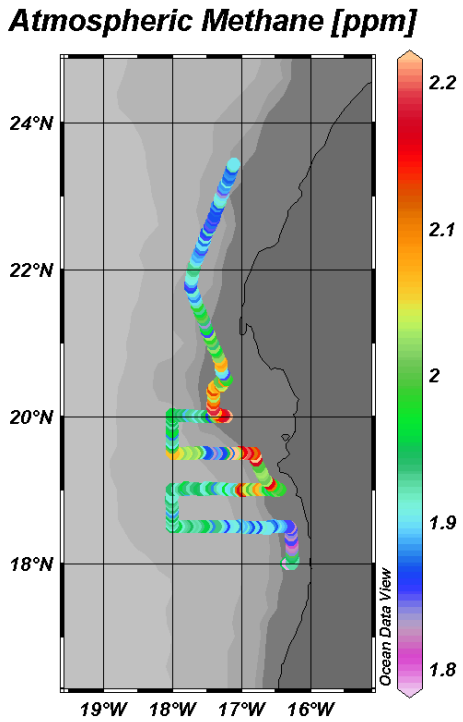

Figure 16: Spatial distribution of atmospheric methane mole fractions measured during P348.

Enhanced concentrations were found particularly between 19°N and 21°N at the shelf edge. This could be due to high CH_4 emissions from the shallow waters of the Banc d'Arguin. The Banc d'Arguin is a very productive ecosystem (and may be comparable to the Wadden Sea in the North Sea) and thus sediments of the Banc d'Arguin should be rich in organic material and favourable for the enhanced formation of methane. Because the waters of the Banc d'Arguin are very shallow, CH_4 produced in the sediments can reach

the atmosphere before being completely oxidized. However, methane measurements from the inner Banc d'Arguin are not available yet.

FIG. 17 shows the backward trajectories of air masses in the surveyed area during the Poseidon 348 cruise that support the assumption of enhanced methane mixing ratios as result of high emissions from the Banc d'Arguin. Trajectories were calculated using the NOAA HYSPLIT model [http://www.arl.noaa.gov/ready/hysplit4.html].

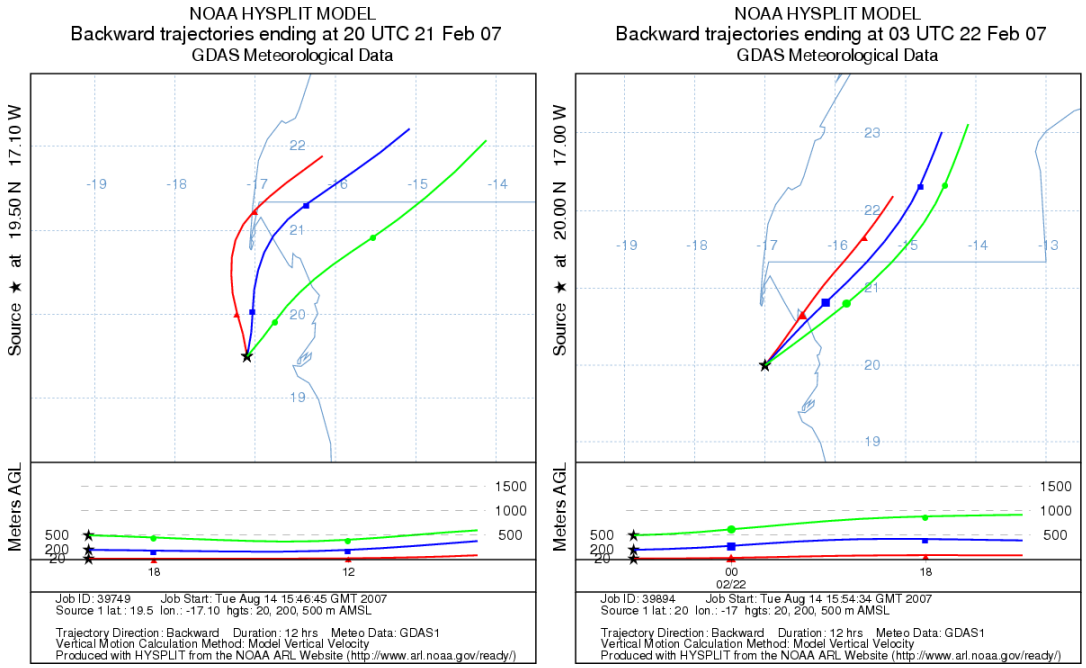

Figure 17: 12 h backward trajectories of air masses that were encountered in the investigated area during the P348 survey. Trajectories were calculated using the NOAA HYSPLIT model [http://www.arl.noaa.gov/ready/hysplit4.html]. The starting point and time were chosen to correspond to the ship's position.

3.3.2 Surface Methane Concentrations

The results of the underway measurements are shown in FIG. 18 and 19. SST and salinity were measured by the ship's thermosalinograph and calibrated against the CTD values from the same depth and time. To determine methane saturation the equilibrium methane concentration was calculated using the in-situ measured atmospheric methane mole fraction.

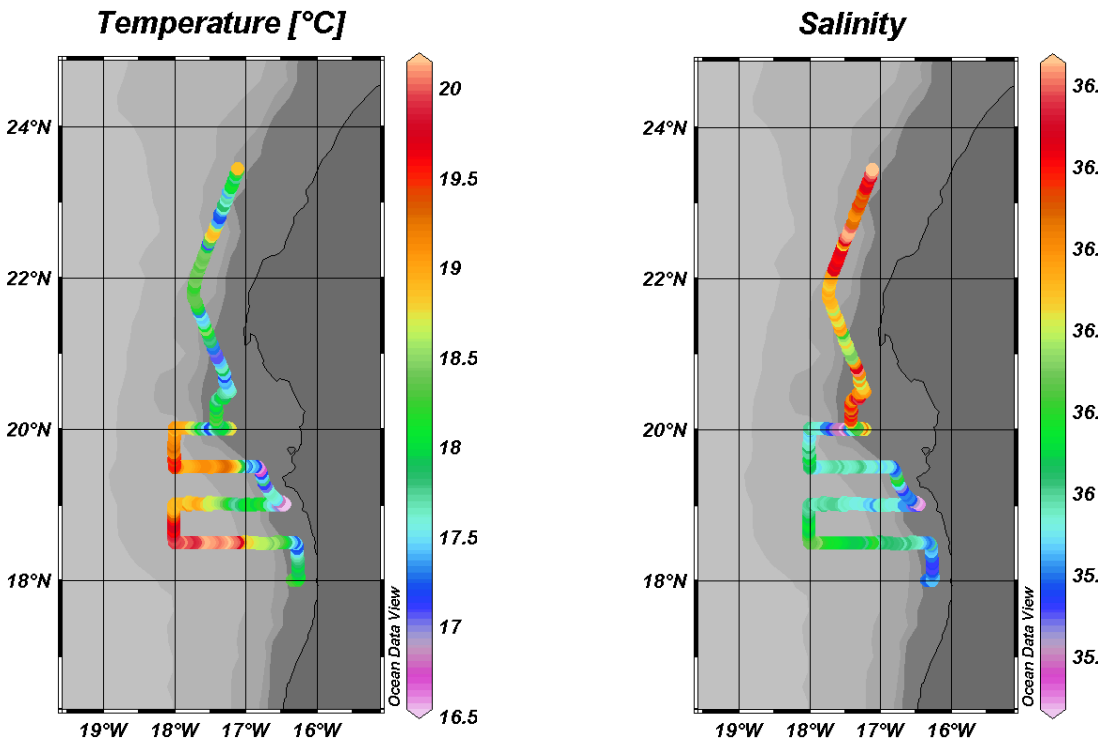

Figure 18: SST and surface salinity during the underway measurements. Time resolution is 22 min for all parameters.

Upwelling can easily be identified by the decline in SST on the continental slope. Lowest temperatures of about 16° C were recorded at 19°N close to the coast while highest SST values of approximately 20° C were measured further offshore at 18.5°N. Furthermore, a salinity decrease of 0.2 could be observed when reaching the upwelling zone [FIG. 18].

While upwelling was easy to identify in the southern part of the investigated area, the situation near the Banc d'Arguin was rather complex. Temperatures were generally lower in this part, and only a slight decrease in temperature was recorded while passing the slope. Even more striking is the change in salinity. North of 20°N, an increase in salinity from less than 36 to 36.5 could be observed. At the shelf edge salinities decreased but still stayed significantly higher than in the southern upwelled waters.

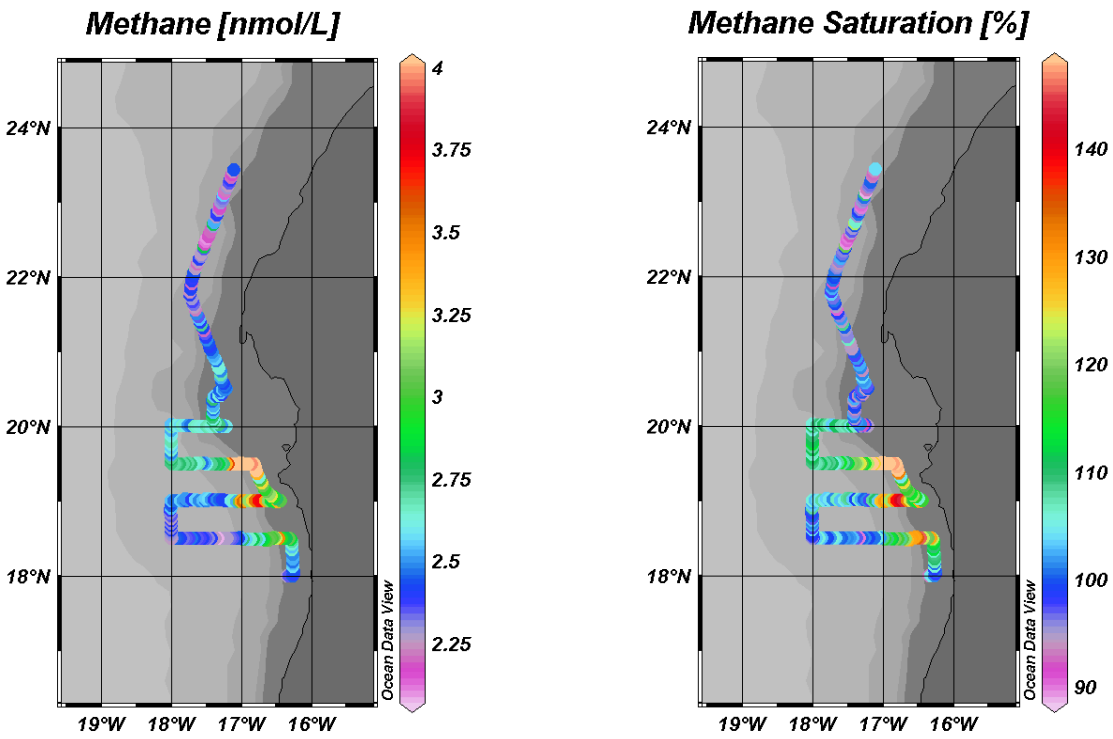

Figure 19: Dissolved methane (left) and methane saturation during the P348 underway measurements.

Surface methane concentrations and surface saturations are shown in FIG. 19. These values should possibly be corrected by a factor of 2 due to the discrepancies between equilibrator and discrete measurements.

South of 20°N, strongly elevated surface methane concentrations were measured in the upwelled water masses. Offshore methane concentrations ranged from 2 to 3 nmol L^{-1} and increased up to 5 nmol L^{-1} in the upwelling zone. No enhancement of methane saturation was recorded in the northern parts, however, providing additional evidence for a change in water mass properties between the southern and the northern part [FIG. 19].

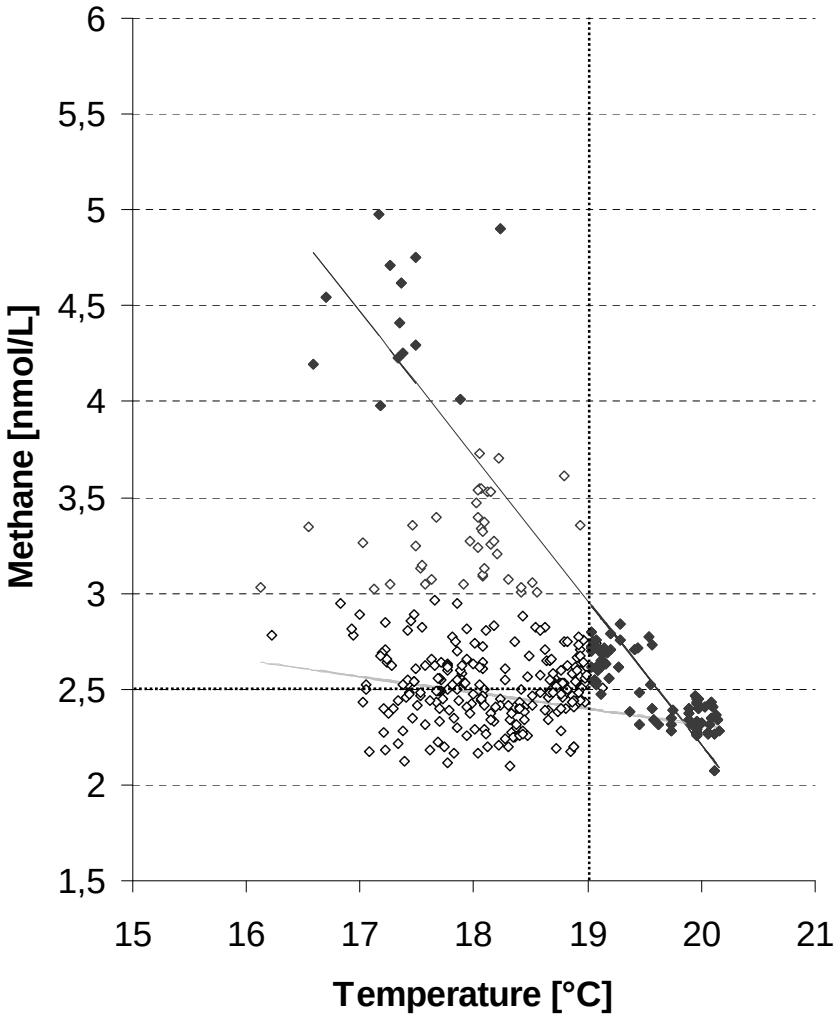

Figure 20: Dissolved methane concentration vs. SST. Concentrations greater than 3.0 nmol L^{-1} and lower than 19 °C were defined as influenced by coastal upwelling (limits indicated by dashed lines). Linear correlation for these clusters of data points is not significant. The grey line indicates the equilibrium methane concentrations calculated with the mean atmospheric mixing ratio from Izaña, Tenerife (see section 5.2.1). Full diamonds were taken as mixing endmembers. Linear correlation gave: $y = -0.753x + 17.25$; $r^2=0.855$.

The correlation between temperature and dissolved methane points out the complexity of the situation even more clearly [FIG. 20]. Enhanced methane concentrations were recorded in waters with temperatures below 19° C only. However, no simple correlation between SST and methane concentration could be found. A great amount of data points was spread over the whole temperature range (16 – 21° C) and showed only slightly enhanced concentrations. On the other hand, clearly enhanced concentrations (> 3.0 nmol L^{-1}) can be found below 19°C, with maximum concentrations of

5 nmol L^{-1} at a temperature of 17°C. Linear correlation for the enhanced values only is insignificant, however.

In order to analyze the effects of mixing between open ocean and upwelling water masses on the CH_4 concentration distribution, the following mixing endmembers were defined: open ocean with T >19°C and upwelling with T <19°C and methane concentrations >3.9 nmol L^{-1}.

The linear correlation of these data points gave a slope of 0.75 ± 0.28 nmol L^{-1} K^{-1}. This is considerably steeper than the slope of about –0.05 nmol L^{-1} K^{-1} reported by GEBHARDT AND BANGE (2006). The discrepancy might be explained with the fact that GEBHARDT AND BANGE (2006) performed their measurements along 17°N, which is south of the area investigated in this study. It might be that CH_4 formation is less effective in the southern parts of the Mauritanian upwelling.

The slope observed during P348 is between the slopes obtained for the Arabian Sea upwelling area (–0.09 nmol L^{-1} K^{-1}) (BANGE, RAMESH ET AL. 1998) and the upwelling area off Oregon (–1.5 nmol L^{-1} K^{-1}) (REHDER, COLLIER ET AL. 2002). Particularly the value from the Arabian Sea demonstrates the differences between the upwelling regions: while a temperature decline of 8°C, associated with a methane concentration rise of 1 nmol L^{-1}, was obtained in the Arabian Sea, a temperature decline of only 4°C effected the increase of the methane levels from 2 to 5 nmol L^{-1} in the Mauritanian upwelling.

The hydrographic properties of the surface waters together with methane concentrations are shown in FIG. 21. The T/S-curves of the predominant water masses, NACW and SACW, are added as straight lines (TOMCZAK AND GODFREY 2002).

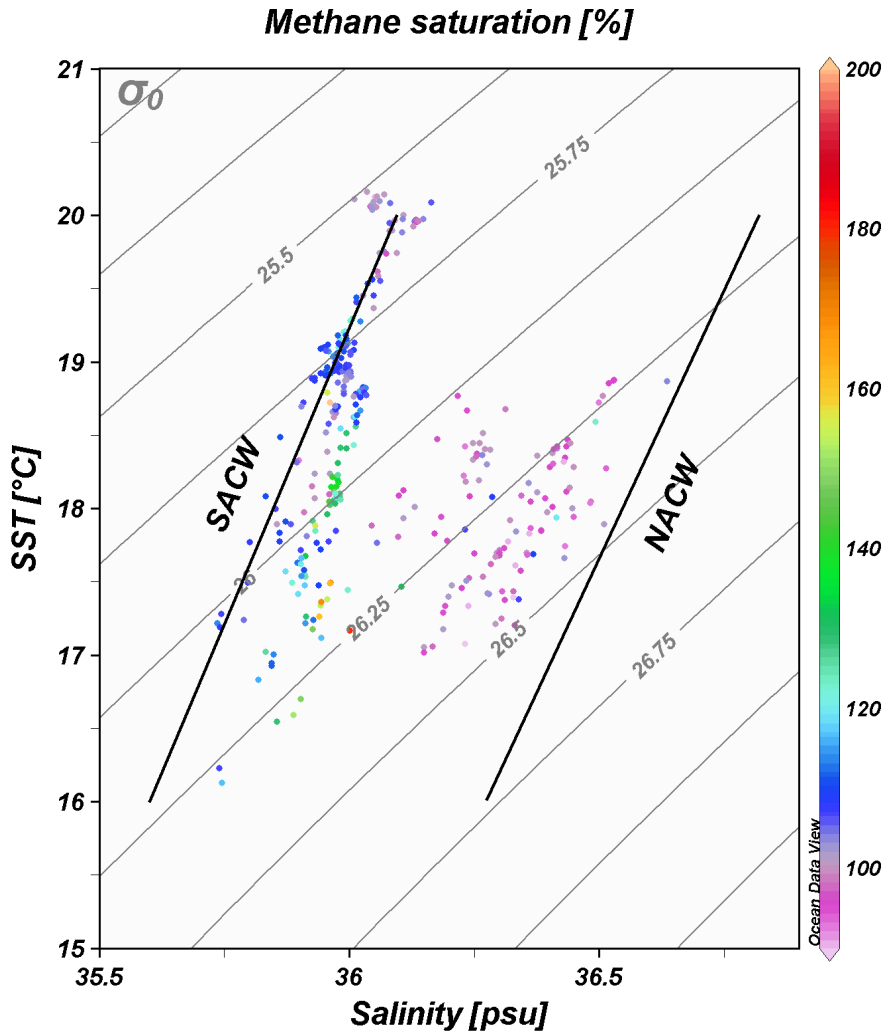

Figure 21: T/S-diagram and methane concentrations for the P348 underway measurements. The T/S properties of the predominant water masses NACW and SACW are characterized by straight lines. (TOMCZAK AND GODFREY 2002).

Waters with temperatures >19°C agreed well with the properties of the SACW. Methane concentrations were in equilibrium with the atmosphere or slightly enhanced for these data points. At temperatures <19°C, data points are between NACW and SACW, suggesting that they were the result of mixing between the two water masses. While the waters with enhanced saturations show a straight T/S relationship with properties close to the SACW, the fraction of NACW was evidently higher for waters around 100% saturation, and no linearity could be recognized.

3.3.3 Gas Exchange

Fig. 22 shows the calculated methane flux densities using the models of LISS AND MERLIVAT (1986) and WANNINKHOF (1992). Highest flux densities were calculated for the region between 19°N and 20°N on the shelf edge, matching the area of highest saturations. Lowest flux densities were calculated off the Banc d'Arguin at 20°N and on the shelf edge at 21°N where saturations and wind speeds were comparatively low.

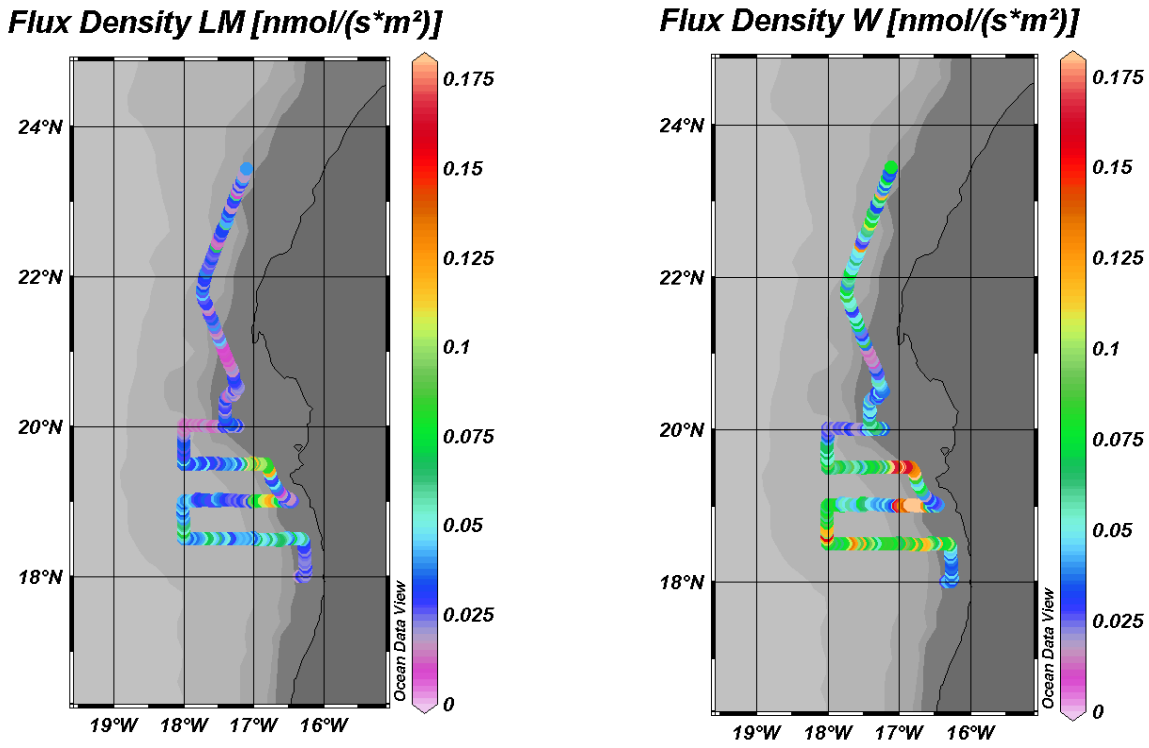

Figure 22: Methane flux densities calculated according to the gas exchange model of LISS AND MERLIVAT (1986) (left) and of WANNINKHOF (1992) (right). To allow comparability of the diagrams the same scales were used for both diagrams.

To estimate the total emissions for the upwelling area off Mauritania, average flux densities based on the upwelling-influenced methane concentrations were calculated and extrapolated to the whole upwelling area off Mauritania. Data points with temperatures <19°C that were associated with methane concentrations >3.0 nmol L^{-1} were defined as "upwelling-influenced" (see FIG. 20). These values were used to calculate the average flux densities from the upwelling area, which was roughly defined as a 50 km wide band near the

shelf edge extending from 21°N to 15°N. This gives a total area of 300 000 km^2. The duration of the upwelling period was determined according to FIG. 13 and averaged over the latitude. The average upwelling period thus was 9 months**.** The calculated emissions are listed in TAB. 3.

Table 3: Calculated emissions from the Mauritanian upwelling and from the Arabian Sea. LM86 stands for LISS AND MERLIVAT (1986) and W92 stands for WANNINKHOF (1992).

	Area [10^{12} m^2]	Flux Density (LM86) [pmol m^{-2} s^{-1}]	Flux Density (W92) [pmol m^{-2} s^{-1}]	Emissions (LM86) [Gg]	Emissions (W92) [Gg]
Mauritanian upwelling	0.3	70.93	118.8	7.55	12.6
Arabian Sea coastal upwelling*	0.2	15.9	27.9	0.5	0.9

*Data from BANGE ET AL. [1998], calculated for 4 months upwelling period.

Despite the fact that the Mauritanian upwelling covers only about 0.1% of the global ocean surface area of 362 10^{12} m^2, the annual CH_4 emissions from the Mauritanian upwelling represent about 1–3 % of the global open ocean CH_4 emssions (0.4–0.8 Tg yr^{-1}). Thus the Mauritanian upwelling represents a hot spot of CH_4 emissions to the atmosphere.

Comparing emission estimates from the Mauritanian upwelling with the estimate reported by BANGE ET AL. (1998) for the Arabian Sea, it is obvious that the Mauritanian upwelling is ventilating more CH_4 to the atmosphere. This is mainly based on the fact the CH_4 surface concentrations in the Mauritanian upwelling are much higher than in the Arabian Sea upwelling (BANGE, RAMESH ET AL. 1998).

Annual emissions for the surveyed area were calculated for an area of 800 000 km^2 which corresponds to the area of the biogeographic CANARY region (FORSTER, UPSTILL-GODDARD ET AL. 2007). It includes coastal upwelling areas as well as open ocean areas. Emissions from the upwelling-influenced areas during the upwelling period are taken from TAB. 3. The mean flux

densities for the data points defined as not influenced by upwelling (see FIG. 20) were used to calculate methane emissions for the remaining area of 500 000 km^2 during the upwelling period and for the whole area during the period of non-upwelling. The results are listed in TAB. 4.

Table 4: Annual methane emissions from the North-African upwelling system.

Period	Area (Name)	Area [10^{12} m^2]	Emissions LM86 [Gg]	Emissions W92 [Gg]
Upwelling Season (9 Months)	Upwelling Area	0.3	7.55	12.6
	Open Ocean Area	0.5	0.737	1.31
Non-Upwelling Season	Open Ocean Area	0.8	0.393	0.698
Whole Year	Whole Area	0.8	7.84	14.6

FORSTER ET AL. (2007) estimated annual methane emissions for the same area to 30 – 50 Gg. However, these values seem questionable due to the fact that a re-calculation of the emissions based on the flux densities for the CANARY area given by FORSTER ET AL. gave values of 10 –17 Gg. These values were in reasonable agreement with the emissions calculated for P348.

The obtained values should be regarded as rough estimates, though. The seasonality of the upwelling and its influence on methane emissions are poorly examined. Local conditions may also have a strong influence on methane saturation. This was already seen in the comparison of the correlation between temperature and methane concentration for the data from P348.

3.4 Depth Profiles along 18° N

3.4.1 Background Settings

The density plot for the upper 500 m of the 18° N section in FIG. 23 shows the rise of the pycnocline from 50-100 m in the offshore regions to the surface near the shelf. Upwelled waters thus stem from a depth of about 100 m.

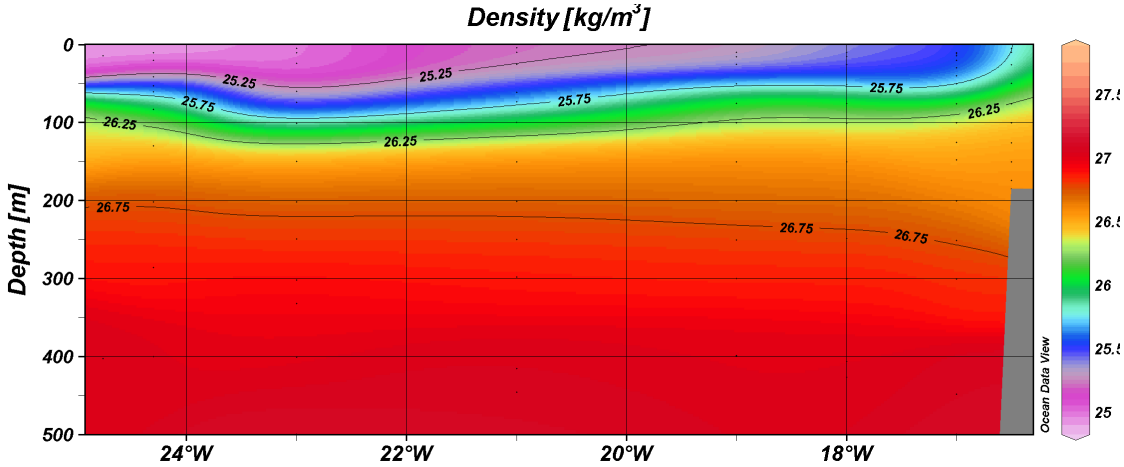

Figure 23: Potential density of the upper 500 m at 18°N during P348.

Depth profiles of nitrate (FIG 24) and phosphate (data not shown) show a considerable enrichment in the water column with a pronounced maximum between 200 and 1000 m. Maximum nutrient concentrations were measured on the continental slope.

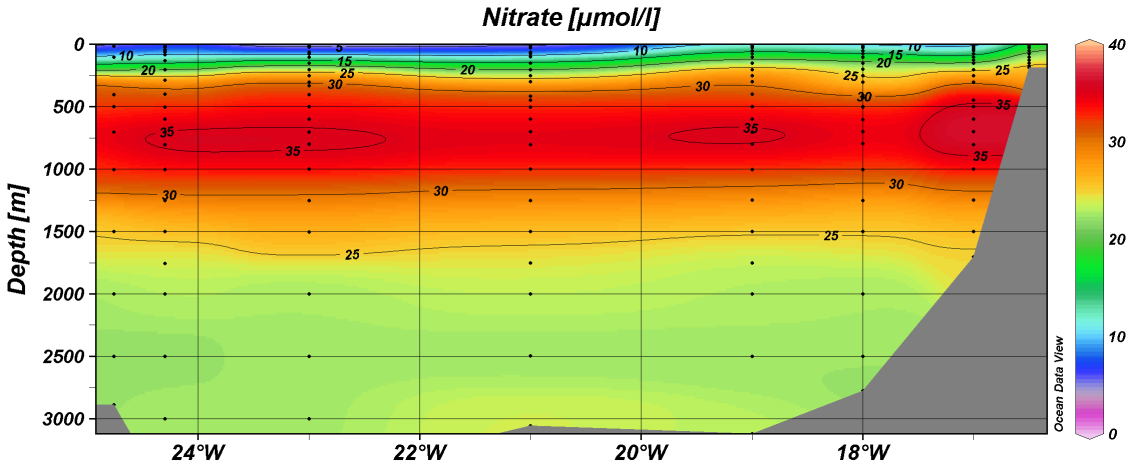

Figure 24: 18°N section for nitrate during P348.

Oxygen depth profiles on the other hand show a minimum zone between 100 and 800 m, which is clearly related to the upwelling [FIG. 25]. Between 16 and 20° W minimum oxygen values were 50 µmol L^{-1}. A less intense minimum was observed between 20 and 22° W.

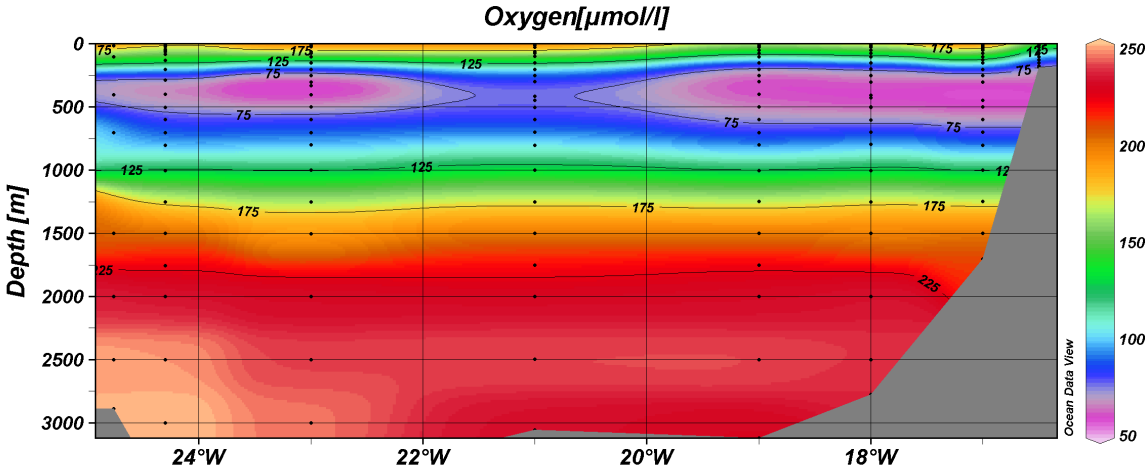

Figure 25: 18°N-section of dissolved oxygen.

3.4.2 Methane Distribution in the Water Column

Dissolved methane concentrations for the 18° N section are shown in FIG. 26 and methane saturations in FIG. 27. As discussed in section 2.8 concentration values should be looked at very carefully. As discussed in section 2.8, they most likely should be corrected to the equilibrator measurements by a factor of 0.5. This would lead to very low concentrations in the deep waters of the open ocean. In the upwelling area surface saturations would be rather modest.

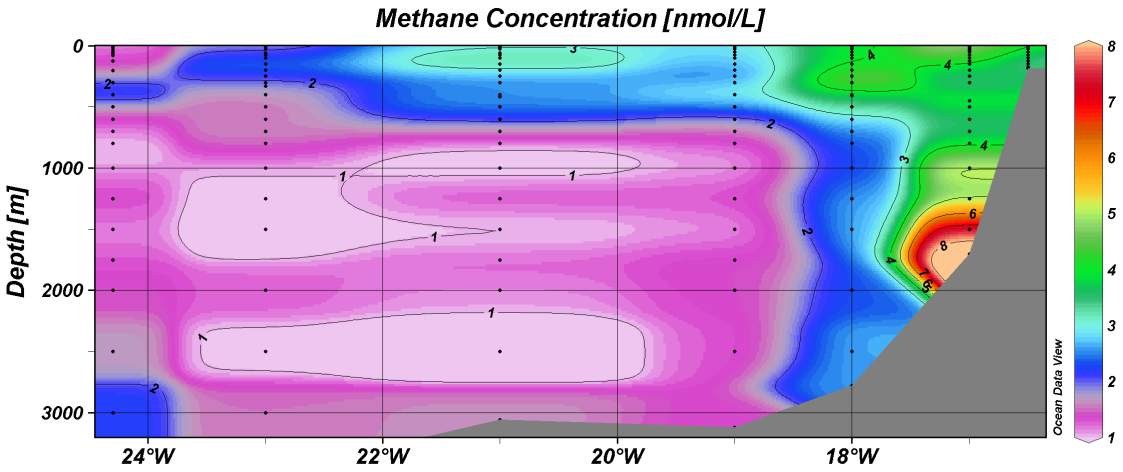

Figure 26: Methane concentrations along 18°N.

Methane saturation values were calculated from the equilibrium methane concentrations based on the mean atmospheric CH_4 mixing ratio of 1.836 ppm measured at Izaña, Tenerife in February 2007 (see section 3.3.1). As atmospheric mixing ratios have been increasing dramatically for the last 200 years, saturations should have been corrected to the mixing rations of the time of last atmospheric contact of the water masses. In this study saturations were not corrected because information on the age of water masses was not available. The calculated saturations thus are underestimated for older water masses.

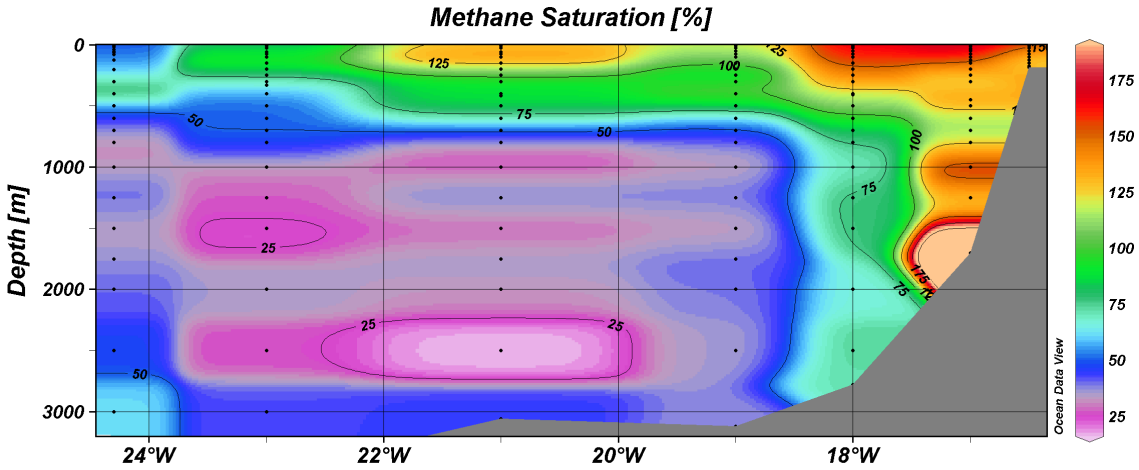

Figure 27: Methane saturation along 18°N. The section was derived from 7 stations (Stations #227 - #236 [see FIG. 15]).

Methane saturation profiles [FIG. 27] reveal several trends: Open ocean surface waters were only slightly supersaturated and saturation declined to less than 50 % below 1000 m. Towards the continental slope the water column was supersaturated. Values up to 250 % were measured in the bottom waters between 17 and 17.5° W, indicating a strong sediment source. REHDER ET AL. (2002) reported a strong coincidence between coastal upwelling and methane sources from the seafloor that could be explained by high export of organic matter to the sediments.

Maximum surface water saturations reached 170 % between 16.5° W and 17.5° W and indicated the upwelling-influenced area. The impact of upwelling on surface water concentrations extended about 200 km offshore. West of 18.5° N, surface and subsurface saturations declined. A pronounced subsurface maximum at 100 m depth was observed between 20 and 22° W [FIG. 27]. The subsurface CH_4 maximum remarkably occurs at the same place where enhanced O_2 concentrations were measured [FIG. 25]. However, the enhanced O_2 was found in a depth of 400m, thus only an indirect link might exist.

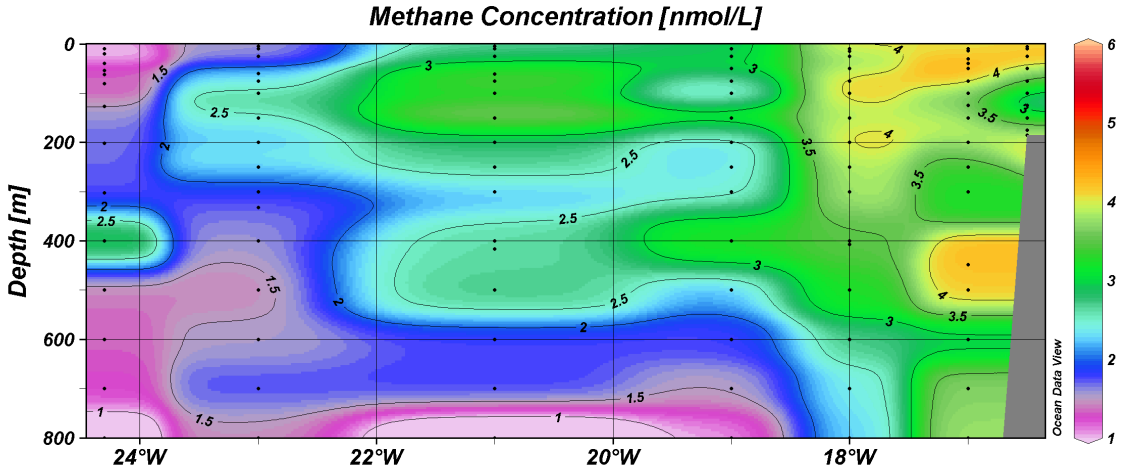

Figure 28: Methane concentration in the upper 800 m of the 18°N section.

Two subsurface maxima were observed near the slope: Enhanced saturations were found at about 100 m and 400 m [FIG. 27]. WARD ET AL. (1993) found comparable concentration profiles in the California Current region and suggested that the deeper maximum results from advection of methane-rich shelf waters and the upper one originates from in-situ production. Surface methane supersaturations stemmed from the upwelling of waters from the upper methane maximum: The enhanced concentrations were lifted into the surface layer when approaching the upwelling.

Because methanogenesis is restricted to strictly anaerobic conditions no correlation between oxygen and methane is expected to occur in the water column. The complex interaction of methane production, consumption, the methane release from the sediments, the mixing processes and the unknown origin of the subsurface methane maximum suggest neither a correlation to oxygen nor to the other nutrients.

4. Methane in the Southwestern Labrador Sea

4.1 Hydrography of the Labrador Sea

The Labrador Sea is a marginal sea of the Northwest Atlantic Ocean and is located between the East coast of Canada and southern Greenland. Its maximum bottom depths are about of 3.900 m. Its surface currents are part of the North Atlantic Subpolar Gyre which circulates cyclonically in the western North Atlantic Ocean [FIG. 28].

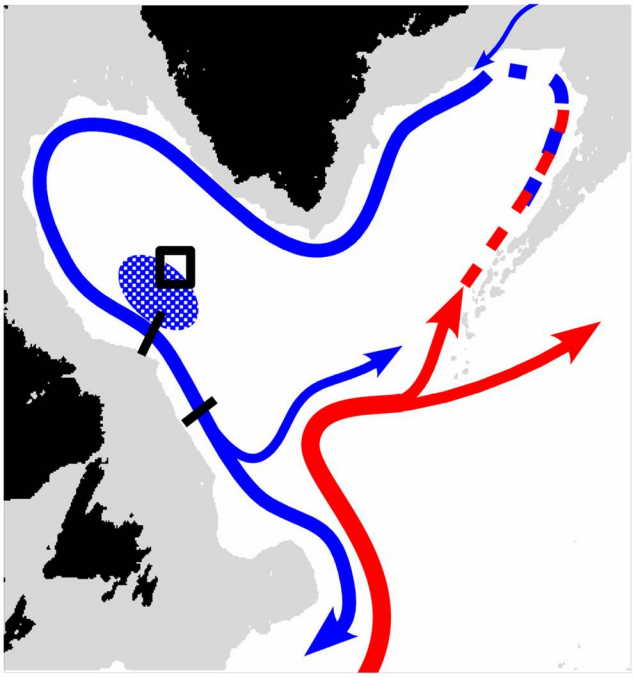

Figure 29: Schematic diagram of the circulation in the North Atlantic Subpolar Gyre. Warm surface waters of the North Atlantic Current (NAC) (red arrows) circulate cyclonically in the Irminger and Labrador Sea, accompanied by a successive cooling. The blue shaded area marks the zone of deep convection in the western Labrador Sea. The cold and dense water masses from convection are exported to the Atlantic by the Deep Western Boundary Current (DWBC) (blue arrow) Black bars indicate the location of frequently surveyed shipboard sections (BÖNING, SCHEINERT ET AL. 2006)

The Labrador Sea is known as a location for deep-water formation due to deep convection in winter (LAVENDER, DAVIS ET AL. 2002) [FIG. 29]. The Labrador Sea Water (LSW) forms the upper part of the North Atlantic Deep

Water (NADW) which spreads southward over the whole Atlantic Ocean and acts as the motor for the thermohaline circulation. Having recently been in contact with the atmosphere, LSW transports the signature of atmospheric gases into the deep ocean (KÖRTZINGER, SCHIMANSKI ET AL. 2004).

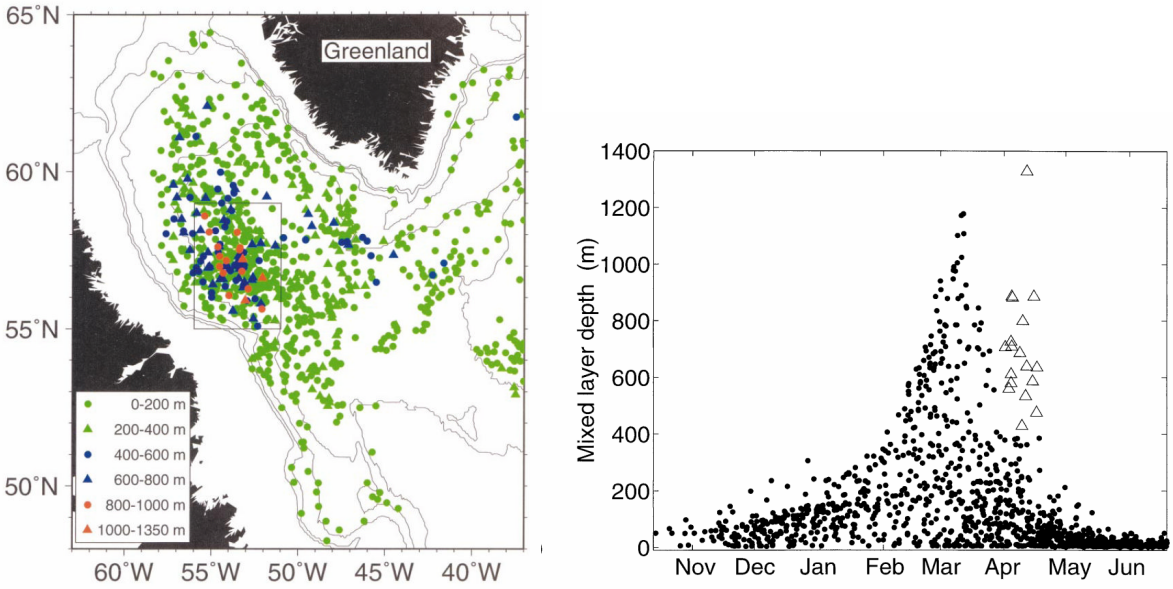

Figure 30: a) Mixed layer depth in winter 1996/1997. The area of deepest convection is located in the western Labrador Sea (marked as the rectangular box). b) Seasonality of deep convection in the Labrador Sea (winter 1996/97). Open triangles represent deep convection events that took place later than expected. Source: (LAVENDER, DAVIS ET AL. 2002).

According to recent investigations deep water formation in the Labrador Sea turns out to be highly variable. Closely linked to the North Atlantic Oscillation (NAO), the LSW formation shows an annual to decadal variability in convection depth and LSW properties (LAZIER, HENDRY ET AL. 2002). AVSIC ET AL. (2006) reported a phase of deep convection with intense deep water formation for the early 1990's followed by years of shallow convection since the second half of the 1990's. The Labrador Sea Water formed in this period was warmer and less dense. It was referred to as Upper Labrador Sea Water (ULSW) to distinguish between the newly formed and the classical water masses (STRAMMA, KIEKE ET AL. 2004).

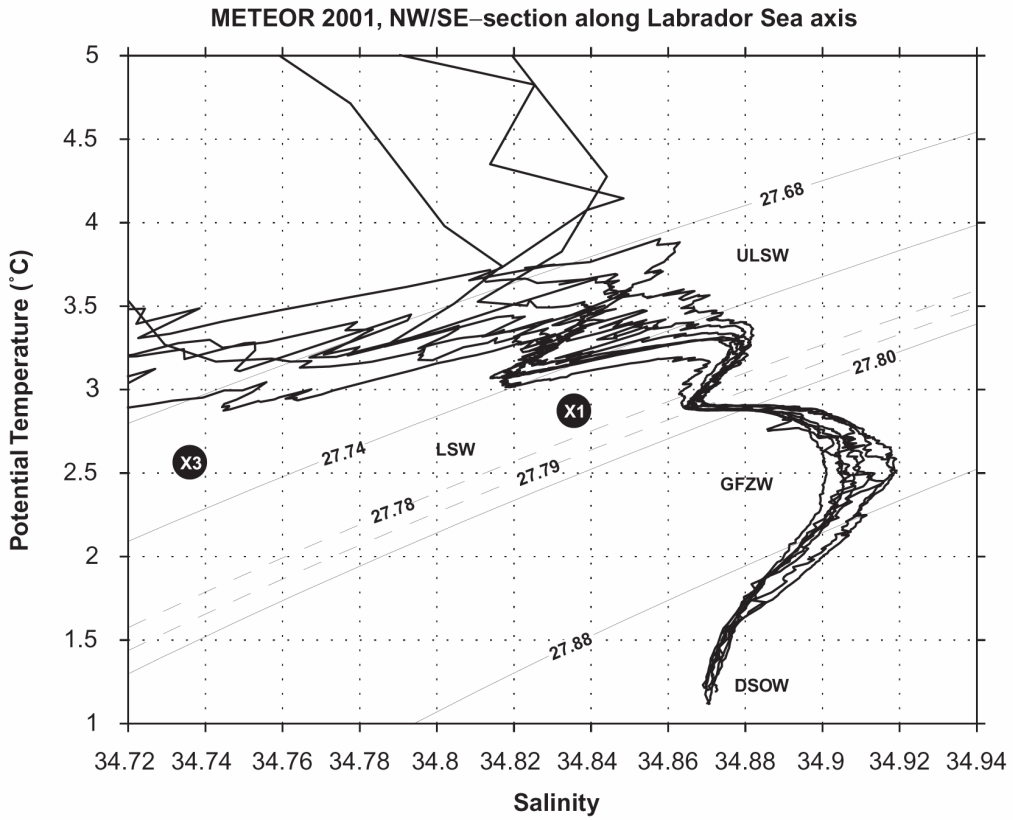

Figure 31: T/S-diagram from CTD casts in the central Labrador Sea 2001 (STRAMMA, KIEKE ET AL. 2004). 4 water masses can be identified: Upper Labrador Sea Water (ULSW): σ_θ = 27.68 – 27.74 kg m^{-3}; (classical) Labrador Sea Water (LSW): σ_θ = 27.74 – 27.80 kg m^{-3}; Gibbs Fracture Zone Water (GFZW): σ_θ = 27.80 – 27.88 kg m^{-3}; Denmark Strait Overflow Water (DSOW): σ_θ > 27.88 kg m^{-3} (STRAMMA, KIEKE ET AL. 2004).

Therefore, four main water masses are expected to occur in the Labrador Sea water column (STRAMMA, KIEKE ET AL. 2004) [FIG. 30]: Recently formed ULSW displays potential densities between 27.68 and 27.74 kg m^{-3} (1000 – 1500 m), and Classical LSW shows potential densities between 27.74 and 27.80 kg m^{-3} (extending to depths down to 2000 m). The water masses below 2000 m are water masses that are transported into the Labrador Sea from the Atlantic Ocean. The Gibbs Fracture Zone Water (GFZW) enters the Labrador Sea from the Northeast Atlantic. It is characterized by a salinity maximum and minimum oxygen saturations, reflecting the older age of this water mass. Bottom waters are formed by Denmark Strait overflow water which originates from the Greenland Sea, where it is fomed by mixing of deep convection waters with Arctic bottom waters. It is significantly colder and younger than the GFZW and shows enhanced trace gas saturations (MAURITZEN 1996).

4.2 The Maria S. Merian Cruise MSM 05/2

The Maria S. Merian cruise MSM 05/2 took place in the southern and western Labrador Sea from May 30 to June 12, 2007. The cruise track is shown in FIG. 31. Samples were taken on two sections from the Labrador shelf towards the central Labrador Sea. On the 53°N section 4 depth profiles (stations #3, #1, #11 and #14) for methane were taken in a narrow range near the shelf break. The second section partly repeated the WOCE AR7W-section with methane sampling at stations #20, #24, #27, #31, #33 and #36.

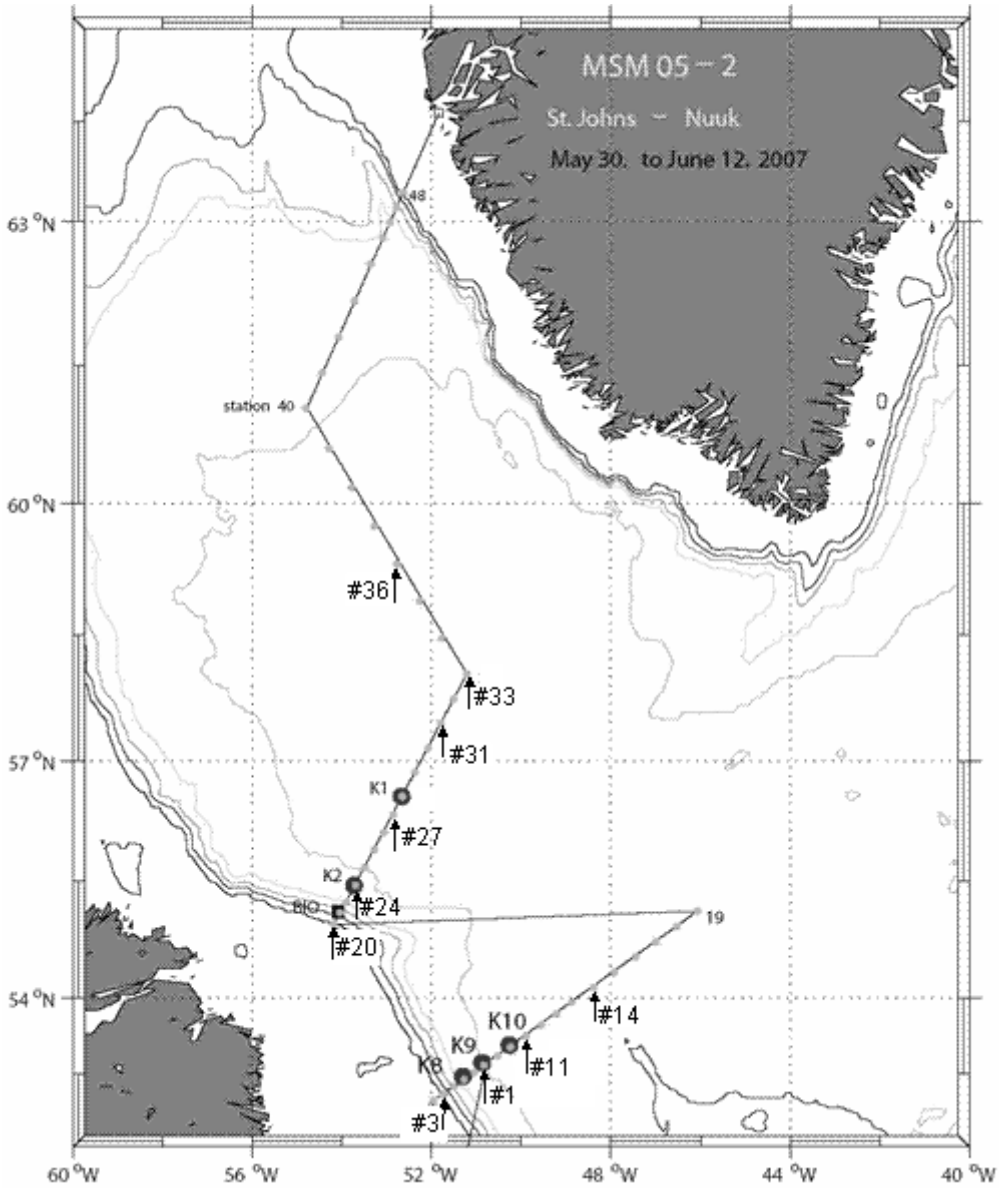

Figure 32: Cruise Track of MSM 05/2, May/June 2007. The stations where methane samples were taken are marked with arrows. K1,K2,K8,K9 and K10 are mooring sites. Modified from FISCHER (2007, unpublished).

4.3 Depth Profiles

4.3.1 Density Distribution

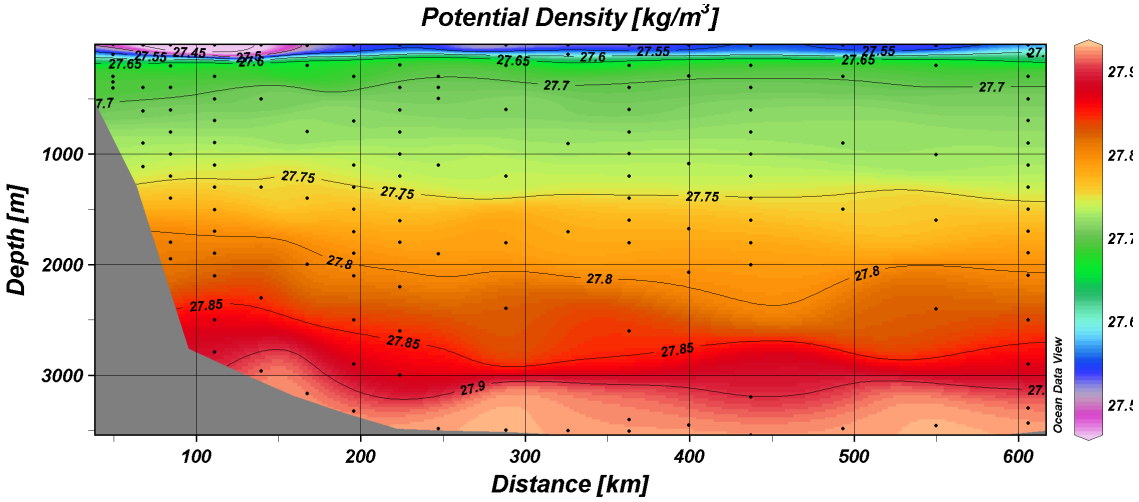

Figure 33: Potential density along the AR7W section in June 2007.

The four water masses mentioned in section 4.1 can be identified in the density plot of the AR7W section [FIG. 32]. In water depths between 200 and 1000 m ULSW was found while water mass characteristics down to 2000 m point to the occurrence of the classical LSW. GFZW occupied depths down to 3000 meters while bottom waters were in the density range of DSOW.

4.3.2 Methane Depth Profiles

The methane depth profiles from the 53°N and AR7W sections are shown in FIG. 33. The measured concentrations should possibly be corrected, too. Equilibrator measurements were not performed during the MSM 05/2 cruise, but the discrepancies between both methods should persist unless they arise in consequence of the storage of the P348-samples.

The methane depth distribution from the 53°N section is rather variable throughout the water column. A trend to higher concentrations in the offshore waters can be recognized.

Along the AR7W section the methane depth profiles are less variable, especially in the deep waters. Deep water methane concentrations were about 2 nmol L^{-1}. In water depths <1500 m methane concentrations ranged from 3 to 4 nmol L^{-1}. Surface waters showed even higher concentrations (up to 6 nmol L^{-1}).

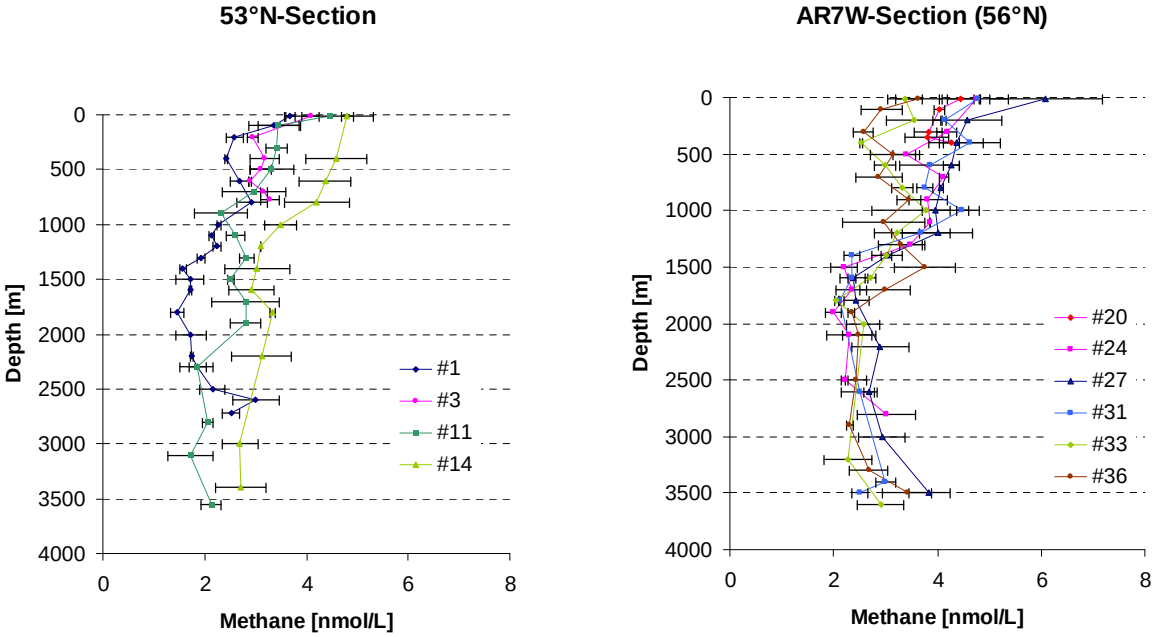

Figure 34: Methane depth profiles for the 53°N and 56°N sections of the MSM 05/2 cruise.

Methane saturations were calculated with equilibrium methane concentrations using the mean atmospheric mixing ratio which was determined occasionally during the cruise. The mean CH_4 mole fraction during MSM 05/2 was 1.823 ± 0.009 ppm (n = 5). This is in good agreement with the monthly mean mixing ratio of 1.838 ± 0.005 ppm measured in June 2006 at the NOAA-Earth System Research Laboratory atmospheric baseline observatory in Summit, Greenland (72.56°N, 38.46°W, elevation 3238 m) [http://www.esrl.noaa.gov/gmd/dv/site/SUM.html].

As mentioned in section 3.4.2 saturation levels for older water masses should have been corrected to the atmospheric mixing ratio difference. However, as information about the age of the water masses is not available yet, saturations were left uncorrected. CFC samples for the determination of the water age were taken but have not been analysed yet. The CFC samples will be analysed by M. Rhein, University Bremen.

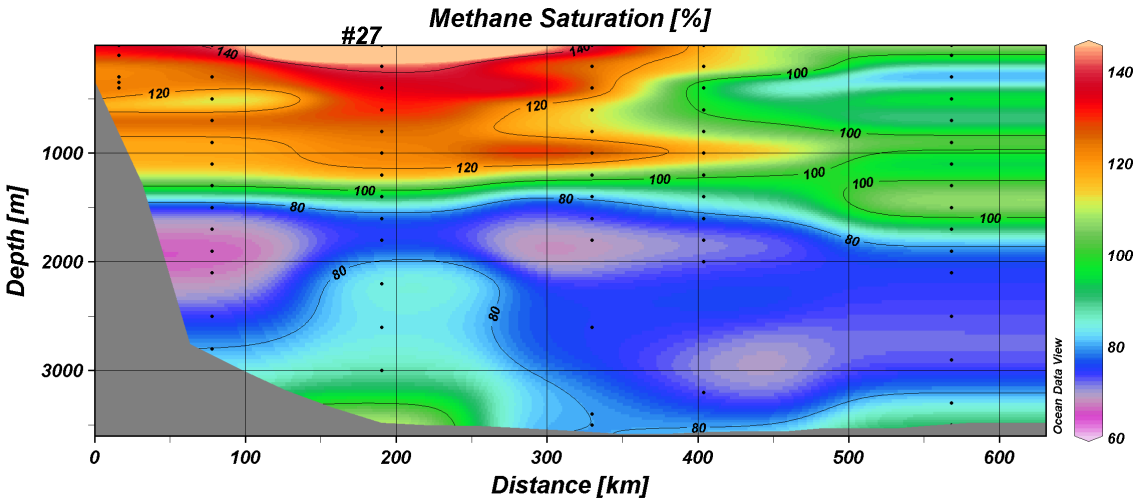

Figure 35: Methane saturation along the WOCE AR7W section.

At all stations along AR7W the methane saturation levels of the upper 1200 m were considerably higher than in the depths >1200 m [FIG 34]. In the upper 1200 m saturation levels ranged from 100 % to 140 %, whereas in water depth >1200 m the saturation was about 70%. Maximum saturations were found in the surface waters of station #27, in the centre of the deep convection zone (see FIG. 34). Further offshore, in the central Labrador Sea, methane saturations were about 100 %. Slightly enhanced saturations were found in the bottom waters close to the continental slope.

The relative uniform water column distribution of methane saturations in the upper 1200 m suggests to appear in consequence of mixing of methane rich waters into the deep ocean rather than of production by in situ biological processes (which, in the case of methane, should be restricted to the surface layer). Thus, in strong contrast to the methane concentration profiles along

18°N off Mauritania, the methane profiles from the Labrador Sea are dominated by oceanographic features: The data from the AR7W section nicely illustrates the transport of methane to deeper water via the deep convection [FIG 34].

The comparatively high saturations measured in the upper 1200 m can be partly explained by air injection during rough weather conditions. Bubble injection leads to disproportionately high concentrations of gases with low solubility in the surface layer, which are then transported to the deep. Stormy weather is often reported for this region in winter.

A simple model of the Labrador Sea deep convection predicts supersaturations of only up to 4 % resulting from bubble injection for gases with low solubility such as N_2 (HAMME AND SEVERINGHAUS 2007). Because the methane solubility is only slightly higher than that of N_2 the measured high methane saturations are most probably explained by advection or in-situ production.

FIG. 35 shows the hydrographic properties together with the methane concentrations of the MSM 05/2 data. The T/S profiles from MSM 05/2 differ slightly from those obtained by STRAMMA ET AL. (2004): The transition from classical LSW to GFZW was difficult to determine. These two water masses showed an almost linear T/S relationship, while STRAMMA ET AL. (2004) reported an S-shaped curve.

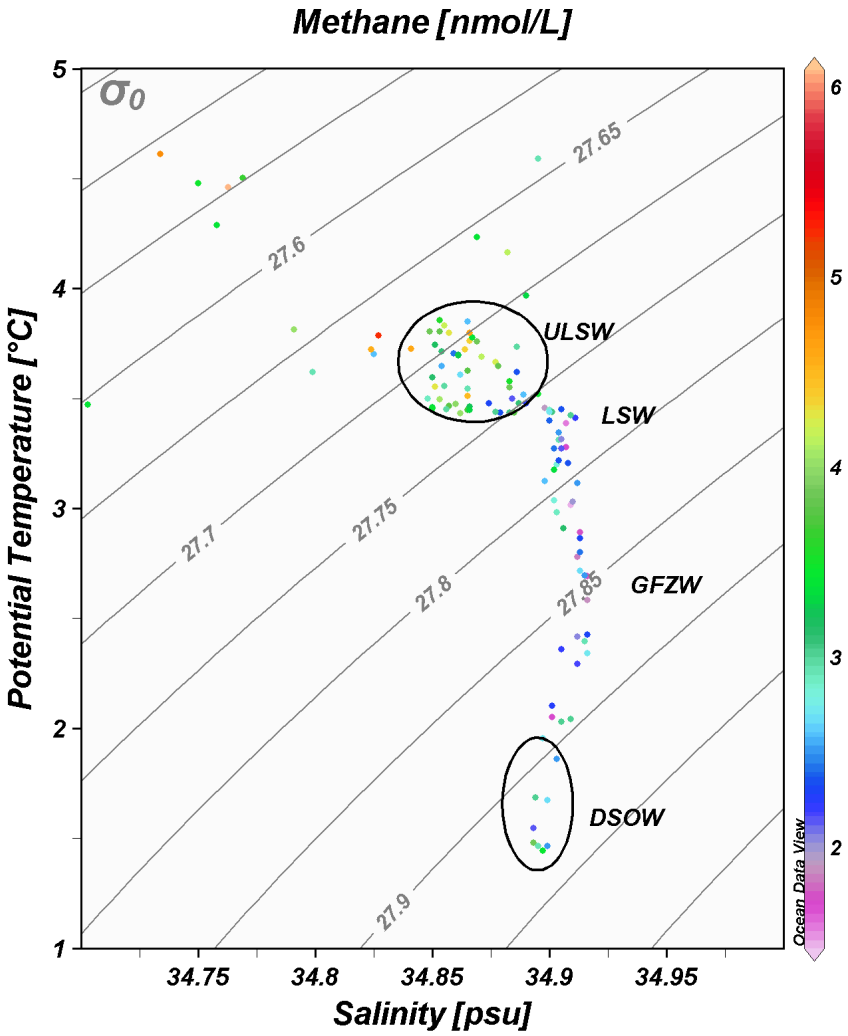

Figure 36: Correlation of hydrographic properties and methane concentrations for the MSM 05/2 data.

Methane concentrations matched the water mass distribution (as described above) quite well [FIG 35]. Maximum concentrations were measured in the surface waters which covered a wide T/S range due to freshwater inputs by precipitation and ice melting. Methane concentrations were considerably high in the ULSW, suggesting that these waters were formed by recent convection. By contrast, methane concentrations were lower in the LSW and in the GFZW and slightly enhanced in the DSOW. The low concentrations for the LSW reflect the long period since intense deep convection in the Labrador Sea. The same phenomenon can be seen when looking at the dissolved oxygen concentrations. Comparable to methane, the O_2 depth profiles along the AR7W section [FIG. 36] reflect the predominant water masses: maximum concentrations of about 350 µmol L^{-1} were found in surface waters.

Concentrations were relatively high in the ULSW, with a trend to higher concentrations in the central Labrador Sea. Lower concentrations (<290 µmol L^{-1}) were observed in the LSW and GFZW, which showed no significant differences in concentration. In contrast, the DSOW >3000 m had concentrations around 300 µmol L^{-1}.

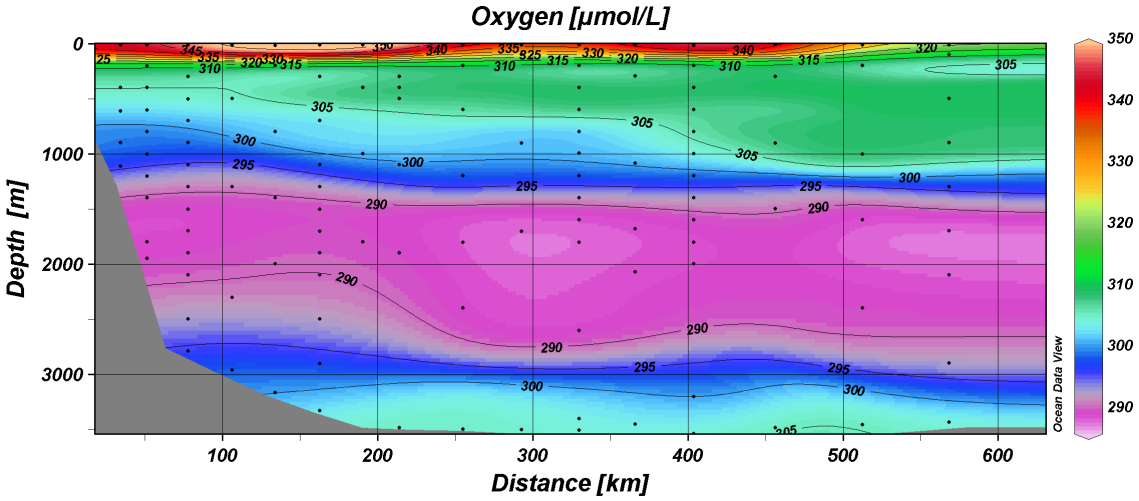

Figure 37: Dissolved oxygen along the AR7W-section.

Methane depth profiles along the AR7W section have been measured during the Meteor cruise M39 by REHDER ET AL. in August 1997 (1999) [FIG. 37]. A comparison with these data revealed two significant differences:

– The methane saturations measured during MSM 05/2 were significantly higher than the saturation measured during M39. This discrepancy might be explained by the general trend to warmer temperatures in the Labrador Sea in 2007 compared to those in 1997 [AVSIC ET AL., 2006] which might lead to an increased input of riverine methane or enhanced release of methane from the adjacent shallow shelf areas.

– During the M39 cruise surface waters were in equilibrium with the atmosphere, and declined to 80 % saturation in 2000 m depth. It seems that the deep convection reached far deeper in August 1997 (down to 2000 m) whereas during MSM 05/2 the convection reached down to only 1200 m. Deep water saturations during M39 were about 60 % which is slightly lower

than during MSM 05/2. However, the saturations from MSM 05/2 have not been corrected for the water mass age (see above) and are most likely underestimated in the deep waters.

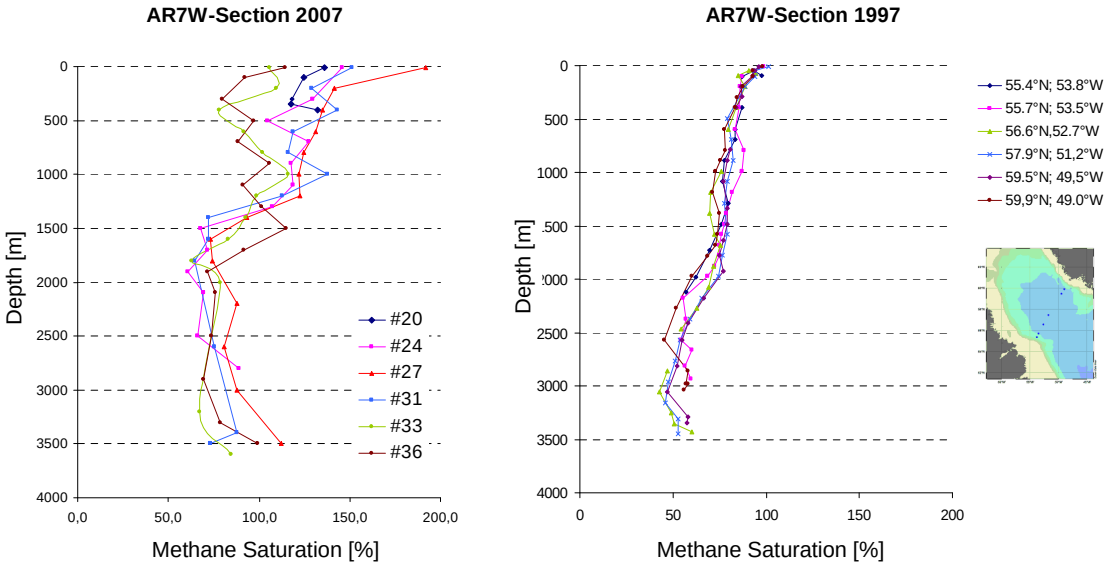

Figure 38: Methane saturations along the AR7W-Section, measured during the MSM 05/2 cruise in June 2007 (left) and during M39 in August 1997 by Rehder et al. (1999) (right).

5. Conclusions

Based on the presented measurements the main conclusions are:

– The comparison of the discrete sampling method to the equilibrator method reveals significant differences between these methods. Different possible sources of errors could be identified, but additional experiments are required before the correction for one of these methods is possible.

– Atmospheric methane mixing ratios in the upwelling area off Mauritania are highly variable and are most probably influenced by high CH4 emissions from the adjacent shallow Banc d'Arguin waters.

– Surface methane concentrations in the upwelling area are variable and seem to be influenced by a patchy distribution of different water masses. No clear relationship between SST and surface methane concentrations was detected. The main source water mass of surface CH_4 is the SACW which is upwelled on the shelf edge from about 100m. Maximum methane surface concentrations was 5 nmol L^{-1} whereas the open ocean concentrations were close to the equilibrium with the atmosphere (about 2.5 nmol L^{-1})

– The resulting total methane emissions from the Mauritanian upwelling during the upwelling season were estimated to range from 7.56 to 12.6 Gg. Thus, the Mauritanian upwelling is a "hot spot" of methane emissions to the atmosphere. CH_4 emissions from the Mauritanian upwelling are considerably higher compared to the coastal upwelling region of the Arabian Sea.

– The water column distribution of methane is influenced by methane which originates from the upwelling area. The CH_4 from the upwelling areas is spread from the coast towards the open ocean. There was a strong sedimentary methane source at the shelf edge. Open ocean deep waters were CH_4-undersaturated due to methane oxidation, though.

– In the Labrador Sea, methane depth distribution was dominated by deep convection down to about 1200m. The methane distribution reflected the age and origin of different water masses.

– A comparison of the methane data along the AR7W section with methane data by REHDER ET AL. (1999) from August 1997 on the same section revealed significant differences which might reflect the ongoing environmental changes in the Labrador Sea: The 2007 data show that methane is transported less deeper in the water column and that the methane concentrations in 2007 were generally higher. Warming of the Labrador Sea might have led to a decrease of the convection depth associated with increased methane input from rivers and/or from the adjacent shelf areas in the Labrador Sea.

6. Zusammenfassung

Folgende Schlussfolgerungen lassen sich aus den vorgestellten Ergebnissen ziehen:

– Der Vegleich zwischen den diskreten Messungen und der Equilibrator-methode offenbart deutliche Unterschiede zwischen beiden Methoden. Verschiedene Fehlerquellen sind denkbar, aber es müssen noch weitere Messungen durchgeführt werden, um eine Korrektur für eine der beiden Methoden vornehmen zu können.

– Das Mischungsverhältnis von Methan in der Atmosphäre zeigt für die Küstenregion vor Mauretanien eine große Variabilität. Ein Einfluss von hohen Methanemissionen aus dem Gebiet der angrenzenden flachen Banc d'Arguin ist wahrscheinlich.

– Oberflächenmethankonzentrationen im Nordwestafrikanischen Auftrieb sind variabel und scheinen von der inkohärenten Wassermassenverteilung in diesem Gebiet beeinflusst zu werden. Es konnte keine einfache Beziehung zwischen der Oberflächenkonzentration von Methan und SST festgestellt werden. Das Methan in der Ozeanoberfläche stammt hauptsächlich aus dem SACW, das an der Schelfkante aus Wassertiefen um 100 m aufgetrieben wird. Die höchste Methankonzentration lag bei 5 nmol L^{-1}, wohingegen Methankonzentrationen im offenen Ozean dem Gleichgewicht mit der Atmosphäre recht nah war (2.5 nmol L^{-1}).

– Die errechneten Gesamtemissionen von Methan aus dem mauretanischen Auftrieb während der Auftriebssaison lagen zwischen 7.56 und 12.6 Gg. Das beweist die Rolle des mauretanischen Auftriebsgebietes als „Hot-Spot" für marine Methanemissionen. Im Vergleich zum Arabischen Meer sind die Emissionen aus dem mauretanischen Auftrieb jedoch um ein Vielfaches höher.

– Die Verteilung von Methan in der Wassersäule ist in diesem Gebiet stark vom Auftrieb beeinflusst. Methan wird aus dem Auftriebsgebiet in den offenen Ozean verbreitet. An der Schelfkante konnte eine große sedimentäre Methanquelle ausgemacht werden, ansonsten war das Tiefenwasser aufgrund von Methanoxidationsprozessen CH_4-untersättigt.

– Winterkonvektion bis zu 1200 m Tiefe bestimmte die CH_4-Verteilung in der Wassersäule der Labradorsee. Die Verteilung von Methan spiegelte Alter und Ursprung verschiedener Wassermassen wider.

– Ein Vergleich der Methanmessungen entlang des AR7W-Abschnitts mit Messungen von Rehder et al. (1999) im August 1997 offenbart deutliche Unterschiede. Diese könnten eine Reaktion auf die sich verändernden Umweltbedingungen in der Labradorsee sein. Die Daten von 2007 zeigen, dass Methan aus der Oberfläche in geringere Tiefen transportiert wurde als zehn Jahre zuvor. Weiterhin waren die Methankonzentrationen während der 2007 durchgeführten Messungen im Allgemeinen höher als 1997. Eine Erwärmung der Labradorsee in den letzten 10 Jahren könnte zu verringerten Konvektionstiefen und zu erhöhten Methaneinträgen aus Flüssen und/oder von angrenzenden Schelfgebieten in die Labradorsee geführt haben.

Danksagung

Prof. Dr. Douglas W. Wallace danke ich dafür, dass er mir die Durchführung dieser Arbeit im Forschungsbereich Marine Biogeochemie ermöglicht hat.

Dr. Hermann Bange danke ich für die Bereitstellung des interessanten Themas und die hervorragende Betreuung dieser Arbeit, sowie für die ausgezeichnete Fahrtleitung während der Forschungsfahrt Poseidon 348.

Dem Kapitän und der Mannschaft der F/S Poseidon sowie den übrigen Fahrtteilnehmern danke ich für die gute Stimmung und das angenehme Arbeitsklima.

Ebenso danke ich dem Fahrtleiter Dr. Jürgen Fischer, dem Kapitän und der Mannschaft der F/S Maria S. Merian und den Fahrtteilnehmern von MSM 05/2 für optimale Arbeitsbedingungen und das entspannte Klima an Bord.

Frank Malien, Tobias Steinhoff, Uwe Koy und Dr. Gerd Krahmann danke ich für die Bereitstellung von Temperatur-, Salinitäts-, Sauerstoff- und Nährstoffdaten für P348 und MSM 05/2.

Ich danke Armin Jordan (MPI für Biogeochemie in Jena) für die Kalibrierung der CH_4-Standards und Ed Dlugogencky (NOAA/ESRL, Boulder, CO, USA) für die Zusendung der CH_4-Daten von Izaña. Desweiteren danke ich Robin Keir für die Methandaten von M39.

Alina Freing und Christian Ostrau danke ich für die herzliche Aufnahme in die „AG Bange“ und die Einführung in die Welt der Gaschromatographie. Für die tatkräftige Hilfe im Kampf mit dem Datendschungel und die Durchsicht meiner Diplomarbeit danke ich besonders Alina Freing.

Björn Fiedler danke ich für die Durchsicht dieser Arbeit und allerlei praktische Tipps und Ratschläge während der „Heißen Phase“.

Den Mitarbeitern im FB2 – Chemische Ozeanographie danke ich für die herzliche Aufnahme und das angenehme Arbeitsklima. Des Weiteren möchte ich allen danken, die mich während meines Chemiestudiums begleitet und unterstützt haben.

Nicht zuletzt danke ich meinen Eltern für ihre bedingungslose Unterstützung während der letzten 24 Jahre.

Die in dieser Studie vorgestellten Arbeiten im tropischen Nordostatlantik wurden vom Bundesministerium für Bildung und Forschung (BMBF, Bonn) im Rahmen des Verbundvorhabens "Surface Ocean Processes in the Anthropocene (SOPRAN)", FKZ 03F0462A, gefördert.

References

Avsic, T., J. Karstensen, et al. (2006). "Interannual variability of newly formed Labrador Sea Water from 1994 to 2005." Geophysical Research Letters **33**(21).

Bange, H. W. (1994). Messungen von Lachgas (N_2O) und Methan (CH_4) in europäischen Nebenmeeren, University of Mainz.

Bange, H. W. (2006). "Nitrous oxide and methane in European coastal waters." Estuar. Coastal Shelf Sci. **70**: 361-374.

Bange, H. W., U. H. Bartell, et al. (1994). "Methane in the Baltic and North Seas and a reassessment of the marine emissions of methane." Global Biogeochem. Cycles **8**: 465-480.

Bange, H. W., R. Ramesh, et al. (1998). "Methane in the surface waters of the Arabian Sea." Geophys. Res. Lett. **25**(19): 3547-3550.

Bange, H. W. and G. Uher (2005). "Photochemical production of methane in natural waters: Implications for its present and past oceanic source." Chemosphere **58**(2): 177-183.

Bates, T. S., K. C. Kelly, et al. (1996). "A reevaluation of the open ocean source of methane to the atmosphere." J. Geophys. Res. **101**(D3): 6953-6961.

Boetius, A., K. Ravenschlag, et al. (2000). "A marine microbial consortium apparently mediating anaerobic oxidation of methane." Nature **407**(6804): 623-626.

Böning, C. W., M. Scheinert, et al. (2006). "Decadal variability of subpolar gyre transport and its reverberation in the North Atlantic overturning." Geophysical Research Letters **33**(21).

Cicerone, R. J. and R. S. Oremland (1988). "Biogeochemical aspects of atmospheric methane." Global Biogeochem. Cycles **2**: 299-327.

David, H. A. (1951). "Further applications of range to analysis of variance." Biometrika **38**: 393-409.

De Angelis, M. A. and C. Lee (1994). "Methane production during zooplankton grazing on marine phytoplankton." Limnol. Oceanogr. **39**(6): 1298-1308.

Dlugokencky, E. J., S. Houweling, et al. (2003). "Atmospheric methane levels off: Temporary pause or a new steady-state?" Geophysical Research Letters **30**(19).

Etheridge, D. M., L. P. Steele, et al. (1998). "Atmospheric methane between 1000 AD and present: Evidence of anthropogenic emissions and climatic variability." Journal of Geophysical Research-Atmospheres **103**(D13): 15979-15993.

Etiope, G. (2004). "New Directions: GEM - Geologic emissions of methane, the missing source in the atmospheric methane budget." Atmos. Environ. **38**: 3099-3100.

Forster, G., R. C. Upstill-Goddard, et al. (2007). "Nitrous oxide and methane in the Atlantic Ocean between 50°N and 52°S: latitudinal distribution and sea-to-air flux." Deep-Sea Res.: in press.

Garratt, J. R. (1977). "Review of the drag coefficients over oceans and continents." Mo. Weath. Rev. **105**: 915-929.

Gebhardt, S. and H. W. Bange (2006). "Nitrous oxide and methane in the upwelling area off Mauritania (NW Africa)." SOLAS news(4, Autumn 2006): 10.

Greinert, J. (1998). Rezente Submarine Mineralbildungen: Abbild Geochemischer Prozesse an aktiven Fluidaustrittsstellen im Aleuten- und Cascadia-Akkretionsprozess. Geomar Forschungszentrum für marine Geowissenschaften. Kiel, Christian-Albrechts-Universität

Hagen, E. (2001). "Northwest African upwelling scenario." Oceanol. Acta **24**: S113-S127.

Hamme, R. and J. P. Severinghaus (2007). "Trace gas disequilibria during deep-water formation." Deep-Sea Res. **54**(6): 939-950.

Houweling, S., T. Kaminski, et al. (1999). "Inverse modeling of methane sources and sinks using the adjoint of a global transport model." J. Geophys. Res. **104**(21): 26,137-26,160.

IPCC (2007). Climate Change 2007: The Scientific Basis. Contribution of Working Group I to the Fourth Assessment report of the Intergovernmental Panel on Climate Change. C. U. Press. Cambridge and New York**:** 539-546.

Jahne, B. and H. Haussecker (1998). "Air-water gas exchange." Annual Review of Fluid Mechanics **30**: 443-468.

Jähne, B., G. Heinz, et al. (1987). "Measurements of the diffusion coefficients of sparingly soluble gases in water." J. Geophys. Res. **92**(C10): 10,767-10,776.

Johnson, J. E. (1999). "Evaluation of a seawater equilibrator for shipbord analysis of dissolved trace gases." Anal. Chim. Acta **395**: 119-132.

Karl, D. M. and B. D. Tilbrook (1994). "Production and transport of methane in oceanic particulate organic matter." Nature **368**: 732-734.

Kelley, C. A. and W. H. Jeffrey (2002). "Dissolved methane concentration profiles and air-sea fluxes from 41°S to 27°N." Global Biogeochem. Cycles **16**(3): doi: 10.1029/2001GB001809.

Keppler, F., J. T. G. Hamilton, et al. (2006). "Methane emissions from terrestrial plants under aerobic conditions." Nature(439): 187-191.

Körtzinger, A., J. Schimanski, et al. (2004). "The ocean takes a deep breath." Science **306**(5700): 1337-1337.

Kvenvolden, K. A. and B. W. Rogers (2005). "Gaia's breath - global methane exhalations." Marine and Petroleum Geology **22**(4): 579-590.

Lavender, K. L., R. E. Davis, et al. (2002). "Observations of open-ocean deep convection in the Labrador Sea from subsurface floats." Journal of Physical Oceanography **32**(2): 511-526.

Lazier, J., R. Hendry, et al. (2002). "Convection and restratification in the Labrador Sea, 1990-2000." Deep-Sea Research Part I-Oceanographic Research Papers **49**(10): 1819-1835.

Lelieveld, J. (2006). "Climate change - A nasty surprise in the greenhouse." Nature **443**(7110): 405-406.

Liss, P. S. and L. Merlivat (1986). Air-sea exchange rates: introduction and synthesis. The Role of Air-Sea Exchange in Geochemical Cycling. P. Buat-Ménard. Dordrecht, D. Reidel Publishing Company. **185:** 113-127.

Mauritzen, C. (1996). "Production of dense overflow waters feeding the North Atlantic across the Greenland-Scotland Ridge .1. Evidence for a revised circulation scheme." Deep-Sea Research Part I-Oceanographic Research Papers **43**(6): 769-806.

Minas, H. J., L. A. Codispoti, et al. (1982). "Nutrients and primary production in the upwelling region off Northwest Africa." Rapp. P.-V. Réun. Cons. Int. Explor. Mer **180**: 148-182.

Mittelstaedt, E. (1983). "The upwelling Area off northwest Africa - a description of phenomena related to coastal upwelling." Prog. Oceanogr. **26**: 307-3331.

Mittelstaedt, E. (1986). Upwelling regions. Landoldt-Börnstein, New Series, Vol. 3, Oceanography. J. Sündermann. Berlin, Springer Verlag. **3:** 135-166.

Mittelstaedt, E. (1991). "The ocean boundary along the northwest African coast: Circulation and oceanography properties at the sea surface." Prog. Oceanogr. **26**: 307-355.

Monteiro, P. M. S., A. Van der Plas, et al. (2006). "Variability of natural hypoxia and methane in coastal upwelling system: Oceanic physics or shelf biology?" Geophys. Res. Lett. **33**: L16614, doi:10.1029/2006GL026234.

Naqvi, S. W. A., H. W. Bange, et al. (2005). "Biogeochemical ocean-atmosphere transfers in the Arabian Sea." Progress in Oceanography **65**(2-4): 116-144.

Peters, H. (1976). "The spreading of water masses of the Banc d'Arguin in the upwelling area off the northern Mauritanian coast." Meteor Forsch. Ergebnisse A **18**: 78-100.

Reeburgh, W. S. (2007). "Oceanic methane biogeochemistry." Chemical Reviews **107**(2): 486-513.

Rehder, G., R. W. Collier, et al. (2002). "Enhanced marine CH_4 emissions to the atmosphere off Oregon caused by coastal upwelling." Global Biogeochem. Cycles **16**(3): doi 10.1029/2000GB001391.

Rehder, G., R. S. Keir, et al. (1999). "Methane in the northern Atlantic controlled by microbial oxidation and atmospheric history." Geophys. Res. Lett. **26**(5): 587-590.

Sansone, F. J., A. W. Graham, et al. (2004). "Methane along the western Mexican Margin." Linmol. Oceanogr. **49**(6): 2242-2255.

Sansone, F. J., B. N. Popp, et al. (2001). "Highly elevated methane in the eastern tropical North Pacific and associated isotopically enriched fluxes to the atmosphere." Geophys. Res. Lett. **28**(24): 4567-4570.

Scranton, M. I. and P. G. Brewer (1977). "Occurrence of methane in the near-surface waters of the western subtropical North-Atlantic." Deep-Sea Res. **24**: 127-138.

Stramma, L., D. Kieke, et al. (2004). "Deep water changes at the western boundary of the subpolar North Atlantic during 1996 to 2001." Deep-Sea Research Part I-Oceanographic Research Papers **51**(8): 1033-1056.

Tomczak, M. and J. S. Godfrey (2002). Regional Oceanography: An Introduction.

Valentine, D. L. and W. S. Reeburgh (2000). "New perspectives on anaerobic methane oxidation." Environmental Microbiology **2**(5): 477-484.

Wanninkhof, R. (1992). "Relationship between wind speed and gas exchange over the ocean." J. Geophys. Res. **97**(C5): 7373-7382.

Ward, B. B. and K. A. Kilpatrick (1993). "Methane oxidation associated with mid-depth methane maxima in the Southern California Bight." Continent. Shelf Res. **13**(10): 1111-1122.

Weiss, R. F. (1970). "The solubility of nitrogen, oxygen and argon in water and seawater." Deep-Sea Res. **17**: 721-735.

Wiesenburg, D. A. and N. L. Guinasso Jr. (1979). "Equilibrium solubilities of methane, carbon monoxide, hydrogen in water and seawater." J. Chem. Eng. Data **24**: 356-360.

Wuebbles, D. J. and K. Hayhoe (2002). "Atmospheric methane and global change." Earth-Sci. Rev. **57**: 177-210.

List of Figures

Table I: Methane in the Surface Waters off the Mauritanian Coast

Date	Time	Longitude [°W]	Latitude [°N]	Temperature [°C]	Salinity	Methane Conc. [nmol L^{-1}]	Methane Saturation [%]	Flux Density LM86 [nmol m^{-2} s^{-1}]	Flux Density W92 [nmol m^{-2} s^{-1}]
19-Feb-07	3:39	16,35	18,00	18,33	35,90	2,273	93,0	0,017	0,027
19-Feb-07	4:01	16,31	18,00	18,31	35,90	2,339	104,6	0,027	0,043
19-Feb-07	4:23	16,27	18,00	18,23	35,93	2,448	101,5	0,023	0,037
19-Feb-07	4:46	16,26	18,02	18,15	35,93	2,377	98,3	0,020	0,032
19-Feb-07	5:08	16,26	18,06	18,07	35,93	2,440	100,9	0,027	0,045
19-Feb-07	5:30	16,26	18,09	17,97	35,91	2,426	98,9	0,023	0,037
19-Feb-07	5:52	16,26	18,12	17,89	35,88	2,583	105,5	0,029	0,047
19-Feb-07	6:15	16,26	18,16	17,89	35,86	2,546	100,9	0,021	0,033
19-Feb-07	6:37	16,27	18,19	18,00	35,85	2,476	106,8	0,024	0,037
19-Feb-07	6:59	16,27	18,22	17,91	35,87	2,531	110,1	0,023	0,035
19-Feb-07	7:21	16,27	18,25	17,83	35,86	2,525	109,4	0,022	0,033
19-Feb-07	7:43	16,27	18,29	17,78	35,86	2,495	108,7	0,024	0,037
19-Feb-07	8:06	16,27	18,32	17,71	35,90	2,488	106,1	0,027	0,043
19-Feb-07	8:28	16,28	18,36	17,63	35,90	2,653	112,9	0,023	0,035
19-Feb-07	8:50	16,28	18,39	17,48	35,94	2,543	109,6	0,029	0,046
19-Feb-07	9:12	16,28	18,43	17,24	35,93	2,638	112,1	0,028	0,044
19-Feb-07	9:34	16,28	18,46	17,22	35,91	2,704	114,1	0,032	0,050
19-Feb-07	9:57	16,29	18,49	17,44	36,00	2,853	122,9	0,044	0,070
19-Feb-07	10:19	16,32	18,50	17,26	35,91	3,048	128,7	0,061	0,101
19-Feb-07	10:41	16,36	18,50	17,42	35,90	2,808	118,9	0,048	0,080
19-Feb-07	11:03	16,40	18,50	17,55	35,91	2,820	119,7	0,048	0,079
19-Feb-07	11:25	16,43	18,50	17,85	35,93	2,949	123,7	0,046	0,073
19-Feb-07	11:48	16,47	18,50	18,02	35,96	3,474	145,6	0,073	0,118
19-Feb-07	12:10	16,50	18,50	18,11	35,97	3,528	147,3	0,060	0,093
19-Feb-07	12:32	16,50	18,50	18,15	35,97	3,253	139,4	0,048	0,074

Date	Time	Longitude [°W]	Latitude [°N]	Temperature [°C]	Salinity	Methane Conc. [nmol L^{-1}]	Methane Saturation [%]	Flux Density LM86 [nmol m^{-2} s^{-1}]	Flux Density W92 [nmol m^{-2} s^{-1}]
19-Feb-07	12:54	16,50	18,50	18,18	35,98	3,274	139,6	0,039	0,060
19-Feb-07	13:16	16,50	18,50	18,20	35,98	3,206	134,1	0,034	0,054
19-Feb-07	13:39	16,53	18,51	18,31	35,98	3,070	129,9	0,042	0,065
19-Feb-07	14:01	16,56	18,51	18,41	35,98	3,003	128,7	0,046	0,073
19-Feb-07	14:23	16,59	18,50	18,41	36,00	3,029	129,2	0,056	0,091
19-Feb-07	14:45	16,62	18,48	18,51	36,00	3,055	128,9	0,062	0,102
19-Feb-07	15:07	16,65	18,48	18,56	36,01	3,006	127,0	0,067	0,115
19-Feb-07	15:30	16,68	18,48	18,43	36,01	2,883	121,4	0,066	0,118
19-Feb-07	15:52	16,72	18,49	18,54	35,98	2,819	118,2	0,064	0,115
19-Feb-07	16:14	16,75	18,49	18,59	36,01	2,575	108,5	0,045	0,080
19-Feb-07	16:36	16,78	18,49	18,62	36,01	2,708	117,0	0,052	0,089
19-Feb-07	16:59	16,82	18,49	18,63	36,01	2,824	119,8	0,065	0,116
19-Feb-07	17:21	16,86	18,49	18,64	36,02	2,647	111,4	0,045	0,078
19-Feb-07	17:43	16,90	18,49	18,67	36,02	2,650	114,3	0,051	0,088
19-Feb-07	18:05	16,94	18,49	18,71	36,01	2,554	109,1	0,050	0,092
19-Feb-07	18:27	16,97	18,49	18,80	36,02	2,745	115,9	0,066	0,123
19-Feb-07	18:50	17,00	18,50	18,83	36,03	2,625	110,9	0,055	0,101
19-Feb-07	19:12	17,00	18,50	18,82	36,03	2,745	113,8	0,051	0,087
19-Feb-07	19:34	17,00	18,50	18,81	36,03	2,402	104,1	0,035	0,062
19-Feb-07	19:56	17,00	18,50	18,79	36,03	2,530	107,8	0,047	0,086
19-Feb-07	20:18	17,00	18,50	18,78	36,01	2,457	106,7	0,040	0,071
19-Feb-07	20:41	17,01	18,51	18,77	36,03	2,470	105,5	0,038	0,067
19-Feb-07	21:03	17,00	18,50	18,76	36,02	2,533	108,2	0,043	0,075
19-Feb-07	21:25		0,00	18,73	36,02	2,381	101,3	0,032	0,056
19-Feb-07	21:47	17,04	18,50	18,76	36,01	2,398	101,9	0,036	0,064

Table I: Methane in the Surface Waters off the Mauritanian Coast

Date	Time	Longitude [°W]	Latitude [°N]	Temperature [°C]	Salinity	Methane Conc. [nmol L^{-1}]	Methane Saturation [%]	Flux Density LM86 [nmol m^{-2} s^{-1}]	Flux Density W92 [nmol m^{-2} s^{-1}]
19-Feb-07	22:09	17,08	18,50	18,98	35,99	2,431	104,9	0,046	0,088
19-Feb-07	22:32	17,12	18,50	19,74	36,10	2,344	101,0	0,041	0,078
19-Feb-07	22:54	17,16	18,50	20,00	36,11	2,321	100,9	0,043	0,085
19-Feb-07	23:16	17,21	18,50	20,05	36,05	2,277	99,1	0,042	0,083
19-Feb-07	23:38	17,25	18,50	20,11	36,01	2,267	101,1	0,043	0,085
20-Feb-07	0:01	17,30	18,50	20,16	36,04	2,284	100,2	0,041	0,081
20-Feb-07	0:23	17,34	18,50	20,12	36,05	2,071	89,9	0,029	0,055
20-Feb-07	0:45	17,38	18,50	20,06	36,04	2,263	97,1	0,036	0,070
20-Feb-07	1:07	17,42	18,50	20,04	36,05	2,403	102,9	0,051	0,102
20-Feb-07	1:29	17,46	18,50	20,07	36,04	2,316	102,1	0,047	0,093
20-Feb-07	1:52	17,51	18,50	20,09	36,05	2,348	101,3	0,038	0,071
20-Feb-07	2:14	17,55	18,50	20,09	36,06	2,403	102,1	0,063	0,119
20-Feb-07	2:36	17,59	18,50	20,13	36,06	2,367	100,3	0,045	0,090
20-Feb-07	2:58	17,63	18,50	20,14	36,07	2,344	100,6	0,051	0,099
20-Feb-07	3:20	17,66	18,50	20,08	36,08	2,415	104,2	0,065	0,124
20-Feb-07	3:43	17,70	18,50	19,94	36,08	2,462	105,7	0,070	0,133
20-Feb-07	4:05	17,74	18,50	19,89	36,09	2,372	102,0	0,054	0,105
20-Feb-07	4:27	17,79	18,50	19,89	36,08	2,337	99,3	0,041	0,081
20-Feb-07	4:49	17,83	18,50	19,96	36,09	2,330	99,9	0,040	0,076
20-Feb-07	5:11	17,86	18,50	19,97	36,11	2,398	103,1	0,036	0,063
20-Feb-07	5:34	17,91	18,50	20,09	36,16	2,430	105,5	0,043	0,078
20-Feb-07	5:56	17,95	18,50	19,97	36,15	2,450	103,7	0,036	0,062
20-Feb-07	6:18	17,98	18,50	19,96	36,13	2,310	98,8	0,040	0,079
20-Feb-07	6:40	18,00	18,50	19,96	36,14	2,273	98,9	0,038	0,074
20-Feb-07	7:03	18,00	18,50	19,97	36,13	2,422	104,9	0,058	0,114

Date	Time	Longitude [°W]	Latitude [°N]	Temperature [°C]	Salinity	Methane Conc. [nmol L^{-1}]	Methane Saturation [%]	Flux Density LM86 [nmol m^{-2} s^{-1}]	Flux Density W92 [nmol m^{-2} s^{-1}]
20-Feb-07	7:25	18,00	18,50	19,96	36,14	2,448	105,8	0,047	0,088
20-Feb-07	7:47	18,00	18,50	19,96	36,13	2,430	104,7	0,055	0,109
20-Feb-07	8:09	18,00	18,50	19,96	36,13	2,264	95,7	0,036	0,072
20-Feb-07	8:31	18,00	18,51	19,95	36,14	2,254	95,7	0,040	0,077
20-Feb-07	8:54	18,00	18,53	19,97	36,14	2,263	98,0	0,046	0,088
20-Feb-07	9:16	18,00	18,56	19,96	36,14	2,286	98,5	0,056	0,106
20-Feb-07	9:38	18,00	18,59	19,92	36,13	2,315	99,3	0,068	0,125
20-Feb-07	10:00	18,00	18,62	19,88	36,11	2,401	103,8	0,085	0,156
20-Feb-07	10:22	18,00	18,65	19,62	36,06	2,315	97,5	0,052	0,097
20-Feb-07	10:45	18,00	18,68	19,57	36,05	2,399	102,2	0,060	0,115
20-Feb-07	11:07	18,00	18,71	19,74	36,06	2,316	101,2	0,062	0,117
20-Feb-07	11:29	18,00	18,74	19,75	36,07	2,389	103,6	0,062	0,119
20-Feb-07	11:51	18,00	18,77	19,74	36,07	2,283	97,0	0,040	0,079
20-Feb-07	12:13	18,01	18,80	19,58	36,06	2,340	100,0	0,044	0,089
20-Feb-07	12:36	18,01	18,84	19,45	36,03	2,316	98,3	0,039	0,077
20-Feb-07	12:58	18,01	18,87	19,36	36,05	2,381	100,2	0,033	0,059
20-Feb-07	13:20	18,01	18,91	19,08	36,01	2,542	108,1	0,047	0,085
20-Feb-07	13:42	18,01	18,94	18,93	36,00	2,452	103,7	0,041	0,076
20-Feb-07	14:04	18,00	18,98	18,90	36,00	2,423	102,6	0,035	0,061
20-Feb-07	14:27	18,00	19,01	18,92	36,00	2,539	105,8	0,044	0,079
20-Feb-07	14:49	17,96	19,01	18,90	36,00	2,477	103,2	0,039	0,070
20-Feb-07	15:11	17,92	19,00	18,86	35,98	2,469	104,5	0,043	0,080
20-Feb-07	15:33	17,88	19,00	18,93	35,98	2,563	107,7	0,046	0,083
20-Feb-07	15:55	17,83	19,00	18,94	35,99	2,505	104,6	0,042	0,076
20-Feb-07	16:18	17,79	19,00	19,13	36,01	2,510	107,0	0,042	0,073

Date	Time	Longitude [°W]	Latitude [°N]	Temperature [°C]	Salinity	Methane Conc. [nmol L^{-1}]	Methane Saturation [%]	Flux Density LM86 [nmol m^{-2} s^{-1}]	Flux Density W92 [nmol m^{-2} s^{-1}]
20-Feb-07	16:40	17,79	19,00	18,97	35,99	2,531	107,4	0,041	0,072
20-Feb-07	17:02	17,79	19,00	18,96	35,99	2,505	107,8	0,040	0,070
20-Feb-07	17:24	17,79	19,01	18,94	36,00	2,439	104,7	0,031	0,051
20-Feb-07	17:46	17,79	19,02	18,88	35,99	2,438	101,9	0,025	0,041
20-Feb-07	18:09	17,80	19,03	18,80	35,99	2,511	103,4	0,027	0,043
20-Feb-07	18:31	17,76	19,02	18,83	35,99	2,502	104,5	0,033	0,054
20-Feb-07	18:53	17,71	19,02	18,87	35,99	2,407	101,4	0,029	0,048
20-Feb-07	19:15	17,66	19,01	18,98	36,00	2,553	106,8	0,035	0,059
20-Feb-07	19:38	17,61	19,00	18,92	36,00	2,481	103,1	0,028	0,045
20-Feb-07	20:00	17,55	19,00	18,78	35,99	2,535	105,4	0,028	0,044
20-Feb-07	20:22	17,50	19,00	18,65	35,97	2,455	103,6	0,034	0,058
20-Feb-07	20:44	17,50	19,00	18,65	35,97	2,340	98,7	0,023	0,038
20-Feb-07	21:06	17,50	19,00	18,66	35,97	2,386	102,1	0,036	0,065
20-Feb-07	21:29	17,50	19,01	18,67	35,97	2,487	104,0	0,036	0,062
20-Feb-07	21:51	17,51	19,02	18,67	35,97	2,482	104,2	0,037	0,066
20-Feb-07	22:13	17,51	19,03	18,68	35,97	2,552	107,8	0,043	0,076
20-Feb-07	22:35	17,47	19,02	18,69	35,98	2,584	108,5	0,038	0,064
20-Feb-07	22:57	17,43	19,02	18,70	35,97	2,507	103,4	0,036	0,064
20-Feb-07	23:20	17,39	19,02	18,62	35,97	2,390	99,3	0,028	0,049
20-Feb-07	23:42	17,35	19,02	18,58	35,96	2,480	106,0	0,030	0,048
21-Feb-07	0:04	17,31	19,02	18,52	35,95	2,461	102,5	0,026	0,042
21-Feb-07	0:26	17,27	19,01	18,38	35,96	2,397	100,3	0,024	0,040
21-Feb-07	0:49	17,23	19,01	18,23	35,96	2,415	101,3	0,027	0,045
21-Feb-07	1:11	17,19	19,01	18,10	35,96	2,419	97,7	0,023	0,039
21-Feb-07	1:33	17,15	19,00	17,76	35,94	2,602	108,1	0,030	0,048

Date	Time	Longitude [°W]	Latitude [°N]	Temperature [°C]	Salinity	Methane Conc. [nmol L^{-1}]	Methane Saturation [%]	Flux Density LM86 [nmol m^{-2} s^{-1}]	Flux Density W92 [nmol m^{-2} s^{-1}]
21-Feb-07	1:55	17,11	19,00	17,72	35,94	2,639	109,9	0,025	0,039
21-Feb-07	2:17	17,06	19,00	17,81	35,92	2,525	103,5	0,019	0,030
21-Feb-07	2:40	17,02	19,00	17,91	35,93	3,047	126,3	0,032	0,049
21-Feb-07	3:02	17,00	19,00	18,06	35,97	3,545	134,8	0,052	0,082
21-Feb-07	3:24	17,00	19,00	18,07	35,97	3,334	127,7	0,047	0,073
21-Feb-07	3:46	16,99	19,00	18,08	35,97	3,086	121,6	0,040	0,062
21-Feb-07	4:08	16,99	19,00	18,08	35,97	3,096	115,3	0,035	0,055
21-Feb-07	4:31	16,99	19,00	18,07	35,98	3,324	130,6	0,080	0,139
21-Feb-07	4:53	16,98	19,00	18,06	35,98	3,550	124,8	0,077	0,132
21-Feb-07	5:15	17,00	19,00	18,04	35,97	3,235	121,4	0,067	0,116
21-Feb-07	5:37	17,00	19,00	18,03	35,96	3,396	127,8	0,086	0,154
21-Feb-07	6:00	16,98	19,00	18,03	35,97	3,542	130,0	0,094	0,169
21-Feb-07	6:22	16,93	19,00	18,10	35,98	3,373	127,6	0,075	0,128
21-Feb-07	6:44	16,89	19,00	18,10	35,97	3,133	122,0	0,076	0,138
21-Feb-07	7:06	16,84	19,00	17,96	35,96	3,268	129,9	0,104	0,203
21-Feb-07	7:28	16,80	19,00	18,14	35,96	3,529	138,6	0,109	0,201
21-Feb-07	7:51	16,75	19,00	18,22	35,97	3,703	141,3	0,119	0,221
21-Feb-07	8:13	16,70	19,00	18,05	35,96	3,726	143,6	0,124	0,230
21-Feb-07	8:35	16,66	19,00	17,67	35,91	3,397	132,3	0,100	0,186
21-Feb-07	8:57	16,61	19,00	17,53	35,91	3,126	124,7	0,072	0,128
21-Feb-07	9:19	16,57	19,00	17,47	35,91	2,892	117,4	0,041	0,066
21-Feb-07	9:42	16,55	19,00	16,94	35,84	2,778	111,5	0,034	0,054
21-Feb-07	10:04	16,55	19,00	16,93	35,84	2,811	111,3	0,034	0,054
21-Feb-07	10:26	16,52	19,00	17,00	35,85	2,887	114,0	0,023	0,036
21-Feb-07	10:48	16,48	18,99	16,54	35,86	3,346	128,1	0,036	0,056

Date	Time	Longitude [°W]	Latitude [°N]	Temperature [°C]	Salinity	Methane Conc. [nmol L^{-1}]	Methane Saturation [%]	Flux Density LM86 [nmol m^{-2} s^{-1}]	Flux Density W92 [nmol m^{-2} s^{-1}]
21-Feb-07	11:10	16,45	19,00	16,13	35,75	3,032	116,6	0,026	0,040
21-Feb-07	11:33	16,49	19,03	16,23	35,74	2,779	106,2	0,016	0,025
21-Feb-07	11:55	16,53	19,05	16,83	35,82	2,943	115,6	0,017	0,029
21-Feb-07	12:17	16,57	19,07	17,49	35,89	3,250	121,4	0,027	0,042
21-Feb-07	12:39	16,60	19,10	17,54	35,90	3,143	114,5	0,018	0,030
21-Feb-07	13:01	16,64	19,12	17,62	35,90	3,073	119,2	0,008	0,019
21-Feb-07	13:24	16,66	19,16	17,66	35,90	2,960	116,4	0,026	0,041
21-Feb-07	13:46	16,69	19,20	17,57	35,87	3,051	118,8	0,039	0,061
21-Feb-07	14:08	16,71	19,24	17,02	35,83	3,260	125,2	0,048	0,076
21-Feb-07	14:30	16,73	19,28	17,12	35,94	3,025	116,6	0,034	0,054
21-Feb-07	14:52	16,75	19,32	17,77	36,06	2,634	104,4	0,028	0,044
21-Feb-07	15:15	16,77	19,37	17,46	36,10	3,357	132,0	0,053	0,084
21-Feb-07	15:37	16,78	19,41	17,17	36,00	4,978	179,4	0,119	0,191
21-Feb-07	15:59	16,80	19,45	16,70	35,90	4,548	148,1	0,080	0,126
21-Feb-07	16:21	16,82	19,49	16,59	35,89	4,192	151,3	0,082	0,131
21-Feb-07	16:43	16,86	19,50	17,18	35,93	3,976	147,3	0,084	0,135
21-Feb-07	17:06	16,91	19,50	17,38	35,96	4,257	154,5	0,100	0,163
21-Feb-07	17:28	16,95	19,50	17,49	35,96	4,753	170,0	0,103	0,163
21-Feb-07	17:50	17,00	19,50	17,26	35,94	4,713	160,4	0,115	0,188
21-Feb-07	18:12	0,00	0,00	17,35	35,93	4,412	152,3	0,086	0,136
21-Feb-07	18:34	17,00	19,50	17,34	35,94	4,225	153,4	0,093	0,150
21-Feb-07	18:57	17,02	19,51	17,36	35,94	4,622	168,2	0,115	0,186
21-Feb-07	19:19	17,05	19,50	17,49	35,96	4,291	161,0	0,089	0,141
21-Feb-07	19:41	17,08	19,50	17,88	35,93	4,016	156,8	0,100	0,165
21-Feb-07	20:03	17,12	19,50	18,23	35,98	4,900	125,6	0,099	0,166

Date	Time	Longitude [°W]	Latitude [°N]	Temperature [°C]	Salinity	Methane Conc. [nmol L^{-1}]	Methane Saturation [%]	Flux Density LM86 [nmol m^{-2} s^{-1}]	Flux Density W92 [nmol m^{-2} s^{-1}]
21-Feb-07	20:26	17,15	19,50	18,72	35,96	8,259	235,1	0,230	0,379
21-Feb-07	20:48	17,19	19,50	18,79	35,96	3,609	155,4	0,064	0,106
21-Feb-07	21:10	17,22	19,50	18,93	35,96	3,354	122,6	0,047	0,086
21-Feb-07	21:32	17,26	19,50	19,07	35,96	2,739	114,1	0,027	0,047
21-Feb-07	21:54	17,29	19,50	19,21	35,99	2,708	118,1	0,035	0,064
21-Feb-07	22:17	17,32	19,50	19,29	36,01	2,840	124,4	0,049	0,094
21-Feb-07	22:39	17,36	19,50	19,28	36,00	2,756	122,4	0,041	0,077
21-Feb-07	23:01	17,39	19,50	19,20	35,99	2,791	120,5	0,037	0,067
21-Feb-07	23:23	17,43	19,50	19,15	35,98	2,716	119,9	0,040	0,077
21-Feb-07	23:45	17,46	19,50	19,10	35,98	2,718	120,4	0,041	0,079
22-Feb-07	0:08	17,49	19,50	19,04	35,97	2,722	116,4	0,038	0,074
22-Feb-07	0:30	17,50	19,50	19,04	35,97	2,745	118,7	0,050	0,097
22-Feb-07	0:52	17,50	19,50	19,04	35,97	2,801	120,5	0,045	0,089
22-Feb-07	1:14	17,49	19,50	19,04	35,97	2,713	113,8	0,034	0,067
22-Feb-07	1:37	17,50	19,50	19,04	35,97	2,614	113,1	0,035	0,070
22-Feb-07	1:59	17,53	19,50	19,06	35,98	2,531	110,1	0,028	0,056
22-Feb-07	2:21	17,57	19,50	19,11	35,98	2,475	107,7	0,021	0,042
22-Feb-07	2:43	17,61	19,50	19,13	36,00	2,680	114,2	0,034	0,067
22-Feb-07	3:05	17,64	19,50	19,12	35,98	2,652	107,8	0,029	0,057
22-Feb-07	3:28	17,68	19,50	19,11	35,99	2,634	105,2	0,028	0,054
22-Feb-07	3:50	17,72	19,50	19,07	35,99	2,759	110,8	0,049	0,091
22-Feb-07	4:12	17,76	19,50	19,03	35,98	2,695	108,3	0,030	0,059
22-Feb-07	4:34	17,80	19,50	18,97	35,98	2,758	109,7	0,030	0,059
22-Feb-07	4:56	17,84	19,50	18,94	35,97	2,704	107,9	0,037	0,070
22-Feb-07	5:19	17,88	19,50	18,92	35,96	2,774	111,2	0,045	0,085

Date	Time	Longitude [°W]	Latitude [°N]	Temperature [°C]	Salinity	Methane Conc. [nmol L^{-1}]	Methane Saturation [%]	Flux Density LM86 [nmol m^{-2} s^{-1}]	Flux Density W92 [nmol m^{-2} s^{-1}]
22-Feb-07	5:41	17,92	19,50	18,92	35,94	2,734	108,2	0,031	0,061
22-Feb-07	6:03	17,96	19,50	19,10	35,95	2,697	107,1	0,029	0,058
22-Feb-07	6:25	17,99	19,50	19,41	36,01	2,705	107,0	0,034	0,065
22-Feb-07	6:47	18,00	19,51	19,56	36,05	2,731	108,8	0,037	0,071
22-Feb-07	7:10	18,00	19,55	19,53	36,04	2,771	110,2	0,050	0,093
22-Feb-07	7:32	18,00	19,58	19,44	36,01	2,714	111,1	0,037	0,074
22-Feb-07	7:54	18,00	19,62	19,55	36,06	2,525	106,0	0,028	0,053
22-Feb-07	8:16	18,00	19,65	19,45	36,05	2,484	106,9	0,027	0,052
22-Feb-07	8:39	18,00	19,68	19,16	35,99	2,629	111,0	0,034	0,069
22-Feb-07	9:01	18,00	19,72	19,18	35,99	2,557	108,0	0,026	0,050
22-Feb-07	9:23	18,00	19,76	19,28	36,02	2,613	113,4	0,035	0,068
22-Feb-07	9:45	18,00	19,79	19,18	35,98	2,687	111,2	0,034	0,067
22-Feb-07	10:07	0,00	0,00	19,15	35,97	2,639	110,8	0,032	0,062
22-Feb-07	10:30	18,00	19,87	19,11	35,96	2,618	109,4	0,024	0,043
22-Feb-07	10:52	18,00	19,91	19,09	35,94	2,596	109,7	0,020	0,036
22-Feb-07	11:14	18,00	19,95	19,08	35,95	2,525	105,2	0,014	0,024
22-Feb-07	11:36	18,00	19,98	18,89	35,93	2,544	107,1	0,016	0,027
22-Feb-07	11:58	18,00	20,00	18,87	35,93	2,580	108,1	0,014	0,023
22-Feb-07	12:21	18,00	20,00	18,89	35,93	2,617	107,6	0,013	0,020
22-Feb-07	12:43	18,00	20,00	18,91	35,95	2,665	109,9	0,017	0,028
22-Feb-07	13:05	18,00	20,01	18,94	35,95	2,669	111,4	0,016	0,024
22-Feb-07	13:27	18,00	20,02	19,07	36,00	2,544	105,6	0,015	0,025
22-Feb-07	13:49	17,97	20,02	19,05	36,00	2,537	105,2	0,013	0,021
22-Feb-07	14:12	17,94	20,01	18,97	35,98	2,627	108,4	0,015	0,023
22-Feb-07	14:34	17,91	20,02	18,99	35,97	2,614	109,4	0,015	0,024

Date	Time	Longitude [°W]	Latitude [°N]	Temperature [°C]	Salinity	Methane Conc. [nmol L^{-1}]	Methane Saturation [%]	Flux Density LM86 [nmol m^{-2} s^{-1}]	Flux Density W92 [nmol m^{-2} s^{-1}]
22-Feb-07	14:56	17,87	20,01	18,99	35,97	2,570	106,8	0,012	0,018
22-Feb-07	15:18	17,84	20,01	18,96	35,96	2,640	110,7	0,016	0,026
22-Feb-07	15:40	17,80	20,01	18,91	35,95	2,597	108,2	0,015	0,024
22-Feb-07	16:03	17,76	20,01	18,72	35,91	2,512	107,0	0,016	0,026
22-Feb-07	16:25	17,72	20,00	18,70	35,90	2,478	103,4	0,012	0,019
22-Feb-07	16:47	17,67	20,00	18,48	35,86	2,669	111,0	0,019	0,031
22-Feb-07	17:09	17,63	20,00	18,08	35,83	2,639	110,3	0,016	0,025
22-Feb-07	17:31	17,59	20,00	17,77	35,80	2,623	107,3	0,012	0,019
22-Feb-07	17:54	17,54	20,00	17,49	35,80	2,605	106,6	0,012	0,019
22-Feb-07	18:16	17,50	20,00	17,28	35,74	2,627	106,7	0,011	0,017
22-Feb-07	18:38	17,50	20,00	17,22	35,74	2,848	113,5	0,019	0,031
22-Feb-07	19:00	17,49	20,00	17,19	35,74	2,690	108,0	0,014	0,023
22-Feb-07	19:22	17,46	20,00	17,24	35,79	2,656	104,8	0,017	0,028
22-Feb-07	19:45	17,42	20,00	17,58	35,91	2,623	110,9	0,028	0,047
22-Feb-07	20:07	17,39	20,00	17,77	35,96	2,617	106,3	0,025	0,043
22-Feb-07	20:29	17,36	20,00	17,85	35,97	2,702	106,2	0,028	0,049
22-Feb-07	20:51	17,33	20,00	17,88	36,04	2,600	97,9	0,020	0,035
22-Feb-07	21:14	17,29	20,00	18,09	36,10	2,496	95,3	0,021	0,037
22-Feb-07	21:36	17,26	20,00	18,47	36,18	2,568	97,0	0,024	0,043
22-Feb-07	21:58	17,23	20,00	18,67	36,24	2,550	94,2	0,022	0,039
22-Feb-07	22:20	17,22	20,00	18,77	36,22	2,595	94,9	0,020	0,035
22-Feb-07	22:42	17,25	20,01	18,68	36,31	2,652	98,1	0,030	0,054
22-Feb-07	23:05	17,29	20,01	18,42	36,23	2,502	92,4	0,021	0,037
22-Feb-07	23:27	17,32	20,02	18,01	36,13	2,737	101,5	0,034	0,061
22-Feb-07	23:49	17,66	22,08	18,11	36,38	2,803	101,9	0,042	0,084

Date	Time	Longitude [°W]	Latitude [°N]	Temperature [°C]	Salinity	Methane Conc. [nmol L^{-1}]	Methane Saturation [%]	Flux Density LM86 [nmol m^{-2} s^{-1}]	Flux Density W92 [nmol m^{-2} s^{-1}]
23-Feb-07	0:11	17,37	20,05	17,93	36,11	2,660	101,7	0,036	0,068
23-Feb-07	0:33	17,40	20,07	17,81	36,10	2,772	97,7	0,031	0,057
23-Feb-07	0:56	17,41	20,10	18,08	36,24	2,607	95,3	0,028	0,054
23-Feb-07	1:18	17,41	20,13	18,36	36,38	2,752	100,9	0,035	0,064
23-Feb-07	1:40	17,41	20,16	18,17	36,36	2,828	102,3	0,036	0,065
23-Feb-07	2:02	17,41	20,19	18,28	36,40	2,544	95,7	0,025	0,045
23-Feb-07	2:25	17,41	20,22	18,08	36,34	2,467	93,9	0,020	0,035
23-Feb-07	2:47	17,41	20,25	18,28	36,45	2,605	99,7	0,028	0,050
23-Feb-07	3:09	17,41	20,28	17,92	36,32	2,530	99,1	0,026	0,048
23-Feb-07	3:31	17,41	20,31	18,05	36,36	2,522	96,9	0,026	0,048
23-Feb-07	3:53	17,41	20,34	18,07	36,39	2,448	94,8	0,021	0,039
23-Feb-07	4:16	17,40	20,37	17,84	36,33	2,752	102,6	0,031	0,055
23-Feb-07	4:38	17,38	20,40	17,71	36,30	2,551	98,2	0,024	0,042
23-Feb-07	5:00	17,35	20,40	17,87	36,36	2,441	93,6	0,013	0,021
23-Feb-07	5:22	17,32	20,41	18,00	36,45	2,634	101,3	0,022	0,035
23-Feb-07	5:44	17,29	20,41	18,05	36,48	2,611	98,9	0,024	0,040
23-Feb-07	6:07	17,28	20,43	17,94	36,45	2,407	93,8	0,017	0,029
23-Feb-07	6:29	17,30	20,46	17,85	36,38	2,551	99,9	0,023	0,038
23-Feb-07	6:51	17,30	20,48	17,73	36,31	2,448	96,8	0,018	0,031
23-Feb-07	7:13	17,27	20,48	17,70	36,29	2,556	101,1	0,028	0,048
23-Feb-07	7:36	17,24	20,49	17,69	36,30	2,492	94,4	0,016	0,027
23-Feb-07	7:58	17,22	20,50	17,68	36,30	2,487	96,1	0,015	0,024
23-Feb-07	8:20	17,22	20,50	17,68	36,30	2,435	97,0	0,021	0,035
23-Feb-07	8:42	17,22	20,50	17,67	36,29	2,493	99,5	0,022	0,037
23-Feb-07	9:04	17,23	20,52	17,62	36,28	2,444	97,2	0,021	0,036

Date	Time	Longitude [°W]	Latitude [°N]	Temperature [°C]	Salinity	Methane Conc. [nmol L^{-1}]	Methane Saturation [%]	Flux Density LM86 [nmol m^{-2} s^{-1}]	Flux Density W92 [nmol m^{-2} s^{-1}]
23-Feb-07	9:27	17,24	20,55	17,52	36,24	2,464	97,1	0,022	0,038
23-Feb-07	9:49	17,26	20,58	17,51	36,23	2,413	102,6	0,026	0,044
23-Feb-07	10:11	17,28	20,61	17,40	36,20	2,457	101,8	0,028	0,048
23-Feb-07	10:33	17,29	20,65	17,42	36,28	2,526	103,9	0,033	0,057
23-Feb-07	10:55	17,29	20,69	17,18	36,19	2,673	101,2	0,027	0,045
23-Feb-07	11:18	17,30	20,74	17,43	36,31	2,481	93,9	0,015	0,025
23-Feb-07	11:40	17,32	20,78	17,89	36,51	2,626	101,4	0,021	0,034
23-Feb-07	12:02	17,34	20,82	17,66	36,43	2,620	102,7	0,015	0,023
23-Feb-07	12:24	17,37	20,88	17,43	36,33	2,476	97,7	0,007	0,011
23-Feb-07	12:46	17,38	20,90	17,42	36,28	2,552	102,1	0,012	0,018
23-Feb-07	13:09	17,40	20,95	17,06	36,17	2,523	97,3	0,009	0,015
23-Feb-07	13:31	17,42	20,99	17,05	36,15	2,494	100,4	0,010	0,016
23-Feb-07	13:53	17,44	21,03	17,02	36,15	2,431	94,2	0,008	0,012
23-Feb-07	14:15	17,46	21,07	17,29	36,19	2,397	94,7	0,010	0,015
23-Feb-07	14:37	17,47	21,12	17,33	36,19	2,439	94,4	0,021	0,038
23-Feb-07	15:00	17,49	21,16	17,86	36,23	2,495	106,9	0,046	0,087
23-Feb-07	15:22	17,51	21,20	17,78	36,20	2,391	96,2	0,023	0,043
23-Feb-07	15:44	17,52	21,24	17,83	36,17	2,344	95,9	0,018	0,031
23-Feb-07	16:06	17,54	21,28	18,12	36,11	2,196	95,3	0,014	0,024
23-Feb-07	16:28	17,55	21,32	18,51	36,27	2,416	100,4	0,024	0,041
23-Feb-07	16:51	17,57	21,36	18,08	36,29	2,722	108,2	0,040	0,071
23-Feb-07	17:13	17,59	21,40	17,69	36,25	2,397	95,1	0,024	0,047
23-Feb-07	17:35	17,60	21,44	17,47	36,21	2,540	102,0	0,036	0,069
23-Feb-07	17:57	17,62	21,47	17,46	36,22	2,349	95,9	0,025	0,050
23-Feb-07	18:19	17,64	21,51	17,54	36,27	2,480	98,6	0,027	0,049

Date	Time	Longitude [°W]	Latitude [°N]	Temperature [°C]	Salinity	Methane Conc. [nmol L^{-1}]	Methane Saturation [%]	Flux Density LM86 [nmol m^{-2} s^{-1}]	Flux Density W92 [nmol m^{-2} s^{-1}]
23-Feb-07	18:42	17,66	21,55	17,33	36,24	2,217	90,6	0,014	0,028
23-Feb-07	19:04	17,67	21,59	17,94	36,18	2,259	94,6	0,017	0,030
23-Feb-07	19:26	17,68	21,63	18,18	36,23	2,333	99,3	0,029	0,057
23-Feb-07	19:48	17,70	21,67	18,33	36,25	2,372	100,6	0,028	0,052
23-Feb-07	20:11	17,72	21,71	18,37	36,26	2,299	96,3	0,026	0,051
23-Feb-07	20:33	17,73	21,75	18,36	36,27	2,406	103,3	0,045	0,086
23-Feb-07	20:55	17,73	21,79	18,35	36,25	2,248	97,4	0,025	0,051
23-Feb-07	21:17	17,73	21,83	18,30	36,28	2,412	102,5	0,038	0,076
23-Feb-07	21:39	17,72	21,87	18,19	36,26	2,403	100,8	0,033	0,063
23-Feb-07	22:02	17,71	21,91	18,22	36,23	2,203	92,4	0,020	0,039
23-Feb-07	22:24	17,71	21,94	18,45	36,25	2,403	100,9	0,031	0,059
23-Feb-07	22:46	17,70	21,98	18,45	36,26	2,384	99,2	0,029	0,057
23-Feb-07	23:08	17,69	22,01	18,40	36,27	2,405	99,9	0,031	0,059
23-Feb-07	23:30	17,68	22,05	18,40	36,28	2,428	101,0	0,038	0,075
23-Feb-07	23:53	16,72	24,36	18,10	36,51	2,290	96,6	0,033	0,063
24-Feb-07	0:15	17,65	22,11	18,42	36,43	2,283	96,0	0,025	0,048
24-Feb-07	0:37	17,64	22,14	18,35	36,43	2,252	95,3	0,026	0,052
24-Feb-07	0:59	17,63	22,17	18,30	36,41	2,199	93,5	0,023	0,045
24-Feb-07	1:22	17,61	22,20	18,47	36,44	2,256	96,0	0,025	0,049
24-Feb-07	1:44	17,60	22,24	18,41	36,42	2,397	102,4	0,033	0,063
24-Feb-07	2:06	17,58	22,27	18,38	36,41	2,316	100,6	0,025	0,047
24-Feb-07	2:28	17,57	22,30	18,40	36,41	2,256	96,5	0,024	0,045
24-Feb-07	2:50	17,56	22,34	18,42	36,42	2,268	96,1	0,026	0,051
24-Feb-07	3:13	17,54	22,37	18,44	36,44	2,341	99,1	0,027	0,050
24-Feb-07	3:35	17,53	22,40	17,94	36,42	2,815	119,4	0,065	0,125

Date	Time	Longitude [°W]	Latitude [°N]	Temperature [°C]	Salinity	Methane Conc. [nmol L^{-1}]	Methane Saturation [%]	Flux Density LM86 [nmol m^{-2} s^{-1}]	Flux Density W92 [nmol m^{-2} s^{-1}]
24-Feb-07	3:57	17,52	22,44	17,08	36,23	2,178	89,2	0,013	0,026
24-Feb-07	4:19	17,51	22,47	17,77	36,32	2,119	90,7	0,014	0,028
24-Feb-07	4:41	17,49	22,51	18,32	36,43	2,095	90,0	0,012	0,023
24-Feb-07	5:04	17,47	22,54	18,72	36,50	2,192	92,2	0,027	0,052
24-Feb-07	5:26	17,46	22,57	18,85	36,52	2,177	95,1	0,023	0,046
24-Feb-07	5:48	17,44	22,61	18,88	36,53	2,201	96,8	0,033	0,062
24-Feb-07	6:10	17,43	22,64	18,87	36,53	2,201	95,2	0,032	0,061
24-Feb-07	6:32	17,41	22,68	18,77	36,51	2,284	99,6	0,031	0,060
24-Feb-07	6:55	17,40	22,70	18,59	36,49	2,802	122,3	0,060	0,109
24-Feb-07	7:17	17,38	22,73	17,38	36,34	2,524	106,3	0,042	0,081
24-Feb-07	7:39		0,00	17,22	36,34	2,181	92,0	0,016	0,032
24-Feb-07	8:01	17,37	22,80	17,20	36,33	2,276	95,3	0,027	0,052
24-Feb-07	8:24	17,36	22,83	17,21	36,29	2,400	101,0	0,040	0,078
24-Feb-07	8:46	17,34	22,86	17,25	36,30	2,374	98,9	0,033	0,065
24-Feb-07	9:08	17,33	22,89	17,37	36,31	2,283	96,1	0,032	0,060
24-Feb-07	9:30	17,31	22,92	17,61	36,33	2,184	89,9	0,016	0,032
24-Feb-07	9:52	17,30	22,95	17,83	36,36	2,168	90,4	0,017	0,032
24-Feb-07	10:15	17,29	22,99	17,85	36,38	2,297	95,6	0,029	0,058
24-Feb-07	10:37	17,27	23,02	17,57	36,34	2,312	96,1	0,028	0,054
24-Feb-07	10:59	17,26	23,05	17,70	36,36	2,331	100,6	0,034	0,068
24-Feb-07	11:21	17,25	23,09	17,69	36,37	2,553	109,4	0,060	0,115
24-Feb-07	11:43	17,24	23,12	17,39	36,33	2,125	88,6	0,009	0,018
24-Feb-07	12:06	17,22	23,16	17,68	36,36	2,220	93,3	0,020	0,039
24-Feb-07	12:28	17,21	23,19	18,01	36,41	2,293	95,9	0,029	0,057
24-Feb-07	12:50	17,19	23,22	18,11	36,43	2,265	96,4	0,019	0,035

Date	Time	Longitude [°W]	Latitude [°N]	Temperature [°C]	Salinity	Methane Conc. [nmol L^{-1}]	Methane Saturation [%]	Flux Density LM86 [nmol m^{-2} s^{-1}]	Flux Density W92 [nmol m^{-2} s^{-1}]
24-Feb-07	13:12	17,17	23,25	18,14	36,44	2,340	100,0	0,029	0,055
24-Feb-07	13:34	17,16	23,29	17,97	36,40	2,374	100,4	0,040	0,077
24-Feb-07	13:57	17,14	23,33	17,74	36,43	2,202	93,0	0,017	0,032
24-Feb-07	14:19	17,13	23,37	18,04	36,48	2,164	92,6	0,019	0,037
24-Feb-07	14:41	17,12	23,40	18,272	36,51	2,243	93,7	0,019	0,034
24-Feb-07	15:03	17,11	23,44	18,868	36,64	2,432	103,9	0,041	0,078

Station Nº	Longitude [°W]	Latitude [°N]	Depth [m]	Temperature [°C]	Salinity	Methane Conc. [nmol L^{-1}]	Statistic Error [%]	Methane Saturation [%]	Nitrate Conc. [µmol L^{-1}]	Dissolved Oxygen [µmol L^{-1}]
227	24,3	17,6	3594	2,47	34,91	2,231	38,56	65,4	23,25	247,5
227	24,3	17,6	3000	2,76	34,94	2,206	16,44	65,3	22,41	252,6
227	24,3	17,6	2500	3,07	34,96	1,667	18,56	49,9	21,99	248,6
227	24,3	17,6	2000	3,58	34,98	1,427	31,39	43,4	22,71	237,3
227	24,3	17,6	1750	3,98	35,00	1,279	13,85	39,3	23,54	225,2
227	24,3	17,6	1500	4,52	35,01	1,077	0,00	33,6	25,13	206,9
227	24,3	17,6	1250	5,56	35,03	1,389	14,29	44,6	29,27	169,4
227	24,3	17,6	1000	6,28	34,94	1,124	7,28	36,8	33,42	131,7
227	24,3	17,6	800	7,51	34,97	0,723	28,92	24,5	36,06	98,3
227	24,3	17,6	700	8,05	35,00	1,259	15,31	43,2	36,91	84,3
227	24,3	17,6	600	9,08	35,11	1,328	13,95	46,7	34,27	80,75
227	24,3	17,6	500	9,76	35,18	1,372	12,55	49,1	32,28	62,95
227	24,3	17,6	400	10,75	35,27	3,020	6,63	110,8	29,85	64
227	24,3	17,6	302	12,09	35,42	1,696	3,83	64,3	31,3	54,4
227	24,3	17,6	202	13,91	35,71	1,674	20,11	66,3	24,52	78,8
227	24,3	17,6	127	15,96	36,00	1,566	47,48	65,0	20,02	93,3
227	24,3	17,6	81	18,12	36,31	1,072	10,23	46,7	15,94	112,5
227	24,3	17,6	62	19,37	36,35	1,647	6,61	73,5	12,8	126
227	24,3	17,6	54	20,72	36,40	1,465	10,83	67,2	8,47	150,6
227	24,3	17,6	40	22,38	36,21	0,787	0,00	37,3	0,58	214,5
227	24,3	17,6	20	22,59	36,10	0,915	4,87	43,5	0	224
227	24,3	17,6	10	22,67	36,11	1,123	11,47	53,5	0,04	223,7
228	23	18	3483	2,5	34,92	2,303	1,20	67,7	23,24	241,9
228	23	18	3500	2,5	34,92	2,160	15,44	63,4	23,39	241,8
228	23	18	3000	2,75	34,93	1,514	21,58	44,8	22,41	246,1
228	23	18	2500	3,11	34,96	0,924	33,51	27,7	22,39	241
228	23	18	2000	3,66	34,99	1,232	6,91	37,5	22,55	232,2

Station Nº	Longitude [°W]	Latitude [°N]	Depth [m]	Temperature [°C]	Salinity	Methane Conc. [nmol L^{-1}]	Statistic Error [%]	Methane Saturation [%]	Nitrate Conc. [µmol L^{-1}]	Dissolved Oxygen [µmol L^{-1}]
228	23	18	1500	4,59	35,01	0,789	13,94	24,7	25,56	201,1
228	23	18	1250	5,56	35,01	0,916	21,46	29,4	28,76	165,9
228	23	18	1000	6,27	34,92	0,936	15,80	30,6	33,94	126,4
228	23	18	800	7,29	34,95	1,440	14,00	48,4	35,83	99,8
228	23	18	700	7,95	34,98	1,718	23,33	58,7	35,96	89,1
228	23	18	600	8,93	35,09	1,539	14,62	54,0	34,96	80,5
228	23	18	500	10,17	35,25	1,403	16,69	50,7	32,84	71,2
228	23	18	400	11,01	35,32	1,534	32,66	56,7	33,85	51,15
228	23	18	332	11,65	35,37	1,682	7,20	63,1	32,37	48,9
228	23	18	300	12,06	35,41	1,634	9,84	61,9	31,63	51,6
228	23	18	250	12,75	35,48	2,641	6,17	101,7	28,63	63,6
228	23	18	200	13,4	35,51	2,117	24,73	82,8	26,57	69
228	23	18	150	14,65	35,65	2,474	11,23	99,5	25,82	61,4
228	23	18	100	17,3	35,90	2,772	12,45	118,2	21,19	71,5
228	23	18	75	21,39	36,20	2,318	7,54	107,6	4,72	179,4
228	23	18	60	22,1	36,09	2,109	24,91	99,2	0,32	217,6
228	23	18	25	22,26	36,08	1,605	13,14	75,7	0	223,4
228	23	18	10	22,26	36,08	1,713	24,15	80,9	0,04	224,4
228	23	18	5	22,26	36,08	1,415	7,32	66,8	0,14	223,5
230	21	18	3057	2,63	34,93	1,608	12,78	47,4	23,73	232,8
230	21	18	2500	3,03	34,95	0,585	1,93	17,5	22,37	241,6
230	21	18	2000	3,57	34,99	1,065	7,69	32,4	22,94	234,1
230	21	18	1750	3,99	35,01	1,332	11,04	41,0	24,02	222,6
230	21	18	1500	4,57	35,03	0,763	16,16	23,9	25,52	203,6
230	21	18	1250	5,56	35,06	1,468	24,84	47,2	28,06	172,1
230	21	18	1000	6,12	34,95	0,822	4,45	26,8	33,08	135,4
230	21	18	800	7,24	34,98	0,510	0,00	17,1	34,79	109,2

Station Nº	Longitude [°W]	Latitude [°N]	Depth [m]	Temperature [°C]	Salinity	Methane Conc. [nmol L^{-1}]	Statistic Error [%]	Methane Saturation [%]	Nitrate Conc. [µmol L^{-1}]	Dissolved Oxygen [µmol L^{-1}]
230	21	18	700	7,89	35,02	1,783	11,45	60,9	35,47	96
230	21	18	600	8,92	35,12	1,751	12,24	61,4	35,46	81,5
230	21	18	500	10,06	35,26	2,095	3,59	75,6	33,26	76,7
230	21	18	400	10,79	35,35	2,706	5,41	99,4	31,63	73,5
230	21	18	500	10,03	35,26	3,288	8,06	118,6	32,83	77,95
230	21	18	416	10,97	35,34	2,508	19,42	92,6	32	68,3
230	21	18	300	12,86	35,59	2,050	11,93	79,2	26,44	77,8
230	21	18	250	13,77	35,73	2,838	3,70	112,0	24,64	83,7
230	21	18	200	14,57	35,86	2,619	7,33	105,3	21,87	92,4
230	21	18	150	15,87	36,05	3,817	5,36	158,1	20,27	96,4
230	21	18	100	17,23	36,16	3,047	1,68	130,0	19,36	85,8
230	21	18	75	21,27	36,47	3,769	0,00	174,9	8,59	159,1
230	21	18	61	21,62	36,39	3,088	1,86	144,2	1,9	207,5
230	21	18	25	21,95	36,39	3,170	16,91	149,0	0	225,8
230	21	18	10	21,96	36,38	2,580	7,47	121,3	0,01	226
230	21	18	5	21,97	36,38	2,564	2,48	120,6	0,04	226,2
232	19	18	3119	2,67	34,93	1,332	0,18	39,3	23,02	229,7
232	19	18	2500	3,03	34,95	1,258	13,10	37,6	22,23	241,9
232	19	18	2000	3,62	34,99	1,322	8,16	40,2	22,86	233,3
232	19	18	1750	4,04	35,01	1,443	30,51	44,4	22,63	228,8
232	19	18	1500	4,63	35,03	0,941	13,66	29,5	25,08	201,6
232	19	18	1250	5,53	35,04	1,393	15,91	44,7	27,91	168,3
232	19	18	1000	6,31	34,97	0,981	0,00	32,2	32,16	129,3
232	19	18	800	7,04	34,93	1,018	15,78	34,0	35,72	96,4
232	19	18	700	7,78	34,99	1,496	28,53	50,9	36,39	79,2
232	19	18	600	8,76	35,08	1,754	25,85	61,2	35,92	67
232	19	18	400	11,45	35,41	3,688	0,00	137,7	31,31	59,95

Station Nº	Longitude [°W]	Latitude [°N]	Depth [m]	Temperature [°C]	Salinity	Methane Conc. [nmol L^{-1}]	Statistic Error [%]	Methane Saturation [%]	Nitrate Conc. [µmol L^{-1}]	Dissolved Oxygen [µmol L^{-1}]
232	19	18	500	10,18	35,26	2,128	5,68	77,0	33,43	65,8
232	19	18	400	11,48	35,41	2,857	6,25	106,7	31,1	59,9
232	19	18	300	12,17	35,40	2,360	9,75	89,6	31,42	50,8
232	19	18	250	12,5	35,40	2,350	12,11	89,9	29,78	59,8
232	19	18	200	12,99	35,41	2,130	2,32	82,4	28,48	63,8
232	19	18	150	13,71	35,47	3,425	9,19	134,8	27,41	62,6
232	19	18	100	14,98	35,62	2,218	3,21	89,8	26,59	55,8
232	19	18	75	16,08	35,72	2,478	8,97	102,9	26,18	51,1
232	19	18	50	17,93	35,77	3,114	50,00	134,5	18,92	83,2
232	19	18	25	20,72	35,93	2,890	6,59	132,2	2,42	224,7
232	19	18	10	20,71	35,89	2,900	3,10	132,6	1,43	244,8
232	19	18	10	20,72	35,89	2,847	2,53	130,3	1,37	245,9
233	18	18	2778	2,83	34,94	2,542	12,65	75,5	22,05	236,95
233	18	18	2500	3,02	34,95	2,629	2,34	78,6	22,24	239,5
233	18	18	2000	3,51	34,97	2,331	1,74	70,7	22,54	234,7
233	18	18	1500	4,46	35,02	2,633	7,71	82,1	24,34	207,1
233	18	18	1250	5,34	35,04	2,633	0,00	84,1	26,87	176,7
233	18	18	1000	6,34	34,98	2,205	3,10	72,3	32,3	131,1
233	18	18	800	7,25	34,97	2,303	7,37	77,3	34,06	104
233	18	18	700	7,93	35,02	2,397	3,29	81,9	35,42	88,4
233	18	18	600	9,34	35,18	2,700	8,98	95,7	33,93	77,8
233	18	18	500	10,19	35,25	2,789	0,00	100,9	33,91	58,1
233	18	18	407	11,27	35,36	3,553	3,00	132,1	32,24	51,6
233	18	18	300	12,62	35,53	6,743	3,96	258,9	11,16	
233	18	18	500	10,17	35,25	3,695	10,82	133,7	34,22	57,6
233	18	18	400	11,11	35,36	3,408	3,92	126,2	32,69	53,3
233	18	18	300	12,82	35,55	3,857	7,94	148,8	27,54	65

Station Nº	Longitude [°W]	Latitude [°N]	Depth [m]	Temperature [°C]	Salinity	Methane Conc. [nmol L^{-1}]	Statistic Error [%]	Methane Saturation [%]	Nitrate Conc. [µmol L^{-1}]	Dissolved Oxygen [µmol L^{-1}]
233	18	18	250	13,7	35,65	3,797	0,00	149,5	26,3	68,6
233	18	18	200	13,52	35,49	4,231	0,00	165,8	26,47	68
233	18	18	150	14,21	35,53	3,812	3,33	151,8	26,81	59
233	18	18	100	15,26	35,61	4,148	0,00	169,1	26,22	53
233	18	18	75	16,97	35,78	4,158	4,74	176,0	23,56	55,7
233	18	18	50	19,6	35,95	3,919	8,40	175,3	7,34	185,7
233	18	18	25	20,23	36,02	3,469	1,39	157,3	3,19	220,4
233	18	18	15	20,34	36,01	4,094	7,65	186,0	3,06	226,7
233	18	18	10	20,35	36,01	4,194	11,07	190,6	2,9	231,2
235	17	18	1704	4,01	34,98	8,879	6,47	273,2	24,31	216,85
235	17	18	1500	4,38	34,99	7,689	7,73	239,1	25,29	203,7
235	17	18	1250	5,29	35,02	4,003	7,42	127,7	28,26	171,8
235	17	18	1000	6,11	34,94	5,824	5,35	189,8	33,34	128,1
235	17	18	800	7,08	34,95	3,753	5,46	125,5	36,2	96,3
235	17	18	700	7,81	34,99	3,665	8,84	124,9	37,49	79,4
235	17	18	600	9,23	35,14	2,907	1,21	102,7	35,82	65,8
235	17	18	500	9,92	35,19	4,099	8,86	147,4	36,12	58,8
235	17	18	448	10,66	35,27	4,246	12,09	155,5	35,47	49,3
235	17	18	300	12,18	35,41	3,224	6,76	122,5	30,88	52,4
235	17	18	10	20,34	35,98	3,961	6,39	179,9	3,26	238,1
235	17	18	250	12,73	35,40	3,247	3,88	124,9	29,25	63,7
235	17	18	200	13,32	35,44	3,803	0,38	148,3	27,72	68,3
235	17	18	150	14,04	35,50	4,143	4,12	164,3	26,85	62,1
235	17	18	125	14,37	35,50	3,530	5,85	141,0	26,47	64,4
235	17	18	100	15,45	35,70	3,618	1,77	148,2	25,83	59,1
235	17	18	75	17,05	35,73	4,428	1,06	187,7	21,9	71,1
235	17	18	50	19,05	35,85	3,981	1,19	176,0	10,33	186,4

Station Nº	Longitude [°W]	Latitude [°N]	Depth [m]	Temperature [°C]	Salinity	Methane Conc. [nmol L^{-1}]	Statistic Error [%]	Methane Saturation [%]	Nitrate Conc. [µmol L^{-1}]	Dissolved Oxygen [µmol L^{-1}]
235	17	18	40	19,48	35,91	4,565	15,75	203,7	6,61	210,9
235	17	18	30	20,1	35,99	4,375	1,41	197,8	4,01	228,2
235	17	18	20	20,27	35,98	9,444	0,31	428,4	3,15	236,6
235	17	18	14	20,31	35,98	3,640	11,33	165,2	3,08	238,1
235	17	18	10	20,34	35,98	4,353	3,62	197,7	3,08	238,4
236	16,5	18	185	13,74	35,47	4,661	11,78	183,5	27,67	58,3
236	16,5	18	175	13,77	35,47	3,682	0,00	145,1	27,94	58,3
236	16,5	18	150	13,86	35,47	2,813	1,67	111,1	27,43	61,5
236	16,5	18	125	14,14	35,49	2,075	18,94	82,4	27,18	61,5
236	16,5	18	100	14,42	35,51	3,087	9,71	123,4	27,13	61,6
236	16,5	18	75	15,31	35,62	3,378	9,86	137,9	25,16	72,9
236	16,5	18	50	16,11	35,73	3,699	6,30	153,7	21,76	95,6
236	16,5	18	25	17,01	35,82	4,451	10,72	188,6	18,99	112,4
236	16,5	18	10	17,84	35,87	4,169	1,66	179,8	7,92	231,9
236	16,5	18	6	18,16	35,86	3,953	5,53	171,7	7,23	245,15

Station Nº	Longitude [°W]	Latitude [°N]	Depth [m]	Temperature [°C]	Salinity	Methane Conc. [nmol L^{-1}]	Statistic Error [%]	Saturation [%]	Oxygen Conc. [µmol L^{-1}]
1	50,87	53,13	2723	2,07	34,90	2,515	6,9	74,0	302,1
1	50,87	53,13	2600	2,23	34,91	3,004	15,0	88,9	307,1
1	50,87	53,13	2500	2,49	34,91	2,152	11,4	64,1	286,6
1	50,87	53,13	2300	2,76	34,92	1,858	9,3	55,8	290,3
1	50,87	53,13	2200	2,86	34,92	1,753	1,5	52,8	290,0
1	50,87	53,13	2000	3,05	34,91	1,731	17,8	52,4	289,9
1	50,87	53,13	1800	3,15	34,91	1,470	9,0	44,6	288,5
1	50,87	53,13	1600	3,33	34,91	1,725	1,9	52,6	287,5
1	50,87	53,13	1500	3,39	34,91	1,714	15,7	52,4	286,6
1	50,87	53,13	1400	3,50	34,91	1,569	3,8	48,1	287,6
1	50,87	53,13	1300	3,56	34,90	1,925	4,0	59,1	290,2
1	50,87	53,13	1200	3,57	34,89	2,231	3,4	68,5	292,5
1	50,87	53,13	1100	3,58	34,88	2,134	2,2	65,5	295,5
1	50,87	53,13	1000	3,55	34,87	2,274	1,8	69,8	301,7
1	50,87	53,13	800	3,60	34,87	2,925	10,4	89,9	304,2
1	50,87	53,13	600	3,65	34,86	2,687	7,0	82,7	306,1
1	50,87	53,13	400	3,73	34,86	2,417	1,1	74,6	306,7
1	50,87	53,13	200	3,71	34,83	2,588	6,5	79,8	319,3
1	50,87	53,13	100	3,48	34,70	3,372	15,2	103,2	319,7
1	50,87	53,13	10	2,74	34,32	3,679	2,7	110,0	341,5
3	51,73	52,73	770	3,75	34,86	3,275	5,4	101,1	305,0
3	51,73	52,73	700	3,75	34,86	3,162	2,0	97,6	305,3
3	51,73	52,73	600	3,74	34,86	2,890	1,0	89,2	305,8
3	51,73	52,73	500	3,75	34,85	3,097	7,0	95,6	306,9
3	51,73	52,73	400	3,77	34,85	3,169	9,0	97,8	304,6

Station Nº	Longitude [°W]	Latitude [°N]	Depth [m]	Temperature [°C]	Salinity	Methane Conc. [nmol L^{-1}]	Statistic Error [%]	Saturation [%]	Oxygen Conc. [µmol L^{-1}]
3	51,73	52,73	200	3,63	34,80	2,937	3,7	90,3	322,9
3	51,73	52,73	10	1,43	33,68	4,089	4,1	117,2	349,7
11	49,89	53,50	3550	1,83	34,89	2,134	9,3	62,4	303,3
11	49,89	53,50	3100	2,30	34,90	1,719	26,0	50,9	290,8
11	49,89	53,50	2800	2,64	34,91	2,058	5,3	61,6	290,0
11	49,89	53,50	2300	2,96	34,91	1,841	17,3	55,6	287,1
11	49,89	53,50	1900	3,19	34,90	2,803	10,6	85,2	287,9
11	49,89	53,50	1700	3,33	34,90	2,806	23,9	85,6	287,0
11	49,89	53,50	1500	3,46	34,90	2,504	2,6	76,7	285,0
11	49,89	53,50	1300	3,55	34,90	2,825	5,0	86,7	285,9
11	49,89	53,50	1100	3,60	34,89	2,607	6,6	80,1	289,4
11	49,89	53,50	900	3,69	34,89	2,319	22,5	71,5	291,5
11	49,89	53,50	700	3,79	34,89	2,970	20,9	91,8	289,9
11	49,89	53,50	500	4,00	34,89	3,321	12,9	103,2	285,4
11	49,89	53,50	300	4,26	34,87	3,402	6,1	106,5	278,3
11	49,89	53,50	100	4,49	34,75	3,451	12,0	108,6	307,6
11	49,89	53,50	10	5,40	34,73	4,462	19,2	143,9	328,4
14	48,87	53,94	3400	2,24	34,90	2,710	18,0	80,2	286,9
14	48,87	53,94	3000	2,59	34,92	2,694	13,2	80,5	280,9
14	48,87	53,94	2200	3,08	34,91	3,116	19,0	94,4	286,4
14	48,87	53,94	1800	3,32	34,90	3,335	1,3	101,7	287,6
14	48,87	53,94	1600	3,44	34,90	2,920	15,0	89,4	285,5
14	48,87	53,94	1400	3,55	34,90	3,034	21,3	93,1	286,1
14	48,87	53,94	1200	3,57	34,89	3,103	0,0	95,3	289,4
14	48,87	53,94	1000	3,65	34,88	3,497	8,9	107,6	292,2

Station Nº	Longitude [°W]	Latitude [°N]	Depth [m]	Temperature [°C]	Salinity	Methane Conc. [nmol L^{-1}]	Statistic Error [%]	Saturation [%]	Oxygen Conc. [µmol L^{-1}]
14	48,87	53,94	800	3,72	34,88	4,206	15,3	129,7	294,2
14	48,87	53,94	600	3,80	34,87	4,365	11,9	134,9	296,9
14	48,87	53,94	400	3,75	34,82	4,577	13,2	141,3	302,0
14	48,87	53,94	10	5,58	34,75	4,800	2,5	155,5	329,9
20	54,18	54,96	400	3,83	34,86	4,268	3,9	132,0	305,2
20	54,18	54,96	350	3,83	34,85	3,803	11,1	117,6	305,8
20	54,18	54,96	300	3,83	34,85	3,829	6,9	118,4	306,0
20	54,18	54,96	100	3,82	34,79	4,029	2,6	124,6	312,3
20	54,18	54,96	10	3,55	34,58	4,441	8,8	136,0	323,6
24	53,73	55,45	2800	2,26	34,91	3,006	18,7	89,0	296,2
24	53,73	55,45	2500	2,56	34,91	2,214	3,1	66,1	292,2
24	53,73	55,45	2100	3,03	34,91	2,301	19,2	69,6	290,1
24	53,73	55,45	1900	3,18	34,91	1,993	7,9	60,5	288,7
24	53,73	55,45	1700	3,34	34,91	2,339	12,2	71,4	288,0
24	53,73	55,45	1500	3,53	34,91	2,202	11,4	67,6	285,8
24	53,73	55,45	1300	3,62	34,90	3,488	6,4	107,3	289,6
24	53,73	55,45	1100	3,63	34,88	3,855	0,1	118,6	294,7
24	53,73	55,45	900	3,71	34,88	3,812	9,8	117,5	298,8
24	53,73	55,45	700	3,74	34,87	4,122	2,2	127,2	302,7
24	53,73	55,45	500	3,81	34,87	3,390	7,5	104,8	303,0
24	53,73	55,45	300	3,85	34,86	4,183	4,4	129,5	305,2
24	53,73	55,45	10	3,61	34,55	4,750	1,1	145,7	341,6
27	52,86	56,34	3500	1,76	34,89	3,844	10,5	112,1	304,8
27	52,86	56,34	3000	2,64	34,92	2,928	15,2	87,6	
27	52,86	56,34	2600	2,93	34,91	2,684	4,1	81,0	

Station Nº	Longitude [°W]	Latitude [°N]	Depth [m]	Temperature [°C]	Salinity	Methane Conc. [nmol L^{-1}]	Statistic Error [%]	Saturation [%]	Oxygen Conc. [µmol L^{-1}]
27	52,86	56,34	2200	3,16	34,90	2,900	19,1	88,0	
27	52,86	56,34	1800	3,42	34,90	2,434	9,9	74,4	287,4
27	52,86	56,34	1600	3,53	34,90	2,387	11,0	73,2	
27	52,86	56,34	1400	3,54	34,88	3,031	10,0	93,0	
27	52,86	56,34	1200	3,52	34,86	4,001	16,8	122,7	
27	52,86	56,34	1000	3,55	34,86	3,971	6,7	121,9	303,8
27	52,86	56,34	800	3,55	34,85	4,066	1,0	124,8	
27	52,86	56,34	600	3,60	34,85	4,260	3,5	130,9	
27	52,86	56,34	400	3,75	34,86	4,367	12,0	134,8	308,7
27	52,86	56,34	200	3,74	34,84	4,584	14,4	141,4	
27	52,86	56,34	10	4,46	34,76	6,095	17,7	191,7	356,6
31	51,79	57,45	3500	1,75	34,90	2,502	6,1	73,0	304,9
31	51,79	57,45	3400	1,96	34,89	2,999	6,2	88,0	301,0
31	51,79	57,45	2600	2,91	34,92	2,496	14,0	75,3	287,4
31	51,79	57,45	1800	3,42	34,91	2,111	1,0	64,6	286,5
31	51,79	57,45	1600	3,58	34,91	2,354	3,6	72,3	285,8
31	51,79	57,45	1400	3,54	34,88	2,341	6,6	71,8	292,0
31	51,79	57,45	1200	3,54	34,87	3,676	15,5	112,8	300,0
31	51,79	57,45	1000	3,59	34,87	4,480	2,6	137,6	300,7
31	51,79	57,45	800	3,68	34,87	3,764	4,0	116,0	298,3
31	51,79	57,45	600	3,80	34,87	3,847	15,1	118,9	309,3
31	51,79	57,45	400	3,83	34,87	4,627	12,5	143,1	309,8
31	51,79	57,45	200	4,18	34,88	4,134	1,0	129,1	302,1
31	51,79	57,45	10	4,61	34,73	4,784	12,4	151,0	336,0
33	51,21	58,04	3600	1,76	34,90	2,902	15,5	84,7	306,0

Station Nº	Longitude [°W]	Latitude [°N]	Depth [m]	Temperature [°C]	Salinity	Methane Conc. [nmol L^{-1}]	Statistic Error [%]	Saturation [%]	Oxygen Conc. [µmol L^{-1}]
33	51,21	58,04	3200	2,37	34,90	2,264	20,3	67,2	293,7
33	51,21	58,04	2000	3,28	34,90	2,573	12,5	78,4	289,5
33	51,21	58,04	1800	3,46	34,91	2,055	2,3	62,9	287,2
33	51,21	58,04	1600	3,56	34,90	2,709	3,8	83,2	288,0
33	51,21	58,04	1400	3,55	34,88	3,017	3,5	92,6	293,2
33	51,21	58,04	1200	3,55	34,87	3,221	13,7	98,9	300,6
33	51,21	58,04	1000	3,54	34,86	3,779	27,5	116,0	304,8
33	51,21	58,04	800	3,52	34,85	3,329	6,1	102,1	307,5
33	51,21	58,04	600	3,60	34,86	2,986	6,7	91,8	306,0
33	51,21	58,04	400	3,68	34,85	2,541	0,9	78,3	309,2
33	51,21	58,04	200	3,87	34,85	3,542	14,6	109,7	307,2
33	51,21	58,04	10	4,29	34,76	3,373	9,8	105,6	352,9
36	52,77	59,32	3500	1,72	34,90	3,413	13,7	99,5	304,8
36	52,77	59,32	3300	1,94	34,90	2,679	13,7	78,5	
36	52,77	59,32	2900	2,66	34,92	2,312	3,3	69,2	290,2
36	52,77	59,32	2500	3,01	34,91	2,430	8,6	73,5	
36	52,77	59,32	2100	3,28	34,91	2,491	13,2	75,9	288,0
36	52,77	59,32	1900	3,37	34,90	2,341	2,6	71,5	
36	52,77	59,32	1700	3,56	34,91	2,988	16,0	91,7	285,5
36	52,77	59,32	1500	3,55	34,89	3,750	15,7	115,1	
36	52,77	59,32	1300	3,55	34,87	3,310	13,1	101,6	298,5
36	52,77	59,32	1100	3,53	34,86	2,962	26,5	90,9	
36	52,77	59,32	900	3,52	34,85	3,446	6,7	105,7	307,9
36	52,77	59,32	700	3,55	34,85	2,871	15,7	88,1	
36	52,77	59,32	500	3,63	34,85	3,147	13,5	96,8	309,1

Station Nº	Longitude [°W]	Latitude [°N]	Depth [m]	Temperature [°C]	Salinity	Methane Conc. [nmol L^{-1}]	Statistic Error [%]	Saturation [%]	Oxygen Conc. [µmol L^{-1}]
36	52,77	59,32	300	3,87	34,87	2,570	7,7	79,6	
36	52,77	59,32	100	4,60	34,90	2,924	13,5	92,4	300,6
36	52,77	59,32	10	4,50	34,77	3,637	12,4	114,5	326,3

Eidesstattliche Erklärung

Ich erkläre hiermit an Eides Statt, dass ich die vorliegende Arbeit selbständig und ohne Benutzung anderer als der angegebenen Hilfsmittel angefertigt habe.

_____

Annette Kock